



UNIVERSIDAD
TECNOLÓGICA
METROPOLITANA
del Estado de Chile

ISSN (ISSN-L) 2735-6817
ISSN (ONLINE) 2735-6817

Volumen 3 • Número especial
<https://doi.org/10.58560/rmmsb.v03.esp.023>
Octubre 2023

Revista de Modelamiento Matemático de Sistemas Biológicos

Mathematical Biology at Springtime in 29S53W

Grupo MatBio-UTEM
Departamento de Matemática
Facultad de Ciencias Naturales, Matemática y Medio Ambiente

Editores Número Especial:
Diomar Cristina Mistro y Luiz Alberto Díaz Rodrigues
Universidade Federal de Santa Maria, Brasil





UNIVERSIDAD
TECNOLÓGICA
METROPOLITANA
del Estado de Chile

ISSN: 2735-6817

Volumen 3 • Número especial
Octubre 2023

Revista de **Modelamiento Matemático de Sistemas Biológicos**

Mathematical Biology at **Springtime in 29S53W**

Grupo MatBio-UTEM
Departamento de Matemática
Facultad de Ciencias Naturales, Matemática y Medio Ambiente

revistammsb.udem.cl



EDICIONES UNIVERSIDAD
TECNOLÓGICA METROPOLITANA

© UNIVERSIDAD TECNOLÓGICA METROPOLITANA
Facultad de Ciencias Naturales, Matemáticas
y Medio Ambiente
Departamento de Matemática
Grupo MatBio-UTEM

Revista Modelamiento Matemático de Sistemas Biológicos
Journal of Mathematical Modelling of Biological Systems

ISSN (ISSN-L) 2735-6817

ISSN (ONLINE) 2735-6817

Volumen 2, Número especial, octubre 2023

REPRESENTANTE LEGAL

Marisol Durán Santis, Rectora UTEM

COMITÉ EDITORIAL

Director

Dr. Miguel Montenegro Concha

Editor jefe

Dr. Ricardo Castro Santis

Editora técnica

Mg. Mariela Ferrada Cubillos

COMITÉ EJECUTIVO

Departamento de Matemática Grupo – MatBio-UTEM

Dr. Daniel Sepúlveda Oehninger

Dr. Francisco Vielma Leal

Ph D. Tomás Veloz

Editores nacionales

Dr. Pablo Aguirre

Universidad Técnica Federico Santa María, Valparaíso, Chile

Dr. Raimund Bürger

Centro de Investigación en Ingeniería Matemática (CI²MA)

Facultad de Ciencias Físicas y Matemáticas

Universidad de Concepción, Chile

Dr. Ramiro Bustamante

Universidad de Chile

Dra. Alejandra Christen

Universidad de Valparaíso, Chile

Dr. Fernando Córdova Lepe

Universidad Católica del Maule, Talca, Chile

Dr. Gonzalo Robledo

Universidad de Chile

Dra. Katia Vogt Geisse

Universidad Adolfo Ibáñez, Santiago, Chile

Editores extranjeros

Dr. Ignacio Barradas

Centro de Investigación en Matemáticas -CIMAT-, Guanajuato,
México

Dr. Diego Griffon

Instituto de Zoología y Ecología Tropical (IZET)

Universidad Central de Venezuela, Caracas

Dra. Nara Guisoni

Universidad Nacional de la Plata, Argentina

Dr. Eduardo Ibagüen-Mondragón

Universidad de Nariño, Pasto – Nariño, Colombia

Dra. Diomar Cristina Mistro

Universidade Federal de Santa María, Santa María – RS, Brasil

Dr. Fernando R. Momo

Universidad de General Sarmiento, Los Polvorines, Provincia
de Buenos Aires, Argentina

Dr. Jorge Velasco-Hernández

Universidad Autónoma de México – UNAM, Querétaro, México

Dra. Alejandra Ventura

Universidad de Buenos Aires, Argentina

COMITÉ TÉCNICO

Coordinación editorial

Nicole Fuentes

Claudio Lobos

Ediciones UTEM

Diagramación y diseño

Yerko Martínez Velásquez

Corrección de estilo

Gonzalo López

Erick Pezoa

Siujen Chiang

Difusión

Paola Valenzuela Fuentes

INFORMACIONES

Revista Modelamiento Matemático de Sistemas Biológicos
Grupo MatBio-UTEM
Departamento de Matemáticas Facultad de Ciencias Naturales,
Matemática y Medio Ambiente

Correspondencia: Las Palmeras 3360, Ñuñoa, Santiago, Chile.
Código Postal 7800003. Teléfono: (56-2) 27877221

Correo electrónico: revista.mmsb@utem.cl



La revista Modelamiento Matemático de Sistemas Biológicos utiliza la Licencia Creative Commons de Atribución 4.0 Internacional (CC BY 4.0). A menos que se indique lo contrario.

LAS IDEAS Y OPINIONES CONTENIDAS SON DE
RESPONSABILIDAD EXCLUSIVA DEL(OS) AUTOR(ES) Y
NO EXPRESAN NECESARIAMENTE EL PUNTO DE VISTA
DE LA REV. MODEL. MAT. SIST. BIOL. - UNIVERSIDAD
TECNOLÓGICA METROPOLITANA.

Comité Científico – Número Especial

NOMBRE	ORCID	INSTITUCIÓN
Cláudia Mazza Dias	0000-0001-7376-1554	Universidade Federal do Rio de Janeiro, Brasil
Eduardo Ibarguen-Mondragon	0000-0001-6308-1344	Universidad de Nariño, Colombia
Cláudia Pio Ferreira	0000-0002-9404-6098	Universidade Estadual Paulista, Brasil
Juan Pablo Aparicio	0000-0001-5434-7454	Centro Científico Tecnológico CONICET Salta-Jujuy, Argentina
Rodrigo Gutiérrez	0000-0002-1119-9989	Universidad Católica del Maule, Chile
Fernando Luiz Pio dos Santos	0000-0003-2774-7297	Universidade Estadual Paulista, Brasil
Lucy Tiemi Takahashi	0000-0002-8918-3899	Universidade Federal de Juiz de For, Brasil
Gustavo Sibona	0000-0003-3013-159X	Universidad Nacional de Córdoba, Argentina
José Geiser Villavicencio Pulido	0000-0003-1085-8556	Universidad Autónoma Metropolitana, México
Mario Ignacio Simoy	0000-0002-8907-5126	Universidad Nacional del Centro de la Provincia de Buenos Aires, Argentina

Políticas Editoriales

1. Carácter: la revista Modelamiento Matemático de Sistemas Biológicos (MMSB) es una publicación en línea, de acceso abierto, universal, gratuita y sin restricciones de circulación de sus contenidos. MMSB busca ser reconocida por su calidad de contenidos y rigurosidad en los procesos de edición y publicación.

2. Misión. Rev. model. mat. sist. biol. busca difundir trabajos originales e inéditos que incrementen el conocimiento y comprensión de sistemas biológicos a través del modelamiento matemático como herramienta principal de análisis. Las áreas temáticas incluidas en la revista son:

- Dinámica de Poblaciones
- Sustentabilidad
- Biodiversidad
- Epidemiología
- Enfermedades no infecciosas
- Biotecnología
- Biomateriales
- Neurociencia
- Genética
- Fisiología
- Biología celular
- Entre otros temas de origen biológico que puedan ser modelados y estudiados matemáticamente

3. Visión. Rev. model. mat. sist. biol. promueve el acceso al conocimiento de manera democrática y sin fines de lucro, libre circulación y acceso inmediato de sus artículos, siempre que se cite adecuadamente la fuente.

La revista busca valorizar la investigación científica producida en América Latina y el Caribe, aunque no de manera restrictiva geográficamente, ofreciendo una plataforma de divulgación científica para los trabajos de investigadores de la región, sin perjuicio de que se trata de una publicación disponible para los investigadores de todo el mundo.

4. Fecha y número de publicaciones anuales: Rev. model. mat. sist. biol. publicará tres números regulares por cada volumen, en los meses de: abril, agosto y diciembre de cada año.

La Rev. model. mat. sist. biol. se reserva el derecho de publicar volúmenes especiales que pueden ser dedicados a una temática específica o vinculados a un evento científico.

5. Alcance idiomático: Español-Inglés.

6. Política de derechos de autor, publicación y acceso a los contenidos: Rev. model. mat. sist. biol., Universidad Tecnológica Metropolitana como editora se reserva las atribuciones de comunicación y difusión según las prácticas del derecho de autor chilenas, y declara una política de acceso abierto (OA), bajo el principio de disponibilidad inmediata y gratuita, bajo la licencia Creative Commons [Reconocimiento 4.0 Internacional License](https://creativecommons.org/licenses/by/4.0/) (CC BY 4.0) (<https://creativecommons.org/licenses/by/4.0/>), siempre que le sea reconocida la autoría de la creación original, a menos que se indique lo contrario.

La revista adhiere a los principios de Investigación Abierta (Open Science) y a los Principios FAIR (Findable, Accessible, Interoperable, and Reusable), para la gestión de datos científicos.

7.- Cargos por envío y/o publicación artículos

La revista no tiene cargos por procesamiento de artículos (APC).

La revista no tiene cargos por envío de artículos.

8. Para los autores: se autoriza establecer copia en repositorios institucionales o personales, de preprint o posprint, siempre y cuando se cite la fuente o sitio institucional donde han sido publicados originalmente. Véase Políticas de apertura de la revista en: [Sherpa Romeo](#) [AURA - Amelica](#)

9. Para los lectores: se autoriza la reproducción total o parcial de los textos aquí publicados siempre y cuando se cite debidamente la autoría y fuente completa, así como la dirección electrónica de la publicación.

10. La responsabilidad de sus autores/as y de las opiniones expresadas no necesariamente reflejan la postura de la editorial, la revista o de la Universidad Tecnológica Metropolitana (UTEM).

Las opiniones y hechos consignados en cada artículo son de exclusiva responsabilidad de sus autores/as, así como de la idoneidad ética como investigadores.

Además, al enviar un trabajo a evaluar para publicación, hacen explícito que el manuscrito es de su autoría y que se respetan los derechos de propiedad intelectual de terceros. También es su responsabilidad asegurarse de tener las autorizaciones para usar, reproducir e imprimir el material que no sea de su propiedad/autoría (cuadros, gráficas, mapas, diagramas, fotografías, etcétera).

Cuando un autor(a) identifica en su artículo un error importante, deberá informar de inmediato a los editores y proporcionar toda la información necesaria para hacer las correcciones pertinentes y/o elaborar una retractación o corrección en caso de que terceros detecten errores.

11. La responsabilidad de los editores

Decisión de publicación: garantizarán la selección de las personas evaluadoras más calificadas y especialistas científicamente para emitir una apreciación crítica y experta del trabajo, con los menores sesgos posibles.

Integridad ética: evalúan los artículos enviados para su publicación sobre la base del mérito científico de los contenidos, sin discriminación ni opinión de género o política de las personas autoras, y en consideración a las políticas de género en la publicación en base a las recomendaciones de la [ANID - Chile 2021](#).

Confidencialidad: se comprometen a la confidencialidad de los manuscritos, su autoría y evaluación, de forma que el anonimato preserve la integridad intelectual de todo el proceso. Respeto de los tiempos: son responsables máximos del cumplimiento de los límites de tiempo para las revisiones y la publicación de los trabajos aceptados, para asegurar una rápida difusión de sus resultados.

12. **Código ético.** La Rev. model. mat. sist. biol. adhiere al Código del Committee on Publication Ethics (COPE) para discutir y o sancionar toda materia relativa a los aspectos de la ética de la publicación. Véase: COPE Principios de Transparencia y Mejores Prácticas en Publicaciones Académicas, disponible en: <https://doi.org/10.24318/cope.2019.1.13>

13. **Conflicto de interés:** La Revista requiere que los autores, revisores, declaren cualquier conflicto de intereses en conexión con el artículo remitido. Si los hay, es imperativo que

los identifiquen, e informen en detalle cuál fue su relación con el trabajo presentado.

14. **Detección o prevención del plagio.** MMSB emplea el sistema de detección de plagio de la Universidad (UTEM) (véase <https://www.urkund.com/es/>), con motivo de salvaguardar la pertinencia u originalidad de los contenidos que se publicarán.

Si posteriormente a la publicación de un artículo el Consejo editorial detecta o es informado de plagio, mala conducta en la investigación, la Revista puede retirar el artículo e informa retractación, adicionalmente puede emprender en contra de las personas autoras las acciones legales que correspondan.

15.- **Preservación de los contenidos.** En [Repositorio Institucional SIBUTEM](#)

Indexación en bases de datos, directorios: Latindex, Sistema Regional de Información Revistas Científicas de América Latina, el Caribe, España y Portugal; ROAD: Directory of Open Access Scholarly Resources; AURA Amelica Unesco; Sherpa Romeo.

Repositorios: Repositorio académico UTEM; Google Académico.

Editorial Policies

1. Character. The Journal of Mathematical Modeling of Biological Systems (MMSM) is an official publication of the Metropolitan Technological University, published through Ediciones UTEM.

2. Mission. MMSB seeks to disseminate original and unpublished works that increase the knowledge and understanding of biological systems through mathematical modeling as the main tool of analysis. The subject areas included in the journal are:

- Population Dynamics
- Sustainability
- Biodiversity
- Epidemiology
- Non-infectious diseases
- Biotechnology
- Biomaterials
- Neuroscience
- Genetics
- Physiology
- Cell biololog
- Among other topics of biological origin that can be modeled and studied mathematically.

3. Vision. MMSM promotes access to knowledge in a democratic and non-profit manner, therefore the journal does not charge authors for publication or access charges for readers, nor does it restrict the free circulation of its articles (however, the source must always be correctly referenced).

In addition, it seeks to value the scientific research produced in Latin America and the Caribbean, offering a showcase for the work of young researchers in the region, without prejudice to the fact that it is a publication available to researchers from all over the world and of all ages.

4. MMSB will publish an annual volume, with three issues per volume, with a publication date in April, August and December of each year.

MMSB will also publish special volumes that can be dedicated to a specific topic or linked to a scientific event.

5. Language scope: Spanish-English.

6. Publication policy and access to content. MMSB has an open access policy, under the principle of free availability, to research products for the general public.

Under the Creative Commons Attribution 4.0 International License.

7. For authors. it is authorized to establish a copy in institutional or personal repositories, preprint or postprint, as long as the source or institutional site where they were originally published is cited.

8. For readers. the total or partial reproduction of the texts published here is authorized as long as the authorship and full source are duly cited, as well as the electronic address of the publication.

9. The opinions expressed by the authors do not necessarily reflect the position of the publisher, the journal or the Universidad Tecnológica Metropolitana (UTEM).

10. Code of Ethics. the Journal adheres to the Code of the Committee on Publication Ethics (COPE) to discuss and or sanction all matters related to ethical aspects of the publication. See: COPE Principles of Transparency and Best Practices in Academic Publications, available at: <https://doi.org/10.24318/cope.2019.1.13>

11. Code of Ethics. Detection or prevention of plagiarism. MMSB uses the University's plagiarism detection system (UTEM) (see <https://www.urkund.com/es/>), in order to safeguard the relevance or originality of the content to be published.

Tabla de contenidos

CÓDIGO	AUTOR(ES)	INSTITUCIÓN	PAÍS	TÍTULO																									
Presentation	Diomar Cristina Mistro	Federal University of Santa Maria	BRASIL	Current trends and perspectives in mathematical biology																									
	Luiz Alberto Díaz Rodrigues					Frank M. Hilker	Universität Osnabrück	ALEMANIA		Pedro Cenci Dal Castel	Indiana University	ESTADOS UNIDOS	e23E00	Luiz Alberto Díaz Rodrigues	Universidade Federal de Santa Maria	BRASIL	Diomar Cristina Mistro	Guilherme S. Y. Giardini	Universidade Federal do Rio Grande do Sul	BRASIL	Marcelo Rossato	Universidade Estadual de Campinas	BRASIL	Philip K. Maini	University of Oxford	REINO UNIDO	e23E01	Joice Chaves Marques	Universidade Federal do Rio Grande
	Frank M. Hilker	Universität Osnabrück	ALEMANIA																										
	Pedro Cenci Dal Castel	Indiana University	ESTADOS UNIDOS																										
e23E00	Luiz Alberto Díaz Rodrigues	Universidade Federal de Santa Maria	BRASIL																										
	Diomar Cristina Mistro				Guilherme S. Y. Giardini	Universidade Federal do Rio Grande do Sul	BRASIL	Marcelo Rossato	Universidade Estadual de Campinas	BRASIL	Philip K. Maini	University of Oxford		REINO UNIDO	e23E01	Joice Chaves Marques	Universidade Federal do Rio Grande	BRASIL	Some effects of population interaction on a multi-population SIRC epidemiological model	Adriano De Cezaro									
	Guilherme S. Y. Giardini	Universidade Federal do Rio Grande do Sul	BRASIL																										
	Marcelo Rossato	Universidade Estadual de Campinas	BRASIL																										
	Philip K. Maini	University of Oxford	REINO UNIDO																										
e23E01	Joice Chaves Marques	Universidade Federal do Rio Grande	BRASIL		Some effects of population interaction on a multi-population SIRC epidemiological model																								
	Adriano De Cezaro																												

CÓDIGO	AUTOR(ES)	INSTITUCIÓN	PAÍS	TÍTULO
e23E02	Lisandra Pitol	Universidade Federal de Pelotas	BRASIL	Modelamiento Matemático de la Fiebre Amarilla: un modelo con migración
	Luciana Rossato Piovesan			
	Fernanda Tumelero			
	Alexandre Sacco de Athayde			
	Régis Sperotto de Quadros			
	Daniela Buske			
	Glênio Aguiar Gonçalves			
e23E03	Poliana Kenderli Pacini Selau	Universidade Federal do Rio Grande do Sul	BRASIL	Pattern Formation in a Resource and Two Consumers Discrete Model
	Diomar Cristina Mistro Luiz Alberto Díaz Rodrigues	Universidade Federal de Santa Maria	BRASIL	
e23E04	Marcelo Cargnelutti Rossato João Frederico da Costa Azevedo Meyer	Universidade Estadual de Campinas	BRASIL	Spatial spread of an epidemic in the context of cellular automata
e23E05	Luciana Renata de Oliveira	Universidade Federal de Santa Maria	BRASIL	Using the Chemical Master Equation to model the interaction network of focal adhesion proteins
	Júlia Vitória Ribeiro			
	Alícia Groth Becker			
	Gabriel Vitorello			
	José Carlos Merino Mombach			

Presentation

**SPECIAL NUMBER V2N2 - MMSB
MATHEMATICAL BIOLOGY AT SPRINGTIME
IN 29S53W**

Diomar Cristina Mistro
Luiz Alberto Díaz Rodrigues

Presentation

This special issue consists of a collection of papers presented at the workshop “Mathematical Biology in Springtime at 29S53W” (MBS29S53W). The meeting took place in the spring 2022, in Santa Maria, which is located at the geographical coordinates 29S53W. It was part of the project “Cooperação Internacional Brasil-Alemanha em Ecologia Teórica” whose main goal is the internationalization of the post-graduation of Rio Grande do Sul. This project was supported by FAPERGS (Fundação de Amparo à Pesquisa do Estado do Rio Grande do Sul) -- a Rio Grande do Sul state foundation for supporting science and research. The COVID-19 pandemics delayed the workshop in one year and, for most participants, it was the first in-person meeting after two years of confinement and social distancing.

The MBS29S53W was aimed at undergraduate and graduate students with the main goals of offering students the opportunity to get to know the state of the art and new trends in Mathematical Biology, publicising the research produced in the Rio Grande do Sul, giving the Brazilian students the opportunity to attend high level talks and lectures, encouraging undergraduate and graduate students to pursue research and attracting new students to join the Mathematical Biology Group in Santa Maria.

The meeting offered plenary talks, short-courses, a round table and a poster section where the students presented their works. Philip Maini (University of Oxford), Frank Hilker (University of Osnabrück), Wilson Castro Ferreira Jr (University of Campinas) and Roberto Kraenkel (University of the State of São Paulo) were the in person speakers. Besides them, Frithjof Lutscher (University of Ottawa), Mirjam Kretzschmar (University of Utrecht) and Claudia Pio Ferreira (University of the State of São Paulo) gave online talks.

Philip Maini opened the workshop with the plenary talk “Modelling collective cell movement in development and disease”.

The second speaker was Claudia Pio Ferreira who gave the talk “Exploring the impact of temperature on the efficacy of replacing the wild *Aedes aegypti* population by Wolbachia-carrying one”. The online talk “Integrodifference equations for spatial spread and invasions” was given by Frithjof Lutscher while “Interplay between health related opinions, risk perception, and epidemic dynamics in infectious disease models” was the title of the talk of Mirjam Kretzschmar. Finally, Roberto Kraenkel finished the meeting with the talk “Challenges in modeling Covid-19 epidemics and lessons for the future”.

The event included two short-courses: “Elementary Mathematical Models in Biology: Ruminations on Art and Craft” and “Population dynamics in patches coupled by dispersal” taught by Wilson C. Ferreira Jr and Frank Hilker, respectively.

Philip Maini and Frank Hilker discussed with the audience about “Trends and Perspectives on Mathematical Biology” in a round-table mediated by Wilson Ferreira Jr. This discussion resulted in an opinion paper written by the two speakers and some of the participants who actively collaborated with the round table. Finally, there was a poster section where the students presented their work; five of them also compose this volume.

The opinion paper by Hilker et al. (2023) address the perspectives in mathematical biology. It discusses the biological topics in the main stream of mathematical modelling, some of the mathematical techniques currently in use and some educational aspects of mathematical biology.

The COVID-19 pandemics have brought new challenges and reinforced the importance of studying epidemiological models. Three papers of this issue analyse infectious diseases. The spatio-temporal dynamics of a SIRC-type diseases is investigated by Marques and De Cezaro (2023).

Pitol et al. (2023) analyse the effects of vaccination in a mathematical model for the Yellow Fever with migration.

The third paper on the epidemiology field considers an Automata Celular model to study the effects of confinement and vaccination on the spatial spread of the COVID-19 epidemics (Rossato and Meyer, 2023).

On a different subject, Oliveira et al. (2023) study the dynamic interactions between proteins in the focal adhesion by using the Chemical Master Equation.

Presentation

Finally, in Selau et al. (2023), the authors propose a Coupled Map Lattice model to analyse the spatio-temporal dynamics of a system of three interacting species: a resource species and two consumers.

Acknowledgments

We are grateful to the authors and the Scientific Committee who contributed to this special issue. We also acknowledge FAPERGS and the Federal University of Santa Maria for their support for the workshop, and all the workshop participants. Finally, our gratitude to the Revista MMSB for the opportunity to publish this special issue.

Presentación

NÚMERO ESPECIAL V2N2 - MMSB
MATHEMATICAL BIOLOGY AT SPRINGTIME
IN 29S53W

Diomar Cristina Mistro
Luiz Alberto Díaz Rodrigues

Este número especial consta de una colección de artículos presentados en el taller "Biología matemática en primavera en 29S53W" (MBS29S53W). El encuentro tuvo lugar en la primavera de 2022, en Santa María, que se encuentra en las coordenadas geográficas 29S53W. Formó parte del proyecto "Cooperação Internacional Brasil-Alemanha em Ecologia Teórica" cuyo principal objetivo es la internacionalización del posgrado de Rio Grande do Sul. Este proyecto fue apoyado por FAPERGS (Fundação de Amparo à Pesquisa do Estado do Rio Grande do Sul), una fundación estatal de Rio Grande do Sul para apoyar la ciencia y la investigación. La pandemia de COVID-19 retrasó el taller en un año y, para la mayoría de los participantes, fue el primer encuentro presencial después de dos años de confinamiento y distanciamiento social.

El MBS29S53W estuvo dirigido a estudiantes de pregrado y posgrado con los principales objetivos: ofrecer a los estudiantes la oportunidad de conocer el estado del arte y las nuevas tendencias en Biología Matemática, dar a conocer las investigaciones producidas en Rio Grande do Sul, brindar a los estudiantes brasileños la oportunidad de asistir a charlas y conferencias de alto nivel, incentivando a estudiantes de pregrado y posgrado a realizar investigaciones y atraer nuevos estudiantes para unirse al Grupo de Biología Matemática en Santa María.

El encuentro contó con charlas plenarias, cursos cortos, una mesa redonda y una sección de carteles donde los estudiantes presentaron sus trabajos. Philip Maini (Universidad de Oxford), Frank Hilker (Universidad de Osnabrück), Wilson Castro Ferreira Jr (Universidad de Campinas) y Roberto Kraenkel (Universidad del Estado de São Paulo) fueron los ponentes presenciales. Además de ellos, Frithjof Lutscher (Universidad de Ottawa), Mirjam Kretzschmar (Universidad de Utrecht) y Claudia Pio Ferreira (Universidad del Estado de São Paulo) impartieron charlas online.

Philip Maini inauguró el taller con la charla plenaria "Modelado del movimiento celular colectivo en el desarrollo y la enfermedad".

La segunda oradora fue Claudia Pio Ferreira quien dio la charla "Explorando el impacto de la temperatura en la eficacia de reemplazar la población silvestre de *Aedes aegypti* por una *Wolbachia* portadora". La charla online "Ecuaciones de integrodiferenciales para la propagación espacial y las invasiones" fue impartida por Frithjof Lutscher, mientras que "Interacción entre opiniones relacionadas con la salud, percepción de riesgo y dinámica epidémica en modelos de enfermedades infecciosas" fue el título de la charla de Mirjam Kretzschmar. Finalmente, Roberto Kraenkel finalizó el encuentro con la charla "Desafíos en el modelado de epidemias de Covid-19 y lecciones para el futuro".

El evento incluyó dos cursos cortos: "Modelos matemáticos elementales en biología: reflexiones sobre arte y artesanía" y "Dinámica de poblaciones en parches acoplados por dispersión" impartidos por Wilson C. Ferreira Jr y Frank Hilker, respectivamente.

Philip Maini y Frank Hilker discutieron con la audiencia sobre "Tendencias y perspectivas en biología matemática" en una mesa redonda mediada por Wilson Ferreira Jr. Esta discusión resultó en un documento de opinión escrito por los dos oradores y algunos de los integrantes del público que participaron activamente con la mesa redonda. Colaboró con la mesa redonda. Finalmente, hubo una sección de carteles donde los estudiantes presentaron sus trabajos; cinco de ellos también componen este volumen.

El artículo de opinión de Hilker et al. (2023) abordan las perspectivas en biología matemática. Analiza los temas biológicos en la corriente principal de modelado matemático, algunas de las técnicas matemáticas actualmente en uso y algunos aspectos educativos de la biología matemática.

La pandemia de COVID-19 ha traído nuevos desafíos y ha reforzado la importancia de estudiar modelos epidemiológicos. Tres artículos de este número analizan las enfermedades infecciosas. Marques y De Cezaro (2023) investigan la dinámica espacio-temporal de las enfermedades de tipo SIRC.

Pitol et al. (2023) analizan los efectos de la vacunación en un modelo matemático para la Fiebre Amarilla con la migración.

Presentación

El tercer artículo en el campo de la epidemiología considera un modelo de Autómata Celular para estudiar los efectos del confinamiento y la vacunación en la propagación espacial de las epidemias de COVID-19 (Rossato y Meyer, 2023).

En otro tema, Oliveira et al. (2023) estudian las interacciones dinámicas entre proteínas en la adhesión focal utilizando la Ecuación Maestra Química.

Finalmente, en Selau et al. (2023), los autores proponen un modelo de celosía de mapas acoplados para analizar la dinámica espacio-temporal de un sistema de tres especies que interactúan: una especie de recurso y dos consumidores.

Agradecimientos

Agradecemos a los autores y al Comité Científico que contribuyeron a este número especial. También agradecemos a la FAPERGS y a la Universidad Federal de Santa María por su apoyo al taller, y a todos los participantes del mismo. Finalmente, nuestro agradecimiento a la Revista MMSB por la oportunidad de publicar este número especial.

Opinion article

CURRENT TRENDS AND PERSPECTIVES IN MATHEMATICAL BIOLOGY

Authors:

Frank M. Hilker¹, Pedro Cenci Dal Castel², Luiz Alberto Díaz Rodrigues³, Guilherme S. Y. Giardini⁴, Diomar Cristina Mistro³, Marcelo Rossato⁵ and Philip K. Maini⁶

1. Institute of Mathematics, Institute of Environmental Systems Research, Osnabrück University, Osnabrück, Germany
2. Intelligent Systems Engineering Department, Indiana University Bloomington, USA
3. Department of Mathematics, Federal University of Santa Maria, Santa Maria, Brazil
4. Instituto de Física, Universidade Federal do Rio Grande do Sul, Porto Alegre, RS, Brazil
5. Institute of Mathematics, Statistics and Scientific Computing, State University of Campinas, Campinas, Brazil
6. Wolfson Centre for Mathematical Biology, Mathematical Institute, University of Oxford, Oxford, UK

ABSTRACT

This communication summarises a “round-table discussion” at a workshop held at the Federal University of Santa Maria, Brazil, on trends and perspectives in mathematical biology. Mathematical biology as a research field has seen many changes over the past few decades. Starting mostly from deterministic differential or difference equations, the mathematical techniques applied to biology have diversified to include stochastic processes, graph theory, topology, combinatorics and many other areas of mathematics. The complexity, heterogeneity and diversity of biological systems represent both challenges and opportunities in modelling. On the one hand, they require and nurture methodological innovations. On the other hand, they allow models to explain biological phenomena as emerging from multiple scales and to elucidate biological mechanisms, thoughts and concepts with the clarity of mathematics. All this makes mathematical biology an exciting and fruitful field. The present paper discusses (1) key biological topics to be addressed in mathematical modelling, (2) some of the mathematical techniques currently in use and the need for further methodological development, and (3) some issues in the training of the next generation of mathematical biologists.

RESUMEN

Esta comunicación resume una “mesa redonda” en un workshop celebrado en la Universidad Federal de Santa Maria, Brasil, sobre tendencias y perspectivas en biología matemática. La biología matemática como campo de investigación ha experimentado muchos cambios en las últimas décadas. Partiendo principalmente de ecuaciones diferenciales o en diferencias deterministas, las técnicas matemáticas aplicadas a la biología se han diversificado para incluir procesos estocásticos, teoría de grafos, topología, combinatoria y muchas otras áreas de las matemáticas. La complejidad, heterogeneidad y diversidad de los sistemas biológicos representan tanto desafíos como oportunidades en la modelización. Por un lado, requieren y fomentan innovaciones metodológicas. Por otro lado, permiten que los modelos expliquen fenómenos biológicos que emergen de múltiples escalas y dilucidan mecanismos, pensamientos y conceptos biológicos con la claridad de las matemáticas. Todo esto hace de la biología matemática un campo apasionante y fructífero. El presente artículo discute (1) temas biológicos clave que se abordarán en la modelización matemática, (2) algunas de las técnicas matemáticas actualmente en uso y la necesidad de un mayor desarrollo metodológico, y (3) algunas cuestiones en la capacitación de la próxima generación de biomatemáticos.

Introduction

The field of mathematical biology (here we will use the term “biology” in a very broad sense, incorporating medicine, ecology, epidemiology, etc.) has grown considerably over the past years from a research area practised by a few visionary pioneers to a well-established sub-field of mathematics that is now taught in most universities worldwide. The type of research done has also changed beyond all recognition (see, e.g., Levin et al., 1997; Cohen, 2004; May, 2004; Reed, 2004, 2015; Maini, 2023).

Mathematical modelling is very high on the radar now due to the COVID-19 pandemic. Epidemic modellers around the world have worked and continue to work on state-of-the-art models to predict the course of the pandemic, assess impact scenarios and compare exit strategies. At the beginning of the pandemic, knowledge about SARS-CoV-2 was virtually non-existent, which posed major challenges to modellers, public health officials, politicians and other decision-makers alike. With mathematical models and simulations playing a prominent role in the response to the pandemic, concepts like exponential growth, R values and herd immunity entered the discussions of the broader public, some modellers also

played an important role influencing public opinion. Thus, the field of mathematical modelling is acknowledged by society probably more than ever.

At the same time, biodiversity and ecosystems are in peril due to global change, which is occurring at unprecedented rates (e.g., Pereira et al., 2010). To make predictions in a changing world, process-based models are required. For mathematical biology these times are, therefore, as important as challenging, and this is further amplified by the availability of increasingly voluminous, varied and quickly processed data, by expanding computer power and by advents in computational algorithms.

This perspective, inspired by a “round-table” discussion at the workshop *Mathematical Biology in Springtime at 29S53W*,¹ aims to highlight three key aspects of the subject of mathematical biology going forward. First, we will put forward what we think are some key scientific topics to be addressed using mathematical modelling. Second, we will discuss some of the mathematical methods that are being used now and the extensions required. Third, we will focus on the type of training needed for young people coming into mathematical biology, as well as ways to keep expanding this field, which, although it has grown significantly, is still comparatively small when compared with other areas of science (cf. Reed, 2015).

TOPICS

As we indicated in the Introduction, the recent research activities in epidemiological modelling due to the COVID-19 pandemic are probably unparalleled in history. Yet, the pandemic proved challenging in many regards. For example, the epidemic curves looked rather different from what simple, off-the-shelf epidemic models predict. Many variables, including age structure, differences in susceptibility or heterogeneity in the exposure to the virus (often related to socio-economic factors) and individual behaviour regarding the adoption of protective measures impact the course of the pandemic. Modellers must take into account limited access to information, difficulties in model validation, uncertainties in measurements and fundamental model limitations, not only as good scientific practices, but also as important caveats when conveying model predictions and possible scenarios to the media and general public.²

The explosion in the interest in the field of epidemiological modelling also led to the integration of many researchers from adjacent fields keen to bring in their expertise. Dangerfield et al. (2023) describe how UK institutions coordinated many

research activities including Virtual Study Groups,³ Scientific Advisory Boards to government⁴ and Rapid Review Groups,⁵ which provided rapid assessments of the emerging research and assisted government advisory groups.⁶ A wide range of similar initiatives or modelling “hubs” emerged in many other countries as well (e.g. Reich et al., 2022).

More generally, consortia of research groups organised around a certain scientific problem can convey a multitude of benefits such as coordinating research activities, collecting and curating data, and leveraging research networks or software products. Such organised research networks allow rapid development of models in large numbers, which frees researchers from having to rely on a single model; a risky bet. With multiple models at hand, it is possible to compare outcomes under various scenarios from different standpoints, which helps to identify inconsistencies and convergences between models. This helps to either promote debate between research groups or build consensus and deliver collective assessments. Such model intercomparison projects have a long tradition in climatology (Cess et al., 1989) and are featured prominently in IPCC (Intergovernmental Panel on Climate Change) assessment reports (Coupled Model Intercomparison Project). Similar initiatives are underway for biodiversity research (Inter-Sectoral Impact Model Intercomparison Project) in the context of IPBES (Intergovernmental Science-Policy Platform on Biodiversity and Ecosystem Services).

Epidemic modelling is very likely to remain a topical issue, given the number of emerging infectious diseases in recent years (e.g., West Nile virus in 1999, SARS-CoV in 2003, H1N1 in 2009, MERS-CoV in 2012, Ebola in 2013, Zika in 2016) and increased cross-species transmissions due to global change.

The field of ecology is at the forefront of studying the consequences of the ongoing rapid global environmental change. According to IPBES (2019), the main direct drivers of biodiversity loss are land and sea use change, direct exploitation of organisms, climate change, pollution and invasive non-native species. They pose major damage, threats and risks to ecosystem functioning and services as well as production of vital goods (Millennium Ecosystem Assessment, 2005). There is increasing recognition of the existence of ecological regime shifts, in which ecosystems abruptly and irreversibly move from one state to another under supercritical forcing (Scheffer et al., 2001). The planetary boundary framework attempts to globally aggregate the anthropogenic impact on nine processes and relate them to sustainable environmental limits (Steffen et al., 2015). These processes are climate change, biogeochemical (nitrogen and phosphorus) flows,

land-system change, freshwater use, aerosol loading, ozone depletion, ocean acidification, loss of biosphere integrity, including functional and genetic biodiversity, and introduction of novel entities, such as toxic chemicals and plastics. With the increasing societal and political recognition of global change, ecological models are increasingly aiming at ‘anticipatory’ rather than ‘explanatory’ predictions (Mouquet et al., 2015; Houlahan et al., 2017; Maris et al., 2018). On the basis of theoretical and empirical advances, ecological models progressively incorporate biological mechanisms rather than relying solely on statistical descriptions (e.g. Urban et al., 2016; Pilowsky et al., 2022). Yet, there is still no consensus emerging regarding the drivers of species richness and ecosystem functioning (Loreau, 2010). When addressing questions about environmental change, models need the ability to project into novel, future conditions (Evans, 2012). This requires not only a solid mechanistic understanding (Mouquet et al., 2015), but also underlines the importance of model transferability, i.e., how well models generalise to new contexts (Houlahan et al., 2017; Yates et al., 2018).

In developmental biology, advances in image analysis and data collection are revealing the complexities underlying cell movement and spatial patterning. These, in turn, provide challenges to experimentalists and modellers alike, who aim to develop a mechanistic understanding of how processes acting across a vast range of spatial and temporal scales combine to produce the cell and tissue level behaviour that we see. Understanding developmental biology is not only of intrinsic scientific interest, it can also help us develop therapies for developmental diseases. For example, in early development, neural crest cells delaminate from the neural tube and migrate long distances before they differentiate into key tissues in the body. If this process does not occur properly, it can lead to developmental deformities (the so-called neurocristopathies, 66 of which have been identified) (Vega-Lopez et al., 2018). A full understanding of this collective migratory behaviour would allow us to understand the mechanisms and therefore suggest ways to combat developmental diseases. Moreover, these cells have many mechanisms in common with those of cancer cells, so an understanding of how these cells are controlled in normal development suggest novel therapies (e.g., Gallik et al., 2017).

The abstract nature of mathematics allows for ideas from one area of science to be translated to other areas. A striking example of this is the employment of mathematical modelling ideas developed in the context of ecology in cancer cell dynamics. Animal competition models, for example, the classical Lotka–Volterra model (originally proposed for chemical

reactions) are now being used in adaptive therapy. Here, the competitors are drug-sensitive and drug-resistant cells. The idea is that, rather than using a drug at the standard of care (maximum tolerated dose) that will kill off all the drug-sensitive cells, allowing the resistant cells to grow unbounded, using the drug more sparsely by having “drug-holidays”, maintaining the tumour at a controlled size, will allow the sensitive cells to compete with the resistant cells. In this setting, mathematical modelling is being used to test out different therapeutic strategies (see, for example, Strobl et al., 2021), and this is a place where ideas from reinforce deep learning can be employed to modify treatment in an ongoing way. Indeed, more generally, mathematical modelling is now being used to inform drug design and extrapolation from the laboratory to the clinic (see, for example, the review by Kondic et al., 2022).

To build models capable of simulating therapeutic interventions in human patients, different interconnected processes have to be taken into account. Infectious diseases and cancer are good examples of how processes in different systems and on different scales (for example, intracellular reactions, intercellular communication, cell migration, and potentially the metabolism in organs far from the tissue site) depend on each other and determine the outcome of the disease. Different approaches may be used to model each temporal and spatial scale, as well as different parts of the human body. Although model interfacing is becoming less challenging (e.g., Zhou, 2014), we lack a standard framework to couple, merge and switch models. A rigorous procedure for multiscale modelling would leverage the development of powerful simulations able to accurately test and calibrate therapeutic interventions in human patients.

Advances in computing power have led to “digital twin” technologies, where in many industries now computer simulations are used to predict how equipment will perform. A key question is, can this technology be used to develop human digital twins? This is an area of research that is now being pursued in many different areas of medicine (see, for example, Laubenbacher et al., 2022).

As data collecting technologies advance, we are now on the cusp of being able to fit models to data to acquire parameter values. This is now pushing the statistical frontiers of parameter estimation and identifiability (see, for example, Browning et al., 2020). Moreover, ideas from persistent homology are now being used to characterise spatial data (see, for example, McGuirol et al., 2020; Skaf and Laubenbacher, 2022).

MATHEMATICAL METHODS

Classical approaches in mathematical biology focus on low-dimensional and deterministic systems, ignoring the complexities of stochasticity and nonlinear dynamics. Traditional mathematical tools involve ordinary and partial differential equations as well as difference equations. Mathematical biology today goes beyond linear theory and standard nonlinear systems to highly complicated nonlinear systems. There are advances in coarse graining, relating fully nonlinear systems, and in approaches involving agent-based models, network and graph theory, boolean analysis, topological data analysis, statistics, probability theory and stochastic and branching processes, to mention a few. Mathematical biology is now both an inter- and intradisciplinary field.

Artificial intelligence (AI) and machine learning (ML) approaches are being increasingly used. It is worth noting that AI is based on biology (e.g., neural networks), so it is per se an example where biology and mathematics meet. ML models require large amounts of data; they base their predictions on going through databases of inputs and outputs of a given problem. Their results can be faster and more accurate compared to classical statistical methods. More challenging, however, is to gain understanding of the causal mechanisms. ML and mechanistic modelling are therefore often seen as different paradigms, but they can complement each other in their methodological strengths and weaknesses (Baker et al., 2018). The coupling of ML and mechanistic models into hybrid approaches provide major opportunities (Reichstein et al., 2019). Examples include improved model parameterisations or the emulation of computationally challenging process-based models by ML algorithms. Also, mechanistic “sub-models” with little theoretical support can be replaced by data-driven ML models; for example, in agent-based systems the decision-making of individual agents based on input from the environment can follow ML models (e.g., Zhang et al., 2021).

A digital twin is, as already indicated, a dynamic digital representation of a real-life system (e.g., cells, tissues, organs or even the natural environment) (Madni et al., 2019). With automatic data flow between the digital and biological object, this allows a real-time monitoring and prediction of systems, with applications especially in medicine and biotechnology. This is another example where multi-scale aspects are important. Relevant spatial scales can range from the molecular to the ecosystem level. Temporal scales can range from protein processes to the billions of years of evolution of life on Earth. At each level, collective dynamics emerge from the behaviour

of individual units. Despite considerable advances in multi-scale mathematical biology, our understanding of these phenomena is still far from complete (e.g., Eftimie, 2022).

The dynamical systems traditionally studied in mathematical biology are usually autonomous and smooth. However, non-smooth dynamical systems become prevalent in the presence of management actions or policy instruments. For instance, pest control programs are triggered beyond certain economic injury levels, harvest moratoria come into place when the harvested population size drops below a critical level or the use of pesticides, fertilisers or irrigation may be forbidden if environmental indicators become flagged. Non-smooth dynamical systems can be considerably more complex in their dynamics than smooth ones. Consider, for example, the transition from regular dynamics to chaos when varying a system parameter in a certain direction. In smooth systems, this transition generally occurs in a sequence of bifurcations, often called a route to chaos (e.g. Anishchenko et al., 2014). In non-smooth systems, by contrast, this transition can take place in a single bifurcation (di Bernardo et al., 2008; Avrutin et al., 2019). Such bifurcations can give rise to dynamical structures entirely different from the ones in smooth systems.

Non autonomous systems occur when there is periodic forcing (e.g., parameters influenced by seasons or circadian rhythms) or a change in environmental conditions such as temperature or precipitation. The latter is often modelled in the form of parameters that evolve or are ramped in a linear or accelerating trend. Just like seasonal forcing can induce complex dynamics, simple trends in parameters due to a changing world can cause rate-induced critical transitions or track system states that are unstable in a constant environment (e.g., Siteur et al., 2016; Vanselow et al., 2019; Arumugam et al., 2021).

When studying the human impact on biological systems, the human influence is often encapsulated in the form of a simple parameter (e.g., a harvest rate or the average vaccination coverage in a population). Conversely, in many socio-economic studies dealing with biological systems, the latter are often simplified to almost static objects (see also Shin et al., 2022). For a full account of the mutual feedbacks between the biological and socio-economic domains, however, one has to take into account the coupled dynamics. This requires connecting biological dynamics with human and social sciences, for which sociology, economics, behavioural psychology, law and other areas come into play. Mathematical methods that can be used in this context include, for example,

evolutionary and differential games, agent-based models and optimal control. Of course, they also deal with different time scales (e.g., slow-fast systems, singular perturbation analysis) and spatial variation (e.g., reaction-diffusion or integrodifferential equations, nonlocal effects), to mention some of the complexities involved. Such coupled social-ecological systems are fascinating in their own right (e.g., Levin et al., 2013; Galvani et al., 2016). They also play an increasing role in behavioural epidemiology. Individual decision-making, social learning and the spread of (mis-)information are key factors in the adoption of preventive measures such as vaccination, social distancing and face masks. Consequently, the spread of infection and the success of public health programmes are affected by individual behaviour (see the reviews by Funk et al., 2010; Chang et al., 2020).

EDUCATION AND TRAINING

Mathematical biology will have a bright future with new generations of scientists that have expertise in both mathematics and biology, i.e., “empiricists with stronger quantitative skills” and “theoreticians with an appreciation for the empirical structure of biological processes” (Hastings and Palmer, 2003). Universities, however, are built on disciplines. Yet, many of the most exciting areas in science are interdisciplinary. How do we overcome the barriers between disciplines and, indeed, within disciplines (intra-disciplinary)? One way to achieve this in graduate education are Centres for Doctoral Training. These are externally funded PhD programmes at universities in the UK and they have been designed to strategically increase a university’s capacity in interdisciplinary research, especially at the interfaces between traditionally organised departments. Similarly, Research Training Groups funded by the German Research Foundation promote innovative and often interdisciplinary PhD programmes at German universities. These and other externally funded initiatives have proven to stimulate lasting changes in university structures.

Such interdisciplinary programmes also promote students in learning the “language” of the other discipline, while being anchored in a home discipline. There will always be some concern about juggling interdisciplinary breadth and intradisciplinary depth. This is something for which tailored solutions can be found in individual development plans⁷, enlisting the supervisor(s)’ experience and depending on the nature of the research project and the student’s needs.

In mathematical biology education more generally, there has been an enormous spectrum of initiatives and considerable changes in the past 1-2 decades. An impressive collection of

these changes are summarised in the review by Jungck et al. (2020). Many, if not most, major research universities now have courses on mathematical biology; some universities even offer degree programmes in this area. However, the majority of universities probably still lack critical mass to offer courses or projects in mathematical biology that build upon each other and could thus reinforce learning. Furthermore, existing courses in mathematical biology are often inaccessible to students who have not yet completed the classical prerequisite courses, e.g., in linear algebra and (multivariable) calculus. A course design with such prerequisites can be an impediment to attract interested students from nearby disciplines (cf. Miller and Alben, 2012).

A major “asset” of mathematical biology is the high motivation of students to learn about applications of mathematics in biology, i.e., in living systems to which they can intuitively relate. Reed (2015, p. 1175) writes:

“Most people acknowledge the traditional important applications of mathematics to physics, from the motions of the planets to quantum mechanics, nuclear fission and the bomb, and fluid flow over airplane wings. Unfortunately, most people just aren’t very interested in physics (Voltaire had it right), so they acknowledge the importance but aren’t that moved. How about the applications of number theory to cryptography? Again, everyone sees that it is important to have secure communications, but they’re not very interested in how it gets done. Leave it to the geeks! But biology is a different story. Everyone is interested in his or her own body and how it works. Everyone wants to be free of disease and live a long time. Everyone (well almost everyone) knows that we’d better be good stewards of our ecosystems or we and our children are doomed. So, when you tell them how mathematics is contributing, they are really interested. And this has the potential, in the long run, to greatly improve the public perception of mathematics.”

To get prospective students (and also the general public) more interested in mathematics and its applications, there are a host of outreach activities. For example, universities or departments organise Open Days, where students and lecturers show how much fun mathematics is and for what it can be “used”. In some countries, including the UK, there is an established tradition of TV programmes with researchers or educators explaining science. More recently, children increasingly use social media platforms to complement their learning with short video tutorials, some of which point out modern applications of mathematics. To reach out to school

teachers, Seshaiyer and Lenhart (2020) describe a number of modelling activities, in which teachers have engaged via professional development programmes and which they have incorporated in the classroom. For undergraduate students, there are offers of summer research opportunities, internships, workshops or bursaries, which often motivate them to pursue mathematical biology in their graduate studies (e.g. de Vries and Hillen, 2008). Undergraduate research experience programmes have also been run by the Mathematical Biosciences Institute and the National Institute for Mathematical and Biological Synthesis. Both institutes have, more broadly, actively supported mathematical biology through workshops, working groups, visitor programmes, fellowships, education and outreach programmes. Synthesis centres have emerged in the past two decades and created community-oriented research infrastructure (Baron et al., 2017).

CONCLUSIONS AND OUTLOOK

As a scientist, it is hard enough to be an expert in one area. To be an expert in two areas is very difficult. So a key aspect is being able to communicate with researchers in other disciplines. This implies having enough knowledge to understand what scientists in other disciplines are talking about. Another key aspect is being able to communicate within your own discipline. For instance, there are so many areas of mathematics coming together in biology now (e.g., from dynamical systems over networks to group theory) that it is impossible to be an expert in all of these areas. Similarly, biology itself is so diverse that its research fields are fragmented (cf. Reed, 2004). Mathematical biologists therefore need both intra- and interdisciplinary competencies.

Considering all the changes in mathematical biology that happened over the last 40 or so years, it is difficult to predict where the field will be in 10-20 years' time. What seems clear is that, on the one hand, biology continues to provide hard challenges for mathematics because of the multiple temporal and spatial scales, the heterogeneity of individuals and evolutionary dynamics. In addition, the enormous data streams in all areas of biology, as well as the pace at which computational predictions grow faster than our understanding of biological systems, will require new mathematical developments. On the other hand, there has been a tighter integration of mathematical biology with experiments over the past years. This can be seen, for example, in the growing number of examples where mathematicians are integrated into clinics and biological departments. At the same time, the progress in biology increasingly requires researchers to use quantitative skills. Biology is becoming so sophisticated

that researchers essentially cannot escape computation and advanced mathematics. Many biology journals nowadays require theory and modelling in addition to data. And they sometimes even feature mathematical approaches as cover articles—something unheard of a while back.

Progress in biology will depend on our ability to formulate theories, for which mathematics provides the quintessential clarity (Cohen, 2004; May, 2004). Therefore, “simple” theoretical models⁸ also continue to be relevant when they capture the mechanistic essence of a complex system, improve our understanding of biological phenomena, and provide novel insights or suggest new experiments (e.g., Segel and Edelman-Keshet, 2013). They can influence the way we understand biological systems and also have an impact on decision-making and management (e.g., DeAngelis et al., 2021).

ACKNOWLEDGMENTS

We are grateful to Roberto A. Kraenkel, Luciana de Oliveira, José Monbach and the workshop participants for the discussion, which was moderated by Wilson Castro Ferreira Junior. The workshop, in which the round-table discussion took place, is part of the project of internationalisation of the post-graduation of Rio Grande do Sul “Cooperação Internacional Brasil–Alemanha em Ecologia Teórica” coordinated by the Biomathematics Group from the Federal University of Santa Maria and supported by FAPERGS.

1. Held at the Federal University of Santa Maria in Santa Maria, RS, Brazil, from October 5–7, 2022.
2. Corner et al. (2015) provide an illustrated handbook with twelve practical principles for the communication about climate change uncertainties.
3. As part of the Virtual Forum for Knowledge Exchange in the Mathematical Sciences (V-KEMS), convened by the International Centre for Mathematical Sciences, Isaac Newton Institute, Newton Gateway to Mathematics and the Knowledge Transfer Network working with various representatives from the mathematical sciences community.
4. E.g., the Scientific Pandemic Influenza Group for Modelling in operational mode (SPI-M-O) became a formal subgroup of the Scientific Advisory Group for Emergencies (SAGE).
5. Established by the Royal Society's Rapid Assistance in Modelling the Pandemic initiative.

6. Recall the almost overwhelming rate of posting of new preprints during the course of the pandemic.
7. Individual development plans are mutual agreements between a graduate student and the supervisor(s). They are intended to identify needs in training, resources or research infrastructure. They clarify responsibilities of both student and supervisor(s), and are thought to improve orientation and transparency in the student's qualification process.
8. Sometimes also called generic, strategic or stylized models; see Evans et al. (2013) and references therein for terminology.

REFERENCES

- [1] Anishchenko, V. S., Vadivasova, T. E., and Strelkova, G. I. (2014). *Deterministic Nonlinear Systems: A Short Course*. Springer, Cham.
- [2] Arumugam, R., Lutscher, F., and Guichard, F. (2021). "Tracking unstable states: ecosystem dynamics in a changing world". *Oikos*, 130:525–540.
- [3] Avrutin, V., Gardini, L., Sushko, I., and Tramontana, F. (2019). *Continuous and Discontinuous Piecewise-Smooth One-Dimensional Maps*. World Scientific, Singapore.
- [4] Baker, R. E., , J.-M. P., Jayamohan, J. and Jérusalem, A. (2018). "Mechanistic models versus machinelearning, a fight worth fighting for the biological community?" *Biology Letters*, 14:20170660.
- [5] Baron, J. S., Specht, A., Garnier, E., Bishop, P., Campbell, C. A., Davis, F. W., Fady, B., Field, D., Gross, L. J., Guru, S. M., Halpern, B. S., Hampton, S. E., Leavitt, P. R., Meagher, T. R., Ometto, J., Parker, J. N., Price, R., Rawson, C. H., Rodrigo, A., Sheble, L. A., and Winter, M. (2017). "Synthesis centers as critical research infrastructure". *BioScience*, 67:750–759.
- [6] Browning, A. P., Warne, D. J., Burrage, K., Baker, R. E., and Simpson, M. J. (2020). "Identifiability analysis for stochastic differential equation models in systems biology". *Journal of The Royal Society Interface*, 17:20200652.
- [7] Cess, R. D., Potter, G. L., Blanchet, J. P., Boer, G. J., Ghan, S. J., Kiehl, J. T., Le Treut, H., Li, Z.-X., Liang, X.-Z., Mitchell, J. F. B., Morcrette, J.-J., Randall, D. A., Riches, M. R., Roeckner, E., Schlese, U., Slingo, A., Taylor, K. E., Washington, W. M., Wetherald, R. T., and Yagai, I. (1989). "Interpretation of cloud-climate feedback as produced by 14 atmospheric general circulation models". *Science*, 245:513–516.
- [8] Chang, S. L., Piraveenan, M., Pattison, P., and Prokopenko, M. (2020). "Game theoretic modelling of infectious disease dynamics and intervention methods: a review". *Journal of Biological Dynamics*, 14:57–89.
- [9] Cohen, J. E. (2004). "Mathematics is biology's next microscope, only better; biology is mathematics' next physics, only better". *PLoS Biology*, 2:e439.
- [10] Corner, A., Lewandowsky, S., Phillips, M., and Roberts, O. (2015). *The Uncertainty Handbook*. University of Bristol, Bristol.
- [11] Dangerfield, C. E., David Abrahams, I., Budd, C., Butchers, M., Cates, M. E., Champneys, A. R., Currie, C. S., Enright, J., Gog, J. R., Goriely, A., Déirdre Hollings-worth, T., Hoyle, R. B., INI Professional Services, Isham, V., Jordan, J., Kaouri, M. H., Kavoussanakis, K., Leeks, J., Maini, P. K., Marr, C., Merritt, C., Mollison, D., Ray, S., Thompson, R. N., Wakefield, A., and Wasley, D. (2023). "Getting the most out of maths: How to coordinate mathematical modelling research to support a pandemic, lessons learnt from three initiatives that were part of the COVID-19 response in the UK". *Journal of Theoretical Biology*, 557:111332.
- [12] de Vries, G. and Hillen, T. (2008). "Teaching mathematical biology in a summer school for undergraduates". In: Deutsch, A., Bravo de la Parra, R., de Boer, R. J., Diekmann, O., Jagers, P., Kisdi, E., Kretzschmar, M., Lansky, P., and Metz, H., editors, *Mathematical Modeling of Biological Systems, Volume II. Modeling and Simulation in Science, Engineering and Technology*, pages 369–377. Birkhäuser, Boston, MA.
- [13] DeAngelis, D. L., Franco, D., Hastings, A., Hilker, F. M., Lenhart, S., Lutscher, F., Petrovskaya, N. and Tyson, R. (2021). "Towards building a sustainable future: Positioning ecological modelling for impact in ecosystems management". *Bulletin of Mathematical Biology*, 83:107.
- [14] di Bernardo, M., Budd, C. J., Champneys, A. R., and Kowalczyk, P. (2008). *Piecewise-Smooth Dynamical Systems*. Springer, London.
- [15] Eftimie, R. (2022). "Grand challenges in mathematical biology: Integrating multi-scale modeling and data". *Frontiers in Applied Mathematics and Statistics*, 8:1010622.

- [16] Evans, M. R. (2012). “Modelling ecological systems in a changing world”. *Philosophical Transactions of the Royal Society B: Biological Sciences*, 367:181–190.
- [17] Evans, M. R., Grimm, V., Johst, K., Knuuttila, T., Langhe, R., Lessells, C. M., Merz, M., O’Malley, M. A., Orzack, S. H., Weisberg, M., Wilkinson, D. J., Wolkenhauer, O., and G. Benton, T. (2013). “Do simple models lead to generality in ecology?” *Trends in Ecology & Evolution*, 28:578–583.
- [18] Funk, S., Salathé, M., and Jansen, V. A. A. (2010). “Modelling the influence of human behaviour on the spread of infectious diseases: a review”. *Journal of the Royal Society Interface*, 7:1247–1256.
- [19] Gallik, K. L., Treffy, R. W., Nacke, L. M., Ahsan, K., Rocha, M., Grren-Saxena, A., and Saxena, A. (2017). “Neural crest and cancer: Divergent travelers on similar paths”. *Mechanisms of Development*, 148:89–99.
- [20] Galvani, A. P., Bauch, C. T., Anand, M., Singer, B. H., and Levin, S. A. (2016). “Human–environment interactions in population and ecosystem health”. *Proceedings of the National Academy of Sciences*, 113:14502–14506.
- [21] Hastings, A. and Palmer, M. A. (2003). “A bright future for biologists and mathematicians?” *Science*, 299:2003–2004.
- [22] Houlahan, J. E., McKinney, S. T., Anderson, T. M., and McGill, B. J. (2017). “The priority of prediction in ecological understanding”. *Oikos*, 126:1–7.
- [23] IPBES (2019). Global assessment report on biodiversity and ecosystem services of the Intergovernmental Science-Policy Platform on Biodiversity and Ecosystem Services. IPBES secretariat, Bonn, Germany.
- [24] Jungck, J. R., Robeva, R., and Gross, L. J. (2020). “Mathematical biology education: Changes, communities, connections, and challenges”. *Bulletin of Mathematical Biology*, 82:117.
- [25] Kondic, A., Bottino, D., Harrold, J., Kearns, J. D., Musante, C., Odinecs, A., Ramanujan, S., Selimkhanov, J., and Schoeberl, B. (2022). “Navigating between right, wrong, and relevant: The use of mathematical modeling in preclinical decision making”. *Frontiers in Pharmacology*, 13:860881.
- [26] Laubenbacher, R., Niarakis, A., Helikar, T., An, G., Shapiro, B., Malik-Sheriff, R. S., Sego, T. J., Knapp, A., Macklin, P., and Glazier, J. A. (2022). “Building digital twins of the human immune system: toward a roadmap”. *npj Digital Medicine*, 5:64.
- [27] Levin, S., Xepapadeas, T., Crépin, A.-S., Norberg, J., de Zeeuw, A., Folke, C., Hughes, T., Arrow, K., Barrett, S., Daily, G., Ehrlich, P., Kautsky, N., Mäler, K.-G., Polasky, S., Troell, M., Vincent, J., and Walker, B. (2013). “Social-ecological systems as complex adaptive systems: modeling and policy implications”. *Environment and Development Economics*, 19:111–132.
- [28] Levin, S. A., Grenfell, B., Hastings, A., and Perelson, A. S. (1997). “Mathematical and computational challenges in population biology and ecosystems science”. *Science*, 275:334–343.
- [29] Loreau, M. (2010). “Linking biodiversity and ecosystems: towards a unifying ecological theory”. *Philosophical Transactions of the Royal Society B: Biological Sciences*, 365:49–60.
- [30] Madni, A. M., Madni, C. C., and Lucero, S. D. (2019). “Leveraging digital twin technology in modelbased systems engineering”. *Systems*, 7:7.
- [31] Maini, P. K. (2023). “Mathematical biology: Looking back and going forward”. In: Morel, J.-M. and Teissier, B., editors, *Mathematics Going Forward*, pages 413–416. Springer, Cham.
- [32] Maris, V., Huneman, P., Coreau, A., Kéfi, S., Pradel, R., and Devictor, V. (2018). “Prediction in ecology: promises, obstacles and clarifications”. *Oikos*, 127:171–183.
- [33] May, R. M. (2004). “Uses and abuses of mathematics in biology”. *Science*, 303:790–793.
- [34] McGuirl, M. R., Volkening, A., and Sandstede, B. (2020). “Topological data analysis of zebrafish patterns”. *Proceedings of the National Academy of Sciences*, 117:5113–5124.
- [35] Millennium Ecosystem Assessment (2005). *Ecosystems and Human Well-being: Synthesis*. Island Press, Washington, DC.
- [36] Miller, L. A. and Alben, S. (2012). “Interfacing mathematics and biology: a discussion on training, research, collaboration, and funding”. *Integrative and Comparative Biology*, 52:616–621.

- [37] Mouquet, N., Lagadeuc, Y., Devictor, V., Doyen, L., Duputié, A., Eveillard, D., Faure, D., Garnier, E., Gimenez, O., Huneman, P., Jabot, F., Jarne, P., Joly, D., Julliard, R., Kéfi, S., Kergoat, G. J., Lavorel, S., Le Gall, L., Meslin, L., Morand, S., Morin, X., Morlon, H., Pinay, G., Pradel, R., Schurr, F. M., Thuiller, W., and Loreau, M. (2015). “Predictive ecology in a changing world”. *Journal of Applied Ecology*, 52:1293–1310.
- [38] Pereira, H. M., Leadley, P. W., Proença, V., Alkemade, R., Scharlemann, J. P. W., Fernandez-Manjarrés, J. F., Araújo, M. B., Balvanera, P., Biggs, R., Cheung, W. W. L., Chini, L., Cooper, H. D., Gilman, E. L., Guénette, S., Hurtt, G. C., Huntington, H. P., Mace, G. M., Oberdorff, T., Revenga, C., Rodrigues, P., Scholes, R. J., Sumaila, U. R., and Walpole, M. (2010). “Scenarios for global biodiversity in the 21st century”. *Science*, 330:1496–1501.
- [39] Pilowsky, J. A., Colwell, R. K., Rahbek, C., and Fordham, D. A. (2022). “Process-explicit models reveal the structure and dynamics of biodiversity patterns”. *Science Advances*, 8:eabj2271.
- [40] Reed, M. C. (2004). “Why mathematical biology is so hard?” *Notices of the AMS*, 51:338–342.
- [41] Reed, M. C. (2015). “Mathematical biology is good for mathematics”. *Notices of the AMS*, 62:1172–1176.
- [42] Reich, N. G., Lessler, J., Funk, S., Viboud, C., Vespignani, A., Tibshirani, R. J., Shea, K., Schienle, M., Runge, M. C., Rosenfeld, R., Ray, E. L., Niehus, R., Johnson, H. C., Johansson, M. A., Hochheiser, H., Gardner, L., Bracher, J., Borchering, R. K., and Biggerstaff, M. (2022). “Collaborative hubs: Making the most of predictive epidemic modeling”. *American Journal of Public Health*, 112:839–842.
- [43] Reichstein, M., Camps-Valls, G., Stevens, B., Jung, M., Denzler, J., Carvalhais, N., and Prabhat (2019). “Deep learning and process understanding for data-driven Earth system science”. *Nature*, 566:195–204.
- [44] Scheffer, M., Carpenter, S., Foley, J. A., Folke, C., and Walker, B. (2001). “Catastrophic shifts in ecosystems”. *Nature*, 413:591–596.
- [45] Segel, L. A. and Edelstein-Keshet, L. (2013). *A Primer on Mathematical Models in Biology*. Society for Industrial and Applied Mathematics, Philadelphia, PA.
- [46] Seshaiyer, P. and Lenhart, S. (2020). “Connecting with teachers through modeling in mathematical biology”. *Bulletin of Mathematical Biology*, 82:98.
- [47] Shin, Y. A., Lacasse, K., Gross, L. J., and Beckage, B. (2022). “How coupled is coupled human-natural systems research?” *Ecology & Society*, 27:4.
- [48] Siteur, K., Eppinga, M. B., Doelman, A., Siero, E., and Rietkerk, M. (2016). “Ecosystems off track: rate induced critical transitions in ecological models”. *Oikos*, 125:1689–1699.
- [49] Skaf, Y. and Laubenbacher, R. (2022). “Topological data analysis in biomedicine: A review”. *Journal of Biomedical Informatics*, 130:104082.
- [50] Steffen, W., Richardson, K., Rockström, J., Cornell, S. E., Fetzer, I., Bennett, E. M., Biggs, R., Carpenter, S. R., de Vries, W., de Wit, C. A., Folke, C., Gerten, D., Heinke, J., Mace, G. M., Persson, L. M., Ramanathan, V., Reyers, B., and Sörlin, S. (2015). “Planetary boundaries: Guiding human development on a changing planet”. *Science*, 347:736.
- [51] Strobl, M. A., West, J., Viosat, Y., Damaghi, M., Robertson-Tessi, M., Brown, J. S., Gatenby, R. A., Maini, P. K., and Anderson, A. R. (2021). “Turnover modulates the need for a cost of resistance in adaptive therapy”. *Cancer Research*, 81(1135-1147).
- [52] Urban, M. C., Bocedi, G., Hendry, A. P., Mihoub, J.-B., Pe’er, G., Singer, A., Bridle, J. R., Crozier, L. G., De Meester, L., Godsoe, W., Gonzalez, A., Hellmann, J. J., Holt, R. D., Huth, A., Johst, K., Krug, C. B., Leadley, P. W., Palmer, S. C. F., Pantel, J. H., Schmitz, A., Zollner, P. A., and Travis, J. M. J. (2016). “Improving the forecast for biodiversity under climate change”. *Science*, 353:aad8466.
- [53] Vanselow, A., Wiczorek, S., and Feudel, U. (2019). “When very slow is too fast - collapse of a predator-prey system”. *Journal of Theoretical Biology*, 479:64–72.
- [54] Vega-Lopez, G. A., Cerrizuela, S., Tribulo, C., and Aybar, M. J. (2018). “Neurocristopathies: New insights 150 years after the neural crest discovery”. *Developmental Biology*, 444:S110–S143.
- [55] Yates, K. L., Bouchet, P. J., Caley, M. J., Mengersen, K., Randin, C. F., Parnell, S., Fielding, A. H., Bamford, A. J., Ban, S., Barbosa, A. M., Dormann, C. F., Elith, J., Embling,



C. B., Ervin, G. N., Fisher, R., Gould, S., Graf, R. F., Gregr, E. J., Halpin, P. N., Heikkinen, R. K., Heinänen, S., Jones, A. R., Krishnakumar, P. K., Lauria, V., Lozano-Montes, H., Mannocci, L., Mellin, C., Mesgaran, M. B., Moreno-Amat, E., Mormede, S., Novaczek, E., Opper, S., Ortuño Crespo, G., Peterson, A. T., Rapacciuolo, G., Roberts, J. J., Ross, R. E., Scales, K. L., Schoeman, D., Snelgrove, P., Sundblad, G., Thuiller, W., Torres, L. G., Verbruggen, H., Wang, L., Wenger, S., Whittingham, M. J., Zharikov, Y., Zurell, D., and Sequeira, A. M. (2018). “Outstanding challenges in the transferability of ecological models”. *Trends in Ecology & Evolution*, 33:790–802.

[56] Zhang, K., Yang, Z., and Başar, T. (2021). “Multiagent reinforcement learning: A selective overview of theories and algorithms”. In: Vamvoudakis, K. G., Wan, Y., Lewis, F. L., and Cansever, D., editors, *Handbook of Reinforcement Learning and Control*, pages 321–384. Springer, Cham.

[57] Zhou, H.-X. (2014). “Theoretical frameworks for multiscale modeling and simulation”. *Current Opinion in Structural Biology*, 25:67–76.

Some effects of population interaction on a multi-population SIRC epidemiological model

Algunos efectos de la interacción poblacional en un modelo epidemiológico SIRC multipoblacional

 Joice Chaves Marques¹ and  Adriano De Cezaro¹,

✉ Joice Chaves Marques: joicec.marques@hotmail.com

¹ Instituto de Matemática, Estatística e Física,
Universidade Federal do Rio Grande
Rio Grande, Brazil

Recepción: 2023-04-05 | Aceptación: 2023-07-30 | Publicación: 2023-10-29

Recommended Citation: Chaves Marques, J *et al.* (2023). 'Some effects of population interaction on a multi-population SIRC epidemiological model'. Rev. model. mat. sist. biol. 3(E), e23E01, doi:10.58560/rmmsb.v03.n02.023.01



This open access article is licensed under a Creative Commons Attribution International (CC BY 4.0) <http://creativecommons.org/licenses/by/4.0/>.
Support:

ABSTRACT

In this work, we analyze the spread of an infectious disease in a not necessarily homogeneous multipopulation that interacts and is distributed in a discrete two-dimensional lattice (network) that acquires only partial immunity to the circulating stain. We use the solution properties of the proposed model to motivate the effects of including space in the dynamics. We show that the dynamics is largely influenced by the topology of the interactions between the different populations. The theoretical results are investigated numerically.

Keywords:

Partial immunity, Multi-Population SIRC, Spatially distributed, Coupled Map Lattice (CML)

RESUMEN

En este trabajo analizamos la propagación de una enfermedad en una multipoblación no necesariamente homogénea que interactúa y se distribuye en una red discreta bidimensional que adquiere solo inmunidad parcial a la mancha circulante. Usamos las propiedades de solución del modelo propuesto para motivar los efectos de incluir el espacio en la dinámica. Mostramos que la dinámica está influenciada en gran medida por la topología de las interacciones entre las diferentes poblaciones. Los resultados teóricos se investigan numéricamente.

Palabras Claves:

Inmunidad parcial, SIRC multipoblación, Distribución espacial, Red de mapas vinculados

2020 AMS Mathematics Subject Classification: Primary: 92B05; Secondary: 92D30, 92C42

1 INTRODUCTION

Infectious diseases are caused by infectious agents or pathogens, such as bacteria, viruses, and fungi, which make their host sick. Most of these pathogens can undergo genetic mutations, known as variants or mutating strains, that increase their spread power, resistance, or pathogenicity (ability to cause symptoms), virulence (intensity of host harm), and risk to the human population, see, for example, Hethcote (2000); Casagrandi *et al.* (2006) and references therein.

The emergence of such mutating strains makes it possible for contagion to occur again even if the host has already had contact with the virus, as the immune system does not recognize these variants. In this situation, the host acquires only temporary immunity, also known as cross-immunity, e.g. Casagrandi *et al.* (2006). Infectious diseases with the ability to mutate strains include the Influenza-type and the Sars-Cov-2, e.g., Andraesen (2020); Grifoni *et al.* (2020); Casagrandi *et al.* (2006) and references.

Since the pioneer work of Bernoulli (1760), mathematical models have gained more and more visibility as a tool for testing biological hypotheses in disease dissemination. Particularly, the effects of their strain mutations over time, for example, Diekmann *et al.* (1995); Casagrandi *et al.* (2006).

Once most infectious diseases pass from an infected host to a susceptible one due to some kind of contact, the model prediction will strongly depend on the probability of contact between susceptible and infected individuals. If the population is assumed to be homogeneous, that is, the probability of contact between susceptible and infectious individuals is the same in the total population, then the so-called SIRC model (Susceptible, Infected, Recovered, Cross Immune), proposed in Casagrandi *et al.* (2006), has become a well-accepted model that includes the assumption of cross immunity (a proportion of individuals that acquire only partial immunity to the undergoing disease Casagrandi *et al.* (2006)) over the well-known SIR-type models Hethcote (1989, 2000); Brauer *et al.* (2019).

Most populations are not well mixed due to factors such as geographical and social barriers, social and work activities, and public transportation, to name a few. As a result, the contact probability among individuals in the total population is non-homogeneous. However, the nonhomogeneous nature of population mixing does not mean that this is a random process; see Sattenspiel and Dietz (1995) and the references therein. Nonrandom mixing among spatially distributed subpopulations has many consequences for the outcomes of disease spread, for example Sattenspiel and Dietz (1995); Lazo and De Cezaro (2021); Rossato *et al.* (2021); Marques *et al.* (2022a) and references therein.

A common approach to analyzing the spatial spread of infectious diseases is modeling by discrete temporal population models, or metapopulation models, for example Rossato *et al.* (2021); Brauer *et al.* (2019); Marques (2019), and references therein. Although there are a significant number of recent references in the literature, for example, Brauer *et al.*

(2019) and references therein, continuous-time mathematical models with spatially distributed populations are less common than discrete epidemiological models.

In Sattenspiel and Dietz (1995), the authors investigate the effects of migration dynamics coupling in a continuous-time multi-population SIR model. In Lazo and De Cezaro (2021) and Marques *et al.* (2023) the emerging of a plateau-like shape of the infected population is analyzed due to the mixed interaction in a multi-population SIR model without migration. In Gomes and De Cezaro (2022), a multi-population SIRD-type model was proposed to analyze the effects of COVID-19 on an age-distributed population as a consequence of the reopening of schools. The well-posedness and numerical simulations for a fractional SIRC model with two populations that interact were presented in Maurmann *et al.* (2023). The simulations presented in Maurmann *et al.* (2023) suggest that the existence of immunological memory in both subpopulations induces a favorable epidemiological situation, with fewer infections and fewer cross-immunities. In Marques *et al.* (2022b), the authors analyze a multi-population SIRC type model numerically. Numerical simulation scenarios were analyzed in which the effect of disease reintroduction after a period of time was simulated, simulating the emergence of a new strain. The simulations presented show a tendency to continue to grow in cross-immunity due to the reinfection.

Main contributions and paper organization: In this contribution, we explore the effects of inclusion of space in the diseases dynamics of the SIRC-type multipopulation model. The proposed SIRC-type model under investigation assumes the existence of different (not necessarily homogeneous) multipopulation interacting and distributed in a discrete two-dimensional grid (network). We used the smoothness and monotonic behavior of the solution of the SIRC model with multiple populations to show that the spread velocity and intensity of the disease in the network are monotonically dependent on the neighborhood topology (denoted by $V_{i,j}$, see below) and the intensity of the interaction (denoted by $\beta_{i,j}$, see below). The theoretical results are examined numerically, providing some clues to the mechanisms of disease spread, loss of host immunity, or partial transient immunity in inhomogeneous populations. Understand the dynamics behavior of diseases in spatial distributed and non-homogeneous populations are essential for surveillance by public health authorities, who propose preventive measures and vaccination strategies to mitigate the impact of an emerging disease.

In Section *Model description and its well-posedness*, we present the spatially distributed multipopulation SIRC model and prove its well-posedness. In Section *The effect of introducing space in the disease dynamics*, we used the behavior trajectory and the smoothness properties of the existing solution for the proposed model to motivate the effects of the introduction of space in the dynamics of diseases. In particular, we show that the diffusion velocity and intensity of diseases are monotonically dependent on the neighborhood topology and interaction intensity between the distinct popu-

lations in the lattice. The results are numerically verified in Subsections *Scenario 1* and *Scenario 2*.

2 MODEL DESCRIPTION AND ITS WELL-POSEDNESS

We assume the existence of a two-dimensional lattice (nomenclature derived from the theory of Coupled Map Lattice (CML) Marques (2019), where each patch (also known as site pixel or cells) (x_i, x_j) is represented by integer coordinates (with $x_i = is, x_j = js$, where s is the size of the site), for $i \in \{1, \dots, k\}, j \in \{1, \dots, n\}$. In each one of the $(n \times k)$ patches is the home of a distinct, spatially distributed subpopulation, in which $N_{i,j}$ represents the individual's density (which corresponds to the total number of individuals in the site). Furthermore, in each of the patches (i, j) , the density of individuals $N_{i,j}$ in the subpopulation is proportionally distributed, at any time $t \geq 0$, in the susceptible compartments $S_{i,j}(t)$, infectious (infected) $I_{i,j}(t)$, recovered (removed) $R_{i,j}(t)$ and cross-immunity $C_{i,j}(t)$. In this case, the proportional cross-immunity of the population refers to individuals who have acquired partial immunity but are susceptible to any mutation of the circulating stain within a short period of time. There is no migration of the population from one site to another, in contrast to the approach in Sattenspiel and Dietz (1995). The infection might occur even in such a situation, due to the interaction between subpopulations during work hours or in public transport. But at the end of the day, everyone is back at his home site, where infections are reported. In other words, the assumption of no migration is satisfied by considering that the interaction between distinct subpopulations occurs in an infinitely small time step relative to the time of the disease dynamics t , such that individuals from different populations interact and return to their reference sites faster than the time $t \rightarrow t + \Delta t$ of the disease dynamics.

Therefore, the population $N_{i,j}$ at each site remains constant for any time $t \geq 0$. The disease is transmitted from infected individuals to susceptible individuals by the following mechanisms: i) If they belong to the same site, then transmission is proportional to the constant contact rate $\beta_{i,j} > 0$, ii) Another source of transmission occurs by contact between susceptible individuals at the site (i, j) with infected individuals in the neighborhood $V_{i,j} := \{\text{sites } (\hat{i}, \hat{j}) : (\hat{i}, \hat{j}) \neq (i, j)\}$. We assume that the transmission between individuals of different populations is proportional to the constant contact rate $\beta_{\hat{i}, \hat{j}} > 0$ if $(\hat{i}, \hat{j}) \in V_{i,j}$ or $\beta_{\hat{i}, \hat{j}} = 0$ if $(\hat{i}, \hat{j}) \notin V_{i,j}$. Therefore, the neighborhood $V_{i,j}$ determines the topology of contact among different subpopulations in the network, and the parameter $\beta_{\hat{i}, \hat{j}}$ is related to the intensity of interaction with the nearby population.

In the following, we represent the proportion of the infected neighborhood as

$$II := \sum_{\hat{i}, \hat{j} \in V_{i,j}} \beta_{\hat{i}, \hat{j}} I_{\hat{i}, \hat{j}}(t). \tag{1}$$

Hence, $S_{i,j}II$ is the probability that susceptible individuals

from the site (i, j) become infected due to contact with individuals from some of neighboring sites in $V_{i,j}$, with rate of contagion $\beta_{\hat{i}, \hat{j}}$.

We assume that disease dynamics is modeled by a spatially distributed multi-population SIRC-type model, with a normalized and constant total population $N_{i,j}$. Using the mass-action law, the dynamics is given by

$$\begin{aligned} \dot{S}_{i,j} &= \mu_{i,j}(N_{i,j} - S_{i,j}) - S_{i,j}(\beta_{i,j}I_{i,j} + II) + \gamma_{i,j}C_{i,j} \\ \dot{I}_{i,j} &= S_{i,j}(\beta_{i,j}I_{i,j} + II) + \sigma_{i,j}\beta_{\hat{i}, \hat{j}}C_{i,j}I_{i,j} - (\mu_{i,j} + \alpha_{i,j})I_{i,j} \\ \dot{R}_{i,j} &= (1 - \sigma_{i,j})\beta_{i,j}C_{i,j}I_{i,j} + \alpha_{i,j}I_{i,j} - (\mu_{i,j} + \delta_{i,j})R_{i,j} \\ \dot{C}_{i,j} &= \delta_{i,j}R_{i,j} - \beta_{i,j}C_{i,j}I_{i,j} - (\mu_{i,j} + \gamma_{i,j})C_{i,j}. \end{aligned} \tag{2}$$

In (2), the parameters $\alpha_{i,j} > 0, \delta_{i,j} > 0, \gamma_{i,j} > 0$ are the inverse of the time that any individual remains in the compartments $I_{i,j}, R_{i,j}$ and $C_{i,j}$, respectively, for $i = 1, \dots, n$ and $j = 1, \dots, k$. The parameter $\sigma_{i,j}$ is the probability of reinfection, while the parameter $\mu_{i,j} > 0$ represents the mortality/birth rate, which we assume to be equal for all subpopulations.

Furthermore, the model given in (2) is considered with the following initial conditions $X_{i,j}(0) := (S_{i,j}(0), I_{i,j}(0), R_{i,j}(0), C_{i,j}(0))^T \in \mathcal{R}_+^4 := \{X_{i,j}(t) := (S_{i,j}(t), I_{i,j}(t), R_{i,j}(t), C_{i,j}(t))^T \in \mathcal{R}^4 : S_{i,j}(t) \geq 0, I_{i,j}(t) \geq 0, R_{i,j}(t) \geq 0, C_{i,j}(t) \geq 0, t \geq 0\}$, for $i \in \{1, \dots, k\}, j \in \{1, \dots, n\}$.

Note 1 The model given in (2) is a generalization of the SIRC model proposed by Casagrandi et al. (2006) for multi-populations that spatially interact without migration dynamics; see Sattenspiel and Dietz (1995). In fact, if all subpopulations are isolated, which is equivalent to setting $II = 0$ in (2) (or equivalently $\beta_{\hat{i}, \hat{j}} = 0$ for all sites $(\hat{i}, \hat{j}) \in V_{i,j}$), we have the SIRC model originally proposed in Casagrandi et al. (2006), for each of the subpopulations. As a result, the term $S_{i,j}II$ in the model given in (2) is related to the probability that susceptible individuals from the site (i, j) become infected due to contact with individuals from neighboring sites in $V_{i,j}$, but without migration.

It is worth mentioning that the specification of $V_{i,j}$ and $\beta_{\hat{i}, \hat{j}}$ determines the topology of the multipopulation interaction in the network. In particular, restriction on $V_{i,j}$ and $\beta_{\hat{i}, \hat{j}}$ (for example, $\beta_{\hat{i}, \hat{j}} = 0$ represents the isolation of subpopulation) and can be seen as a control strategy. In this case, if a disease starts in a subpopulation, it will become confined in such a population, insofar as there is no interaction between different subpopulations ($\beta_{\hat{i}, \hat{j}} = 0$), see Marques et al. (2022a) and the references therein. If the network size is too small or $V_{i,j}$ contains as many neighborhood sites, then the model dynamics given in (2) is expected to behave as a single population model with a variable transmission rate $\beta_{i,j}$. See also the discussion in the next section. The topology of the multipopulation interaction is the main subject of the numerically simulated scenarios in Section numerically simulated scenarios.

The assumption of non-migratory dynamics and the birth / mortality rates to be constant implies that the number of in-

dividuals in each subpopulation $N_{i,j}$ remains constant. The nonmigration assumption allows us to analyze the effects of the neighborhood interaction topology analytically, as shown in Section Effects of introducing space in the disease dynamics. However, it is one of the weaknesses of the proposed model. We aim to analyze the model given in (2) with some migration patterns, for example, the one proposed in Sattenspiel and Dietz (1995) in future contributions.

In the following, we present the well-posedness of the model given in (2), which supports the forthcoming analysis and the numerically simulated scenarios and their interpretations presented in Section Numerical simulated scenarios.

Theorem 1 *Let the parameters of the model given in (2) be constant and the initial conditions given by $X_{i,j}(0)$. Then, there exists a unique, continuously differentiable and non-negative solution $X(t)$ (a vector with $n \cdot k$ coordinates corresponding to $(S_{i,j}(t), I_{i,j}(t), R_{i,j}(t), C_{i,j}(t))$, for all, $i = 1, \dots, n, j = 1 \dots, k$, with non-negative coordinates) for any $t \in [0, +\infty[$, that continuously depends on the model parameters and initial conditions.*

Sketch of the Proof: Since there is no migration, then summing over all the equations in the model given in (2), it follows that the total population at each site remains constant for all t . As a result, $S_{i,j}, I_{i,j}, R_{i,j}$ and $C_{i,j}$ are uniformly bounded. Therefore, the Jacobian matrix corresponding to the right-hand side of model defined in (2) is uniformly bounded. Then, from the Mean Value Theorem Hale (1980) we see that the right-hand side of (2) is right-hand continuous with respect to t and Lipschitz continuous with respect to $S_{i,j}, I_{i,j}, R_{i,j}$ and $C_{i,j}$, for $i = 1, \dots, n, j = 1, \dots, k$. The continuity of $S_{i,j}, I_{i,j}, R_{i,j}$ and $C_{i,j}$, for $i = 1, \dots, n, j = 1, \dots, k$, also follows straightforward arguments. It follows from classical results on dynamical systems, e.g., Hethcote (2000), the existence of a unique smooth and positive solution $X(t)$ as stated in the Theorem, in the interval $[0, T]$, for some $T > 0$. Since the solution is uniformly bounded by $N_{i,j}$, it follows that the right-hand side of the system proposed in (2) can be bounded by an affine function depending only on the solution of the model $X(t)$ and the model parameters. Therefore, using the classical results of the dynamical system Hale (1980), the solution can be continuously extended to the positive real line. \square

3 EFFECTS OF INTRODUCING SPACE IN THE DISEASE DYNAMICS

In this section, we address some interesting conclusions about some of the effects of space inclusion in disease diffusion dynamics based on the behavior and properties of the solution of the model given in (2).

First, it should be noted that Theorem 1 implies that II (defined in (1)) is a monotonically increasing function of the neighborhood topology $V_{i,j}$ and its intensity $\beta_{i,\hat{j}}$, at any given time $t \geq 0$, as a result of $I_{i,j}(t) \geq 0$.

Hence, from the first equation in the model given in (2), we can see that $S_{i,j}(t)$ remains a decreasing function of t whenever

$$C_{i,j} \leq \frac{(S_{i,j}(\beta_{i,j}I_{i,j} + II) - \mu_{i,j}(N_{i,j} - S_{i,j}))}{\gamma_{i,j}}. \tag{3}$$

In the early stages of the diseases, $C_{i,j} = C_{i,j}(0) = 0$ or $I_{i,j} = 0$ (in the remaining non-infected sites).

The basic reproduction number¹

In any case, if the neighborhood $V_{i,j}$ is not empty and has some proportion of infected individuals such that $\mathcal{R}_0^{(i,j)} > 1$, then it follows from the second equation of the model given by (2) that $I_{i,j}$ will increase. Since $N_{i,j}$ is constant, it follows that $I_{i,j}(t) < \infty$, for all $t \geq 0$.

As a result of the properties mentioned above and the smoothness of $I_{i,j}(t)$ (see Theorem 1), we conclude that there will be a solution trajectory for $I_{i,j}(t)$ (depending on the neighborhood topology of II) that has a concave hump, as shown in Figure 4-a). Therefore, $I_{i,j}(t)$ reaches its maximum at a point $t_p^{i,j} \in]0, +\infty[$, known as the turning point, within $I_{i,j}(t_p^{i,j}) \neq 0$. From the maximality of $I_{i,j}$ at $t_p^{i,j}$ we have $\dot{I}(t_p^{i,j}) = 0$. Hence, from the second equation in the model given by (2) that

$$S_{i,j}(t_p^{i,j}) = \frac{(\mu_{i,j} + \alpha_{i,j}) - \sigma_{i,j}\beta_{i,j}C_{i,j}(t_p^{i,j})}{\beta_{i,j}} \left(\frac{1}{1 + \frac{II(t_p^{i,j})}{\beta_{i,j}I_{i,j}(t_p^{i,j})}} \right). \tag{5}$$

The analysis of equation (5) reveals some possibilities whose consequences is worth exploring is as follows:

- i) In the first analysis, (3) implies that $C_{i,j}$ increases with II . On the other hand, since the number of susceptibles is always non-negative (see Theorem 1), then (5) implies the following threshold for the cross-immunity, given by

$$C_{i,j}(t_p^{i,j}) \leq \frac{(\mu_{i,j} + \alpha_{i,j})}{\sigma_{i,j}\beta_{i,j}}. \tag{6}$$

Such bound is independent of the neighborhood topology. This phenomena is observed numerically in Figures 2 and 4-b).

¹Quantity that expresses the expected number of cases directly generated by one case in a population and within the selected population at the initial phase of the infection Diekmann (1990); van den Driessche and Watmough (2002). of the population (i, j) , calculated using the next generation matrix Diekmann (1990); van den Driessche and Watmough (2002), is given by

$$\mathcal{R}_0^{(i,j)} = (\mu_{i,j} + \alpha_{i,j})^{-1} \left(\beta_{i,j} + \sum_{\hat{i}, \hat{j} \in V_{i,j}} \beta_{\hat{i}, \hat{j}} \right). \tag{4}$$

Therefore, we can have $\mathcal{R}_0^{(i,j)} > 1$, even when the basic reproductive number of totally isolated subpopulations $\tilde{\mathcal{R}}_0^{(i,j)} := \frac{\beta_{i,j}}{\alpha_{i,j} + \mu_{i,j}} < 1$ (which corresponds to the case where $\beta_{\hat{i}, \hat{j}} = 0$). As a consequence, the asymptotical stability of the disease-free equilibrium point at a site (i, j) also depends on the neighborhood topology given in (1), (see the analysis derived in Marques et al. (2023) for the spatially distributed SIR model).

ii) In an isolated population, that is, in a site (i, j) where $V_{i,j}$ is empty (or $\beta_{i,\hat{j}} = 0$), then the number of susceptibles at $t_p^{i,j}$ is

$$S_{i,j}(t_p^{i,j}) = \frac{(\mu_{i,j} + \alpha_{i,j}) - \sigma_{i,j}\beta_{i,\hat{j}}C_{i,j}(t_p^{i,j})}{\beta_{i,j}}. \quad (7)$$

iii) Increasing the network topology $V_{i,j}$ or the intensity interaction $\beta_{i,\hat{j}}$, causes $S_i(t_p^i)$ to decrease (since the denominator in (5) increases), and therefore $I(t_p^i)$ increases. Figures 1, 10 and 12 depicted this situation.

iv) As a consequence of items ii) and iii), $S_i(t_p^{i,j})$ remains at its highest possible value in the scenario where there is minimal interaction between populations and cross-immunity.

The effects of introducing space into the model dynamics proposed in (2) and its relation to above-mentioned situations i), ii), iii) and iv) will be addressed numerically in the following subsection.

4 NUMERICAL SIMULATED SCENARIOS

In this subsection, we investigate numerically the effect that the interaction between distinct subpopulations following the dynamics given in (2) has on the disease dynamics that reflect the situations i), ii), iii) and iv) described above. In all the presented simulations, the solution $X(t)$ of the model given in (2) is numerically obtained using the Euler method with a step-size of $h = 10^{-4}$ that guarantee the numerical accuracy of the approximation and avoids the stiffness phenomena, see da Silva *et al.* (2023.No Prelo). The network has 14×14 sites, which means that $n = k = 14$. Furthermore, the parameters $\alpha_{i,j} = 52.14$, $\delta_{i,j} = 0.75$, $\mu_{i,j} = 0.00001$, $\gamma_{i,j} = 0.35$ and $\sigma_{i,j} = 0.12$, for $i, j \in \{1, \dots, 14\}$, based on the parameters given in Casagrandi *et al.* (2006), are kept fixed in all simulations. Therefore, as previously announced in Remark 1, we shall see below the effects of the neighborhood of interaction topology $V_{i,j}$ and its intensity given by the parameter $\beta_{i,\hat{j}}$ on the disease behavior for the infected and cross-immunity portions of each of the populations.

SCENARIO 1: EFFECTS ON DISEASE DYNAMICS DUE TO VARIATION OF THE DISTINCT POPULATION INTENSITY INTERACTION $\beta_{i,\hat{j}}$, WHILE THE NEIGHBORHOOD OF INTERACTION TOPOLOGY $V_{i,j}$ IS KEPT FIXED

In all simulations presented in this first scenario, we assume that each population located in the patch (i, j) of the lattice interacts only with the four neighbors in a rectangular vicinity $V_{i,j}$ that has a common face interception, also called the Neumann-type neighborhood, e.g. Marques (2019). In Figures 1 and 2, we see the effects on the dynamics of the total infected and cross-immunity population for different choices of interaction intensity $\beta_{i,\hat{j}} \neq 0$ for $(i, \hat{j}) \in V_{i,j}$ and zero elsewhere. More specifically, in all simulated scenarios, we have:

- 1) The density $N_{i,j}$ is constant, corresponding to a total population of 100 individuals in all the 14×14 patches;
- 2) Infection starts at two distinct sites simultaneously at $t = 0$. They correspond to the sites of the positions (10,5) and (5,11) in the lattice. The total number of infected individuals in such patches is $I_{10,5}(0) = I_{5,11}(0) = 20$.
- 3) The initial conditions $X_{i,j}(0)$ are such that $S_{i,j}(0) = 100$ and $I_{i,j} = 0$ if $(i, j) \neq (10,5)$ or $(i, j) \neq (5,11)$ and $S_{10,5} = S_{5,11} = 80$ (see item 2) and $R_{i,j}(0) = C_{i,j}(0) = 0$ in all patches.
- 4) The distinct population interaction intensity is such that $\beta_{i,\hat{j}} = \beta_{i,j}/\kappa$ in $V_{i,j}$ and $\beta_{i,\hat{j}} = 0$, otherwise, the values of κ are chosen for simulated sub-populations with a large or a small interaction in the vicinity $V_{i,j}$ as follows:

Case 1, $\kappa = 15000$; It corresponds to $\beta_{i,\hat{j}} = 0.00783$ and is the lower intensity interaction in the simulated scenarios.

Case 2, $\kappa = 1500$; It corresponds to $\beta_{i,\hat{j}} = 0.0783$ and is the middle-lower intensity interaction in the simulated scenarios.

Case 3, $\kappa = 150$; It corresponds to $\beta_{i,\hat{j}} = 0.783$ and is the middle-large intensity interaction in the simulated scenarios.

Case 4, $\kappa = 15$. It corresponds to $\beta_{i,\hat{j}} = 7.83$ and is the large intensity interaction in the simulated scenarios.

In Figures 1-4, we presented the simulated scenarios using the settings of this subsection. It is possible to see in Figure 1 that in Case 1 and 2 for the choices of $\beta_{i,\hat{j}}$ the total infected proportion of the population presents an oscillatory behavior due to the time it takes for the diseases to spread between different sites (compare with equation (5)). This behavior is not observed for the interaction of medium-large and high intensity $\beta_{i,\hat{j}}$, because in such cases the spread velocity of the diseases between different populations is large, see red and pink curves in Figure 1 (since κ is large in (5)). The intensity of interaction between different populations $\beta_{i,\hat{j}}$ is also monotonically related to the proportion of the infected population at the time of selection of infection (see Figure 1 and compare with Equation (5)). Monotonic behaviors are reflected in the proportion of cross-immunity of the population in terms of the choices for $\beta_{i,\hat{j}}$, as presented in Figure 2. The spatial distribution of the cross immunology for Case 1 at time $t = 0.4$ and Case 4 at time $t = 0.25$ is presented in Figure 3 on the right side. As can be observed in Figure 3, the cross-immunity front wave does not cover the lattice in Case 1, but has fulfilled all the patches for Case 4, even considering an earlier time for the last case. Such a behavior implies that cross-immunity achieves stability early for a large distinct population interaction $\beta_{i,\hat{j}}$, as presented in Figure 2. A similar distribution can be observed in the

infected population Figure 3 on the left.

In Figure 4, we show the evolution of the dynamics for infected and cross-immunity populations in different lattice patches for the intensity of interaction, representing Cases 1 and 4, respectively. The main difference in infected populations is the time at which the peaks occur (see also (5)). At the patch (5, 11) where the disease started, we observe the first and more intense peak (see the Figure 4(a)). Another interesting fact is the time interval in which the dynamics between sites occurs when comparing cases 1 and 4. When there is more interaction (Case 4), the time interval between one curve and another is much shorter than in Case 1, in other words, the diffusion of the disease in the space is faster (see the $\mathcal{R}_0^{i,j}$ in (4)).

SCENARIO 2: EFFECTS ON THE DISEASES DYNAMICS DUE TO VARIATION OF NEIGHBORHOOD TOPOLOGY $V_{i,j}$

In this subsection, we present numerical simulation scenarios for distinct choices of the neighborhood topology $V_{i,j}$ and will discuss its effect on the dynamics of the disease. In particular, it shows another point of view of the effects of the space interaction on the dissemination of diseases. The results presented in Figures 10- 13 show the distinct dynamics of disease dissemination in the following neighborhoods:

- *Neumann neighborhood*: In such a neighborhood, each population (patch) interacts only with the four neighbors in a rectangular vicinity $V_{i,j}$ that has a common face of interception (see Figure 5);
- *V neighborhood*: In such a neighborhood, each population (patch) interacts only with the eight neighbors in a plus-shaped (not rectangular) vicinity $V_{i,j}$ (see Figure 6);
- *V* neighborhood*: In such a neighborhood, each population (patch) interacts only with the eight neighbors in a plus-shaped (not-rectangular) vicinity $V_{i,j}$ but the intensity of the distinct population interaction $\beta_{\hat{i},\hat{j}}$ is 1/2 of the neighbor site that has a common face interception (see Figure 7);
- *Moore neighborhood*: In such a scenario, each population (patch) interacts with the eight neighbors in a rectangular vicinity $V_{i,j}$ (see Figure 8);
- *Moore* neighborhood*: This is a variation of the Moore neighborhood, where we considered that each population (patch) interacts with the eight neighbors in a rectangular vicinity $V_{i,j}$ but, in the absence of a common face interception in the vicinity, the intensity of the distinct population interaction $\beta_{\hat{i},\hat{j}}$ is 1/2 of the neighbor site that has a common face interception (see Figure 9);

In all simulations presented in this subsection, we used the intensity of interaction between the different subpopulations in the vicinity to be chosen as $\beta_{\hat{i},\hat{j}} = \beta_{i,j}$ if $(\hat{i}, \hat{j}) \in V_{i,j}$ and

$\beta_{\hat{i},\hat{j}} = 0$ elsewhere. The remaining parameters of the model given in 2 are the same as those described at the beginning of this section. Therefore, the effect of space throughout the neighborhood topology $V_{i,j}$ is what makes the analysis different from the SIRC model with homogeneous population analyzed elsewhere in Casagrandi *et al.* (2006). See also the comments on Remark 1.

In Figure 10, we show the dynamics of the infected proportion of the total population for different configurations of $V_{i,j}$ as explained above. We can observe that for $V_{i,j}$ with the same number of neighbors, the curves are very close (see the blue and green curves in Figure 10 for example and compare them with equation 5). The proportion of cross-immunity in the population has a more evident peak for smaller neighborhoods (see the blue curve in Figure 11).

We will present two situations for distinct initial conditions, indeed: a) the disease started in two patches, namely the patches (10,5) and (5,11), respectively. For such a scenario, the initial conditions are the same as those described in Subsection *Scenario 1*. b) The disease started in only one patch, namely (5, 11). In such a case, the initial conditions are such that $I_{10,5} = 0$ and then $S_{10,5} = 100$. The remaining initial conditions remain the same as before.

In Figure 12, we show the dynamics of the total infected population in the network due to the distinct choices of the neighborhood and the initial conditions, in three distinct sections of the simulated time intervals. The early dynamics of the infection is presented in Figure 12,-a). It is worth noting that infection pick is monotonically decreasing with the number of neighborhood sites in the vicinity $V_{i,j}$ and the intensity interaction $\beta_{\hat{i},\hat{j}}$. Moreover, it suffers a small shift in time and a considerable decrease in its maximum due to the initial conditions, with the infection beginning at only one site. Figure 12 b) and c) show an oscillating and time shift with the prevalence of the diseases in the long run of the model (2) dynamics, that are independent of the simulated initial conditions. In particular, this result shows that (5) remains true.

In Figure 13, we present the dynamics of the proportion of cross-immunity of the total population, for the simulated scenarios described in this subsection. The simulations presented show that the dynamics of the cross-immunity is independent of the vicinity $V_{i,j}$ and the initial conditions in the short duration of the diseases (up to $t = 0.5$). Then, it presents a monotonically decreasing behavior with the number of neighborhoods and the intensity interaction $\beta_{\hat{i},\hat{j}}$ in the neighborhood topology $V_{i,j}$. Then it presented and shifted the oscillatory behavior independent of the vicinity topology or initial conditions. Therefore, (6) is numerically verified.

In Figure 14 we present the spatial distribution of the infected population at the beginning of the infection $t = 0.002$ for different types of neighborhoods. Note that the sites

(subpopulations) already affected by the infection differ significantly in each case. For the type V neighborhood, we observed that the sites with the presence of infected people already exceeded half of the network. This fact is also observable in the Figure 10(a), in which the largest fractions of the affected population correspond to the V and V^* neighborhoods.

The simulation regarding distinct topologies for vicinity choices shows a monotonically increasing and a shifted pick of infection. Also, there is a monotonically decreasing pick of cross-immunity in the total population with respect to the number of neighbors in the vicinity. This monotonic behavior is also observed due to the number of infected sites in the initial conditions for the total infected populations, but is not observed in the cross-immunity dynamics (see (6) and (5)). The number of neighbors in the vicinity implies a shifting oscillatory behavior and the permanence of the disease infection and cross-immunity in the total population.

5 CONCLUSION AND FUTURE DIRECTIONS

In this contribution, we discuss the effects of space inclusion on the behavior dynamics of a disease in which distinct and not necessarily homogeneous interacting multi-populations, distributed in a discrete two-dimensional network, acquire only partial immunity to circulating stain, modeled by a compartmental multi-population SIRC-type model without migration. The properties of the model solution were used to show that the spread velocity and intensity of the disease to reach its peak of infection in the network are monotonically dependent on the topology of the neighborhood $V_{i,j}$ and the intensity of the interaction $\beta_{i,j}$, while the cross-immunity is uniformly bounded independently of such quantities. These theoretical results are examined numerically in some particular cases for neighborhood topology $V_{i,j}$ and interaction intensity $\beta_{i,j}$ (see Subsection *Scenario 1-Scenario 2*). As far as the authors are aware, such results were not investigated elsewhere. The results obtained provide some clues about the mechanisms of disease spread and loss of host immunity or transient partial immunity in inhomogeneous populations.

Future developments of this approach include the analysis of equilibrium points and stability.

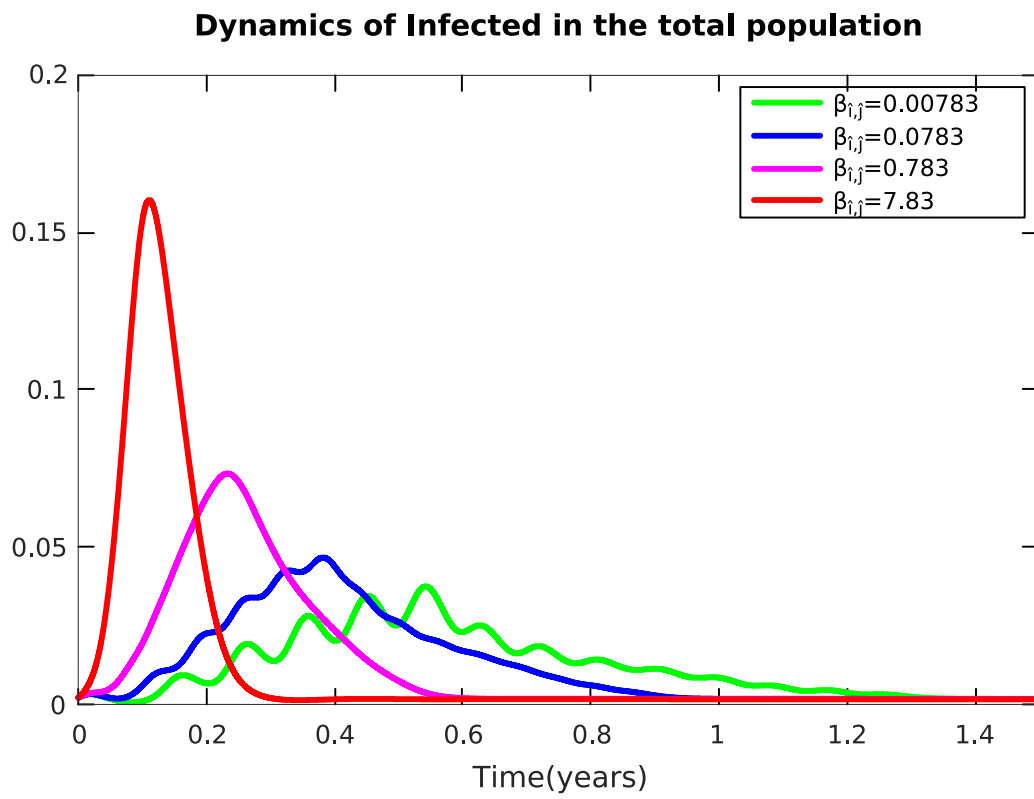


Figure 1: The dynamic behavior of the proportion of the total infected population for distinct choices of the intensity of the population interaction in a Neumann type neighborhood.

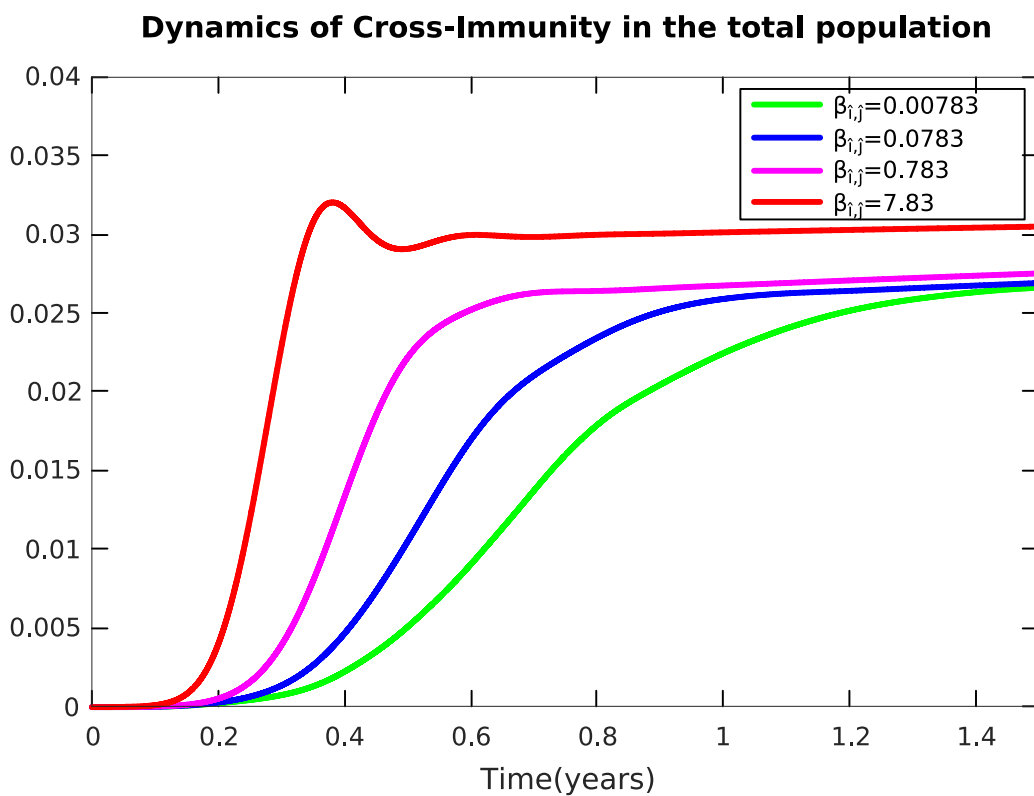
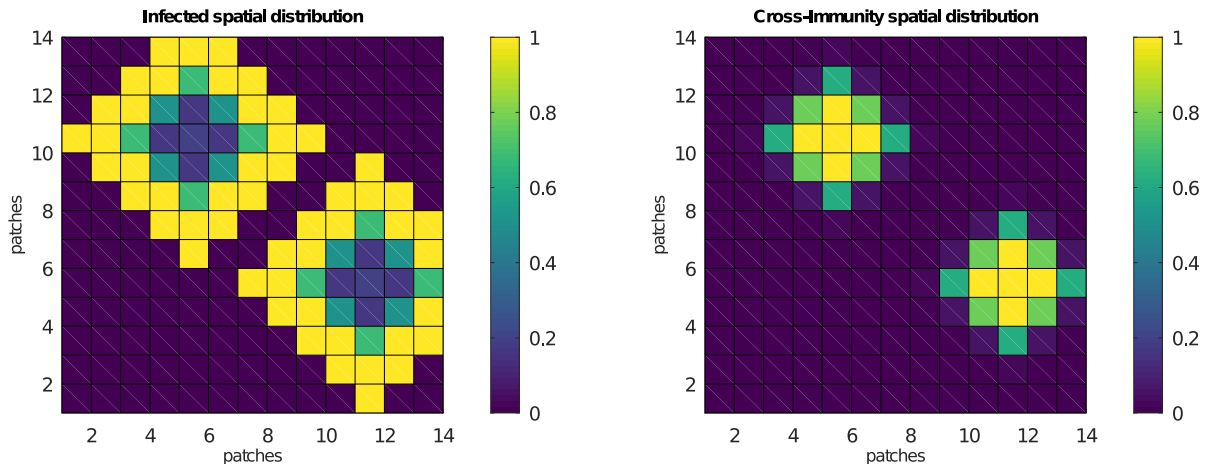
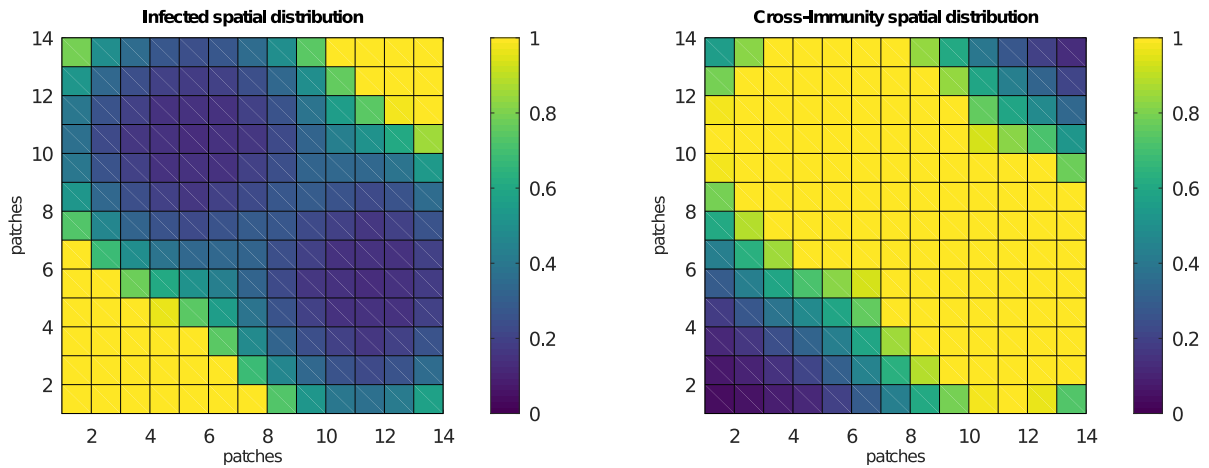


Figure 2: The dynamic behavior of the proportion of the total cross-immune population, for distinct choices of the intensity of the population interaction in a Neumann type neighborhood.



(a) Spatial distribution of the infected and cross-immune population in the lattice at time $t = 0.4$, in the scenario of lower sub-population interaction, in a Neumann type neighborhood - Case 1.



(b) Spatial distribution of the infected and cross-immune population in the lattice at time $t = 0.25$ in the scenario of large sub-population interaction in a Neumann type neighborhood - Case 4.

Figure 3

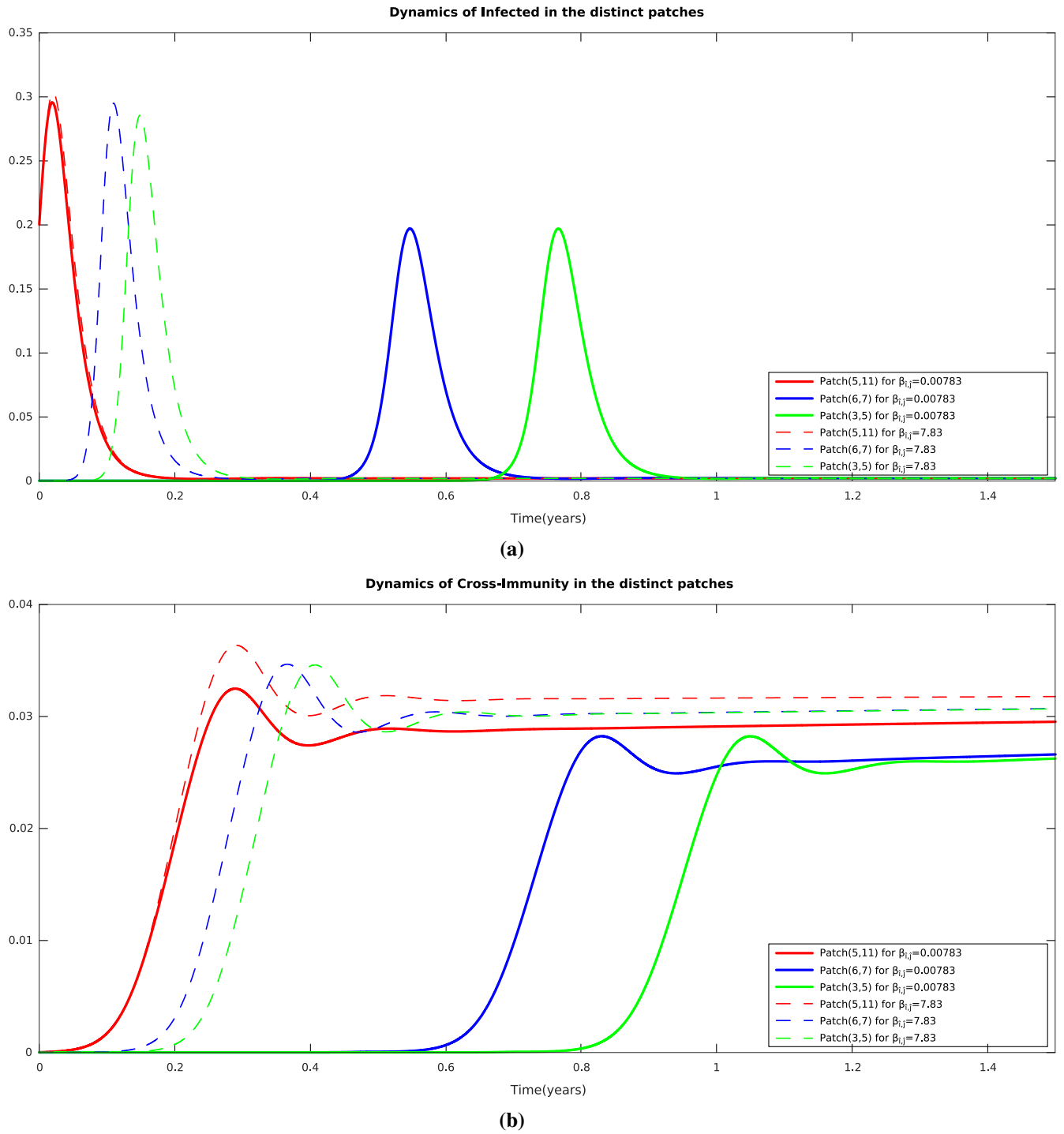


Figure 4: (a) The dynamic behavior of the proportion of the infected population in distinct patches for the parameter setting in the scenario 1, for $\kappa = 1.500$ and $\kappa = 15$, respectively. (b) The dynamic behavior of the proportion of the population of the cross-immunity in distinct patches for the parameter setting in scenario 1, for $\kappa = 1.500$ and $\kappa = 15$, respectively.

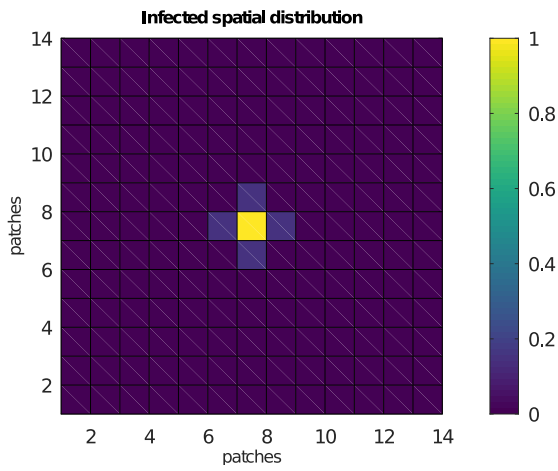


Figure 5: An example of spatial distribution in the case of a Neumann neighborhood.

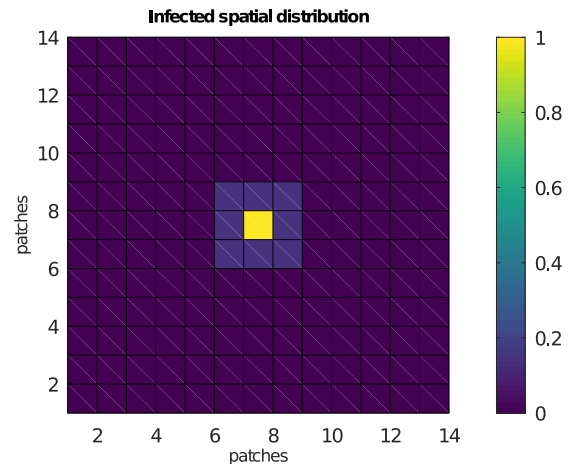


Figure 8: An example of spatial distribution in the case of a Moore neighborhood.

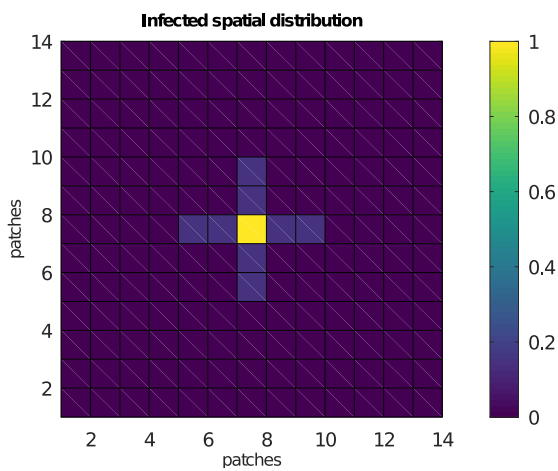


Figure 6: An example of spatial distribution in the case of a V neighborhood.

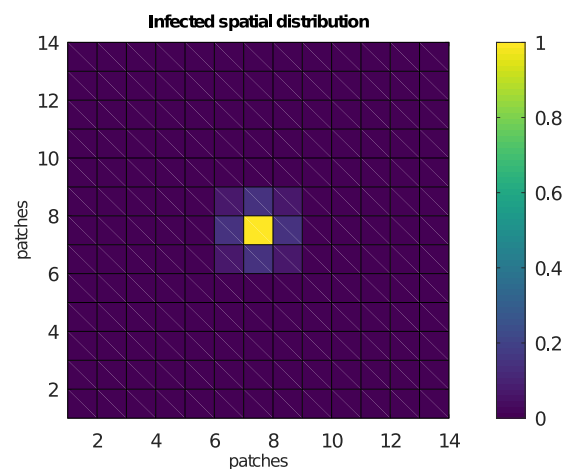


Figure 9: An example of spatial distribution in the case of a Moore* neighborhood.

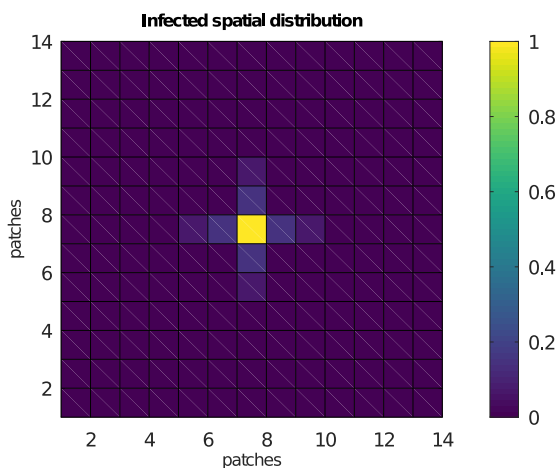


Figure 7: An example of spatial distribution in the case of a V* neighborhood.

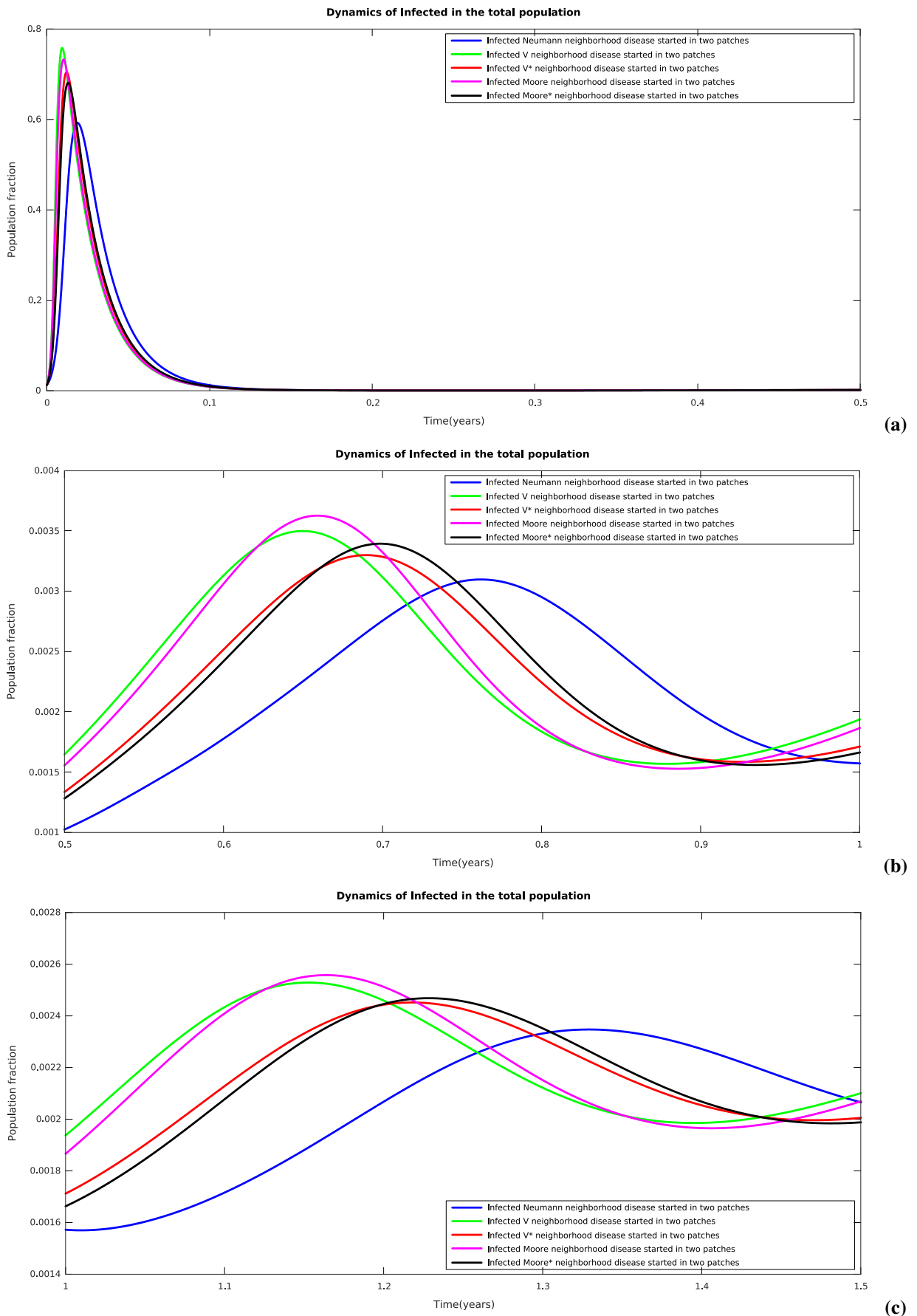


Figure 10: The dynamic behavior of the proportion of the total infected population in different time intervals for distinct neighborhoods for the parameter settings and neighborhood of the scenario 2.

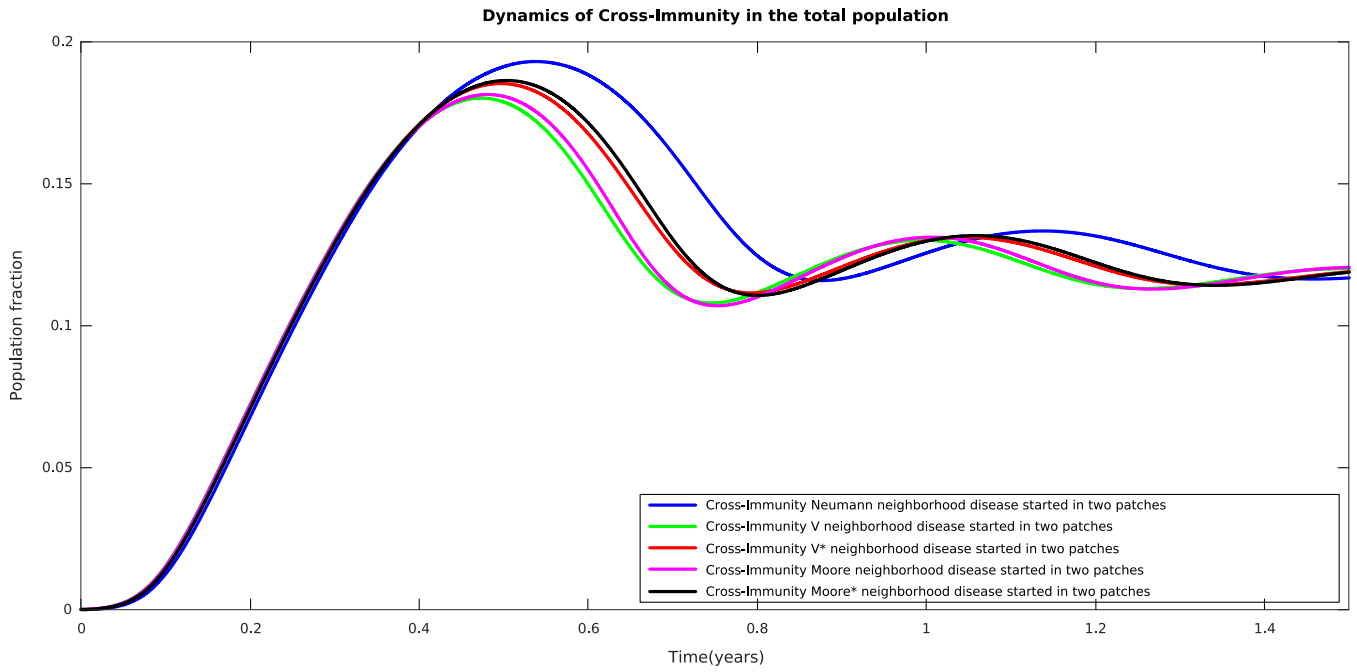


Figure 11: The dynamic behavior of the proportion of the total Cross-immunity population for distinct neighborhoods for the parameter settings and neighborhood of the scenario 2.

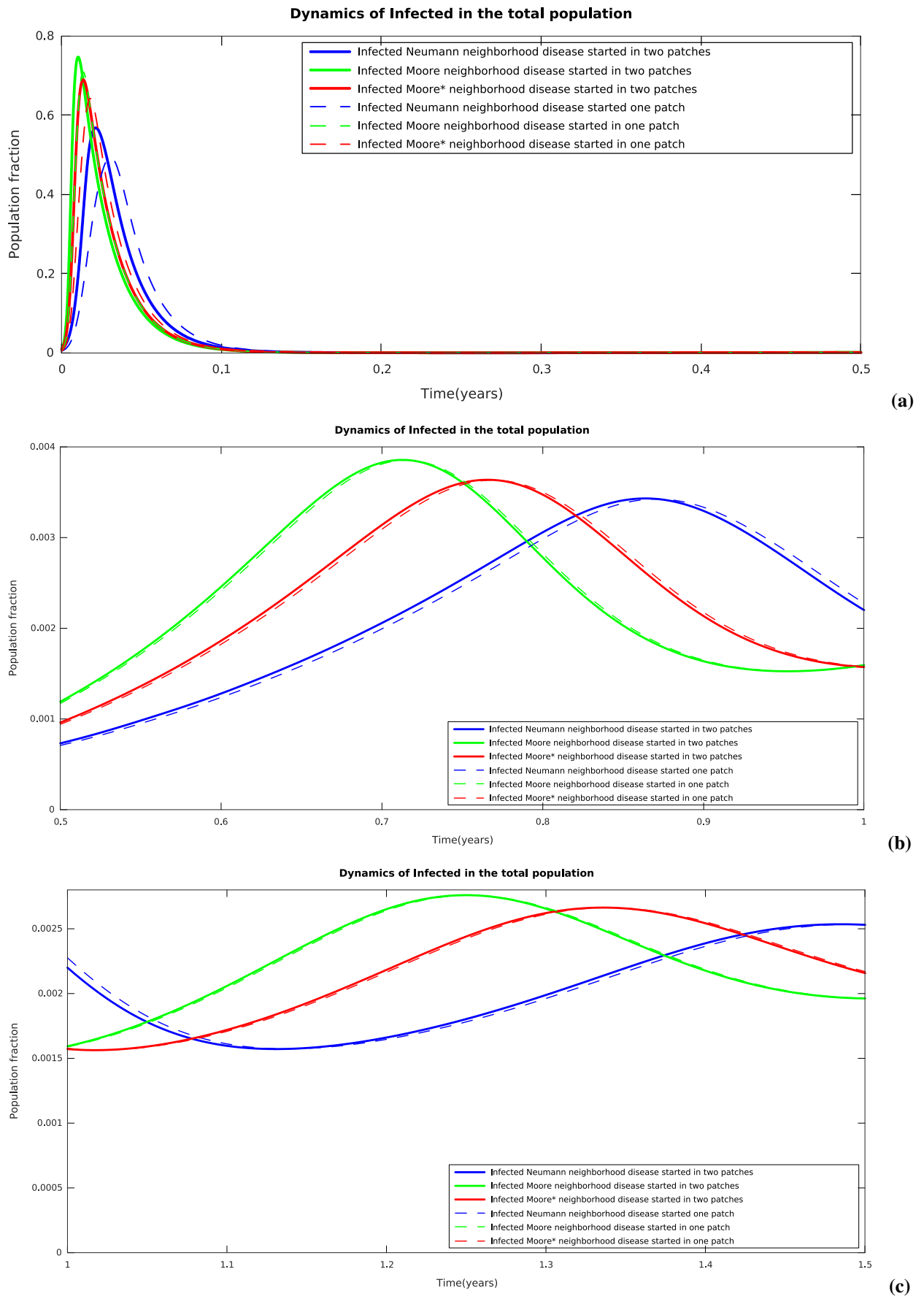


Figure 12: The dynamic behavior of the proportion of the total infected population in different time intervals for distinct neighborhoods according to choices a) and b) for the initial conditions and for the parameter settings and neighborhood of the scenario 2.

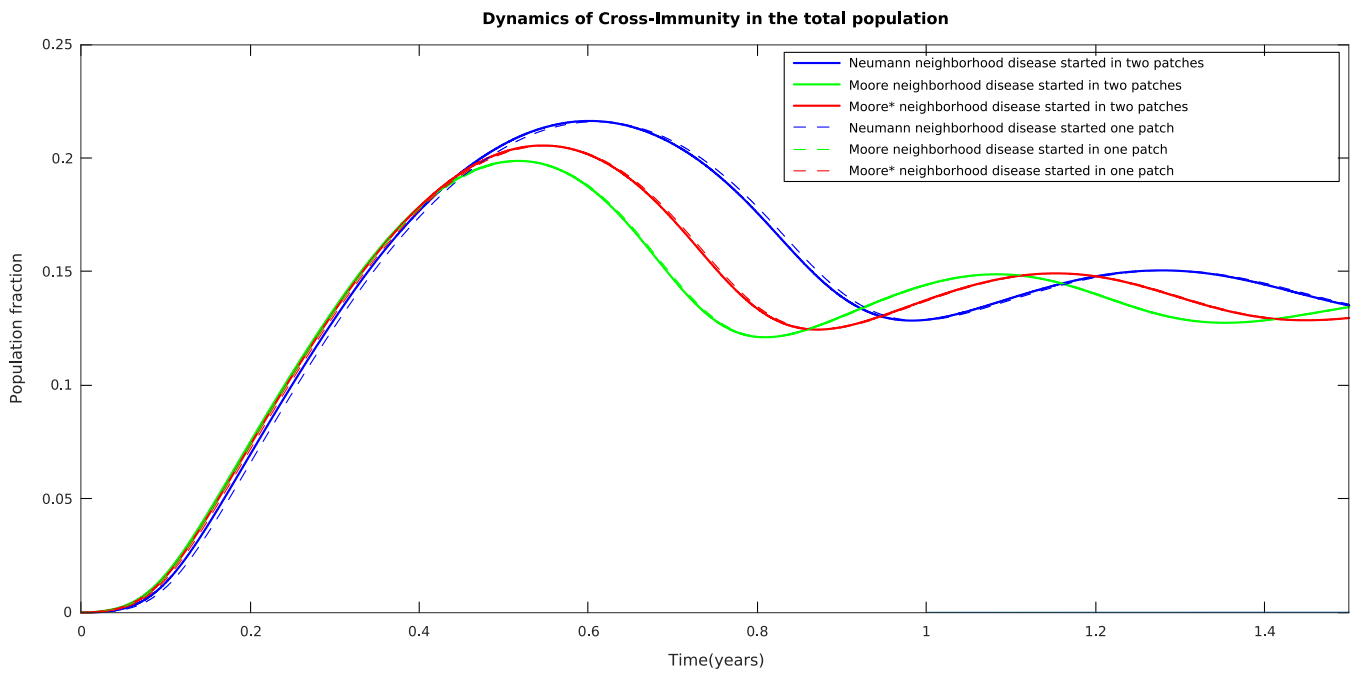


Figure 13: The dynamic behavior of the proportion of the total cross-immune population for distinct neighborhoods according to choices a) and b) for the initial conditions and for the parameter settings of scenario 2.

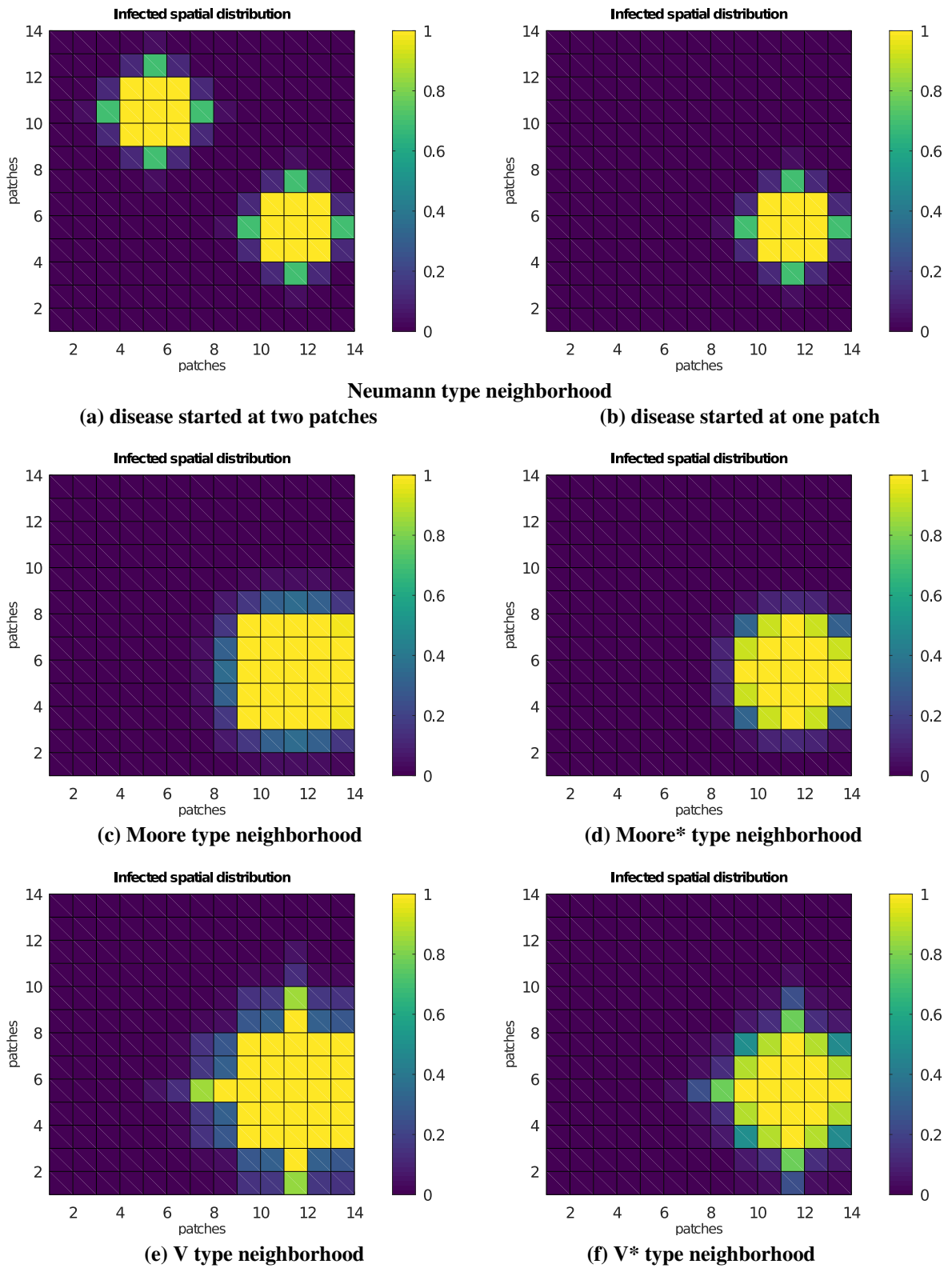


Figure 14: Comparison between different neighborhoods in $t = 0.002$.

REFERENCES

- Andreasen, V.; Gog, J. (2020) 'Pease (1981): The evolutionary epidemiology of influenza a.' *Theoretical Population Biology*, 133, pp. 29–32.
- Bernoulli, D. (1760) 'Essai d'une nouvelle analyse de la mortalité causée par la petite vérole, et des avantages de l'inoculation pour la prévenir'. *Histoire de l'Acad., Roy. Sci.(Paris) avec Mem.*, pp. 1–45.
- Brauer, F., Castillo-Chavez, C. and Z., F. (2019) *Mathematical Models in Epidemiology*. Springer.
- Casagrandi, R. et al. (2006) 'The SIRC model and Influenza A'. *Mathematical Biosciences*, 200(2), pp. 152–169.
- Diekmann, O., H.J.M.J. (1990) 'On the definition and the computation of the basic reproduction ratio r_0 in models for infectious diseases in heterogeneous populations'. *J. Math. Biol.*, 1(28), pp. 365–382.
- Diekmann, O., Metz, J. and Heesterbeek, J.A.P. (1995) 'The legacy of kermack and mckendrick'. *Epidemic Models: Their Structure and Relation to Data Mollison, D. E. (ed.)*, Cambridge University Press, Cambridge., (1).
- Gomes, A.C.F.N. and De Cezaro, A. (2022) 'A model of social distancing for interacting age-distributed multi-populations: An analysis of students' in-person return to schools'. *Trends in Computational and Applied Mathematics*, 23(4), pp. 655–671.
- Grifoni, A., Weiskopf, D., Ramirez, S.I., Mateus, J., Dan, J.M., Moderbacher, C.R., Rawlings, S.A., Sutherland, A., Premkumar, L., Jardi, R.S., Marrama, D., de Silva, A.M., Frazier, A., Carlin, A.F., Greenbaum, J.A., Peters, B., Krammer, F., Smith, D.M., Crotty, S. and Sette, A. (2020) 'Targets of t cell responses to sars-cov-2 coronavirus in humans with covid-19 disease and unexposed individuals'. *Cell*, 181(7), pp. 1489–1501.e15. doi:<https://doi.org/10.1016/j.cell.2020.05.015>. Available at: <https://www.sciencedirect.com/science/article/pii/S0092867420306103>.
- Hale, J.K. (1980) *Ordinary Differential Equations (2nd ed.)*, vol. 1. Malabar: Robert E. Krieger Publishing Company.
- Hethcote, H.W. (1989) 'Three basic epidemiological models'. In *Applied mathematical ecology*. Springer, pp. 119–144.
- Hethcote, H.W. (2000) 'The mathematics of infectious diseases'. *SIAM Review*, 42(4), pp. 599–653.
- Lazo, M.J. and De Cezaro, A. (2021) 'Why can we observe a plateau even in an out of control epidemic outbreak? a seir model with the interaction of n distinct populations for covid-19 in brazil.' *Trends in Computational and Applied Mathematics*, 22(1), pp. 109–123.
- Marques, J.C. (2019) *Modelos para dispersão de javalis { Sus scrofa }*. Ph.D. thesis, Universidade Federal do Rio Grande do Sul.
- Marques, J.C., De Cezaro, A. and Lazo, M.J. (2022a) 'A sir model with spatially distributed multiple populations interactions for disease dissemination'. *Trends in Computational and Applied Mathematics*, 23(1), pp. 143–154.
- Marques, J.C., De Cezaro, A. and Lazo, M.J. (2023) 'On an emerging plateau in a multi-population sir model'. *preprint*, (1), pp. 1–21.
- Marques, J.C., Gomes, A.C.F.N. and De Cezaro, A. (2022b) 'A numerical study of the effect of population interaction on disease dissemination and cross immunity'. In: *McSul*, 9, formato virtual.
- Maurmann, A.C., Travessini De Cezaro, F. and De Cezaro, A. (2023) 'A fractional sirc model for the spread of diseases in two interacting populations'. *LATIN-AMERICAN JOURNAL OF COMPUTING*, to appear, pp. 1–8.
- Rossato, M.C., RODRIGUES, L.A.D. and Mistro, D.C. (2021) 'Padrões espaciais de agregação populacional em modelos discretos'. *CIÊNCIA E NATURA*, 42, pp. 1–13.
- Sattenspiel, L. and Dietz, K. (1995) 'A structured epidemic model incorporating geographic mobility among regions.' *Mathematical biosciences*, 128(1-2), pp. 71–91.
- da Silva, M.I., Marques, J.C., Conza, A.O., De Cezaro, A. and Gomes, A.C.F.N. (2023.No Prelo) 'The stiffness phenomena for the epidemiological sir model: a numerical approach'. In: *Latin-American Journal of Computing*.
- van den Driessche, P. and Watmough, J. (2002) 'Reproduction numbers and sub-threshold endemic equilibria for compartmental models of disease transmission'. *Mathematical Biosciences*, 180(1), pp. 29–48.

Recommended Citation: Chaves Marques, J *et al.* (2023). 'Some effects of population interaction on a multi-population SIRC epidemiological model'. *Rev. model. mat. sist. biol.* 3(E), e23E01, doi:10.58560/rmmsb.v03.n02.023.01





This open access article is licensed under a Creative Commons Attribution International (CC BY 4.0) <http://creativecommons.org/licenses/by/4.0/>.
Support:

Modelamiento Matemático de la Fiebre Amarilla: un modelo con migración

Mathematical Modeling of Yellow Fever: a model with migration

 Lisandra Pitol¹,  Luciana Rossato Piovesan²

 Glênio Aguiar Gonçalves¹  Fernanda Tumelero¹  Alexandre Sacco de Athayde¹

 Régis Sperotto de Quadros¹ y  Daniela Buske¹

✉ Daniela Buske: danielabuske@gmail.com

¹ Instituto de Física e Matemática,
Universidade Federal de Pelotas,
Pelotas / RS, Brasil

² Centro de Engenharias,
Universidade Federal de Pelotas,
Pelotas / RS, Brasil

Recepción: 2023-04-05 | Aceptación: 2023-08-10 | Publicación: 2023-10-29

Citación recomendada: Pitol, L. *et al.* (2023). 'Modelamiento Matemático de la Fiebre Amarilla: un modelo con migración'. Rev. model. mat. sist. biol. 3(E), e23E02, doi:10.58560/rmmsb.v03.n02.023.05



This open access article is licensed under a Creative Commons Attribution International (CC BY 4.0) <http://creativecommons.org/licenses/by/4.0/>.
Support:

RESUMEN

En este trabajo nos limitamos al estudio de un modelo matemático para la Fiebre Amarilla (FA), una enfermedad febril aguda transmitida por vectores (en este caso, mosquitos). Este es un modelo compartimental conocido, propuesto por Esteva *et al.* (2019), que divide a la población en tres ciclos, según la dinámica de transmisión de la enfermedad: ciclo epidémico forestal, ciclo entre humanos en la región forestal y ciclo urbano (epidemia urbana de fiebre amarilla sostenida por humanos migratorios infecciosos). A pesar de tener otros vectores, solo se consideró la presencia de dos vectores principales: el *Aedes aegypti* (transmisor urbano) y el *Haemagogus* (principal transmisor en la región forestal). Además, proponemos una modificación al modelo: la inclusión de la vacunación. Así, a través de simulaciones en el *software* Scilab, fue posible obtener gráficas del comportamiento de cada una de las poblaciones (tanto hospedantes como vectores) en un ambiente con y sin presencia de vacunación, permitiendo un análisis más detallado del impacto de la vacunación en una población humana susceptible.

Palabras Claves:

Modelo Epidemiológico, Fiebre Amarilla, Sistema de Ecuaciones Diferenciales, Vacunación

ABSTRACT

In this work we limit ourselves to the study of a mathematical model for Yellow Fever (YF), an acute febrile disease transmitted by vectors (in this case, mosquitoes). This is a known compartmental model, proposed by Esteva *et al.* (2019), which divides the population into three cycles, according to the dynamics of disease transmission: forest epidemic cycle, human-to-human cycle in the forest region and urban cycle (urban yellow fever epidemic sustained by infectious migratory humans). Despite having other vectors, only two main vectors were considered: the *Aedes aegypti* (urban transmitter) and the *Haemagogus* (main transmitter in the forest region). In addition, we propose a modification to the model: the inclusion of vaccination. Thus, through simulations in the Scilab software, it was possible to obtain graphs of the behavior of each of the populations (both hosts and vectors) in an environment with and without the presence of vaccination, allowing a more detailed analysis of the impact of vaccination on a susceptible human population.

Keywords:

Epidemiological Model, Yellow Fever, System of Differential Equations, Vaccination

2020 AMS Mathematics Subject Classification: Primary: 92B05; Secondary:

1. INTRODUCCIÓN

La epidemiología es el campo de la ciencia que estudia los patrones de salud y enfermedad, así como sus factores asociados en una población (Martcheva, 2015). En este contexto, las matemáticas se convierten en un importante aliado a través del estudio de modelos capaces de describir el comportamiento de una enfermedad en una población y, con ello, poder predecir el comportamiento de la enfermedad en el tiempo, decidiendo qué medidas son más eficientes. Reducir el contagio, verificar qué factores son más relevantes en la propagación de la enfermedad, entre otros.

Se han desarrollado modelos matemáticos para representar la propagación de enfermedades y no es diferente con la Fiebre Amarilla (FA). Esteva *et al.* (2019), basado en una variación del modelo de Ross-MacDonald y en trabajos previos sobre transmisión vectorial, buscó evaluar el riesgo de adquirir FA a través de migrantes en áreas forestales, además de verificar la potencial introducción de esta enfermedad en áreas urbanas. Para ello, se consideraron en el modelo dos vectores diferentes, que son el mosquito *Aedes aegypti* y el mosquito *Haemagogus* y diferentes ciclos epidémicos, que son el ciclo forestal, el ciclo entre humanos en una región forestal y el ciclo que representa epidemia de FA urbana sostenida por humanos infecciosos que regresan de la región forestal (migrantes). Danbaba and Garba (2020), a su vez, estudió la dinámica de transmisión de FA en un entorno donde hay interacción entre humanos y mosquitos en presencia de vacunación, asumiendo que la transmisión vertical ocurre en la población de mosquitos. Kalra and Ratti (2020) presenta un modelo que considera el entorno humano-mosquito con múltiples medidas de control. Las medidas de control adoptadas por Kalra and Ratti (2020) aparecen en una clase denominada protegida y comprenden individuos que adquirieron protección temporal a través del uso de repelente de insectos. Además, también se tiene en cuenta el tema de la vacunación. Los modelos que consideran el uso de una vacuna imperfecta se pueden encontrar en los trabajos de Raimundo *et al.* (2015) y Raimundo *et al.* (2016). Massad *et al.* (2005) intentó estimar la proporción ideal de la población a vacunar, teniendo en cuenta los posibles riesgos de eventos adversos graves causados por la vacuna y teniendo en cuenta la edad de los individuos. Massad *et al.* (2017) presenta un modelo para estimar la densidad de mosquitos *Aedes aegypti* a partir de datos sobre la incidencia de un brote de dengue, donde se analizan los riesgos existentes para la ocurrencia de una reintroducción de FA urbana en áreas infestadas de dengue. Codeço *et al.* (2007) ya estudió cuál sería el momento más adecuado para vacunarse contra la FA, comprobando las ventajas y desventajas de vacunarse de forma preventiva o durante un brote en zonas libres de la enfermedad.

Así, este trabajo tiene como objetivo estudiar un modelo matemático que describa la FA. La FA es una enfermedad

vírica hemorrágica transmitida por vectores, que son los mosquitos (principalmente mosquitos *Aedes aegypti*, *Haemagogus* y *Sabethes*), se presenta con mayor frecuencia en las regiones tropicales de África y América, especialmente en América del Sur, y tiene gran importancia epidemiológica, ya que fue la primera enfermedad humana atribuida a un virus (Sacchetto *et al.*, 2020). Según la Organización Panamericana de la Salud – OPS/OMS. (2022), se registran alrededor de 200.000 casos de FA y un total de 30.000 muertes por la enfermedad al año. Por lo general, la enfermedad se desarrolla de manera leve, sin embargo, alrededor del 15 al 25% desarrolla una forma más grave, donde el riesgo de muerte es mayor, según la Organización Panamericana de la Salud – OPS/OMS. (2022). Los síntomas pueden incluir fiebre, dolor de cabeza, dolores musculares, náuseas, vómitos, fatiga, hemorragias en la piel e ictericia. Una vez que el individuo desarrolla la enfermedad, cuando se recupere, adquirirá inmunidad para el resto de su vida. Es importante resaltar que esta enfermedad no tiene un tratamiento específico, solo tiene la vacuna como medio de prevención.

Este trabajo adapta un modelo epidemiológico desarrollado por Esteva *et al.* (2019) que describe la transmisión del virus que causa la FA, incluida la vacunación.

2. METODOLOGÍA

Los modelos matemáticos se han utilizado ampliamente para estudiar la dinámica de la propagación de enfermedades infecciosas. En el caso de la FA, estos modelos matemáticos suelen estar compuestos por ecuaciones diferenciales ordinarias, las cuales se encargan de describir el proceso de transmisión del virus que provoca la enfermedad entre mosquitos, humanos y monos. En la construcción de estos modelos se tienen en cuenta datos biológicos y de comportamiento de las poblaciones involucradas. Con una recopilación de esta información, es posible tener una comprensión más profunda del proceso de transmisión de la enfermedad.

Propuesto originalmente por Esteva *et al.* (2019), este es un modelo compartimental, que considera tres ciclos de transmisión de FA diferentes, cada uno con sus propias particularidades: ciclo epidémico forestal, ciclo entre humanos en la región forestal y ciclo urbano (epidemia de Fiebre Amarilla sostenida por migrantes humanos infecciosos).

En el modelo se considera que todo individuo infectado también es infeccioso y que ningún humano entra al bosque infectado, solo puede salir de él portando la enfermedad. Además, se tiene en cuenta que todas las poblaciones involucradas en la dinámica de transmisión son constantes.

El ciclo epidémico forestal, como su nombre lo indica, ocurre en el bosque y los agentes que participan en esta

etapa son los mosquitos *Haemagogus* (solo se consideró este transmisor) y los monos. Estos últimos, al ser más sensibles a la enfermedad, acaban muriendo más fácilmente, provocando epizootias. Estas epizootias se convierten en un indicador de alerta, ya que suelen preceder a los casos de FA humana (CEVS-RS, 2021), ya que, cuando los mosquitos no encuentran una gran cantidad de monos susceptibles de los que alimentarse, buscan otras alternativas, en este caso humanos, que se vuelven accidentales anfitriones (que es el caso presentado en el próximo ciclo). El ciclo entre humanos en la región forestal también ocurre en la selva y está compuesto por mosquitos *Haemagogus* y seres migrantes humanos, es decir, individuos que originalmente residen en las ciudades, pero que por alguna razón (ya sea por trabajo o por ocio, por ejemplo) necesitaban mudarse al bosque por un cierto período de tiempo. Finalmente, el ciclo urbano se refiere a la transmisión de la FA en las ciudades, provocada, en este modelo, principalmente por el retorno de migrantes humanos desde la región forestal. Este último ciclo merece atención, ya que humanos infectados pueden transmitir el virus de la FA a mosquitos *Aedes aegypti* (transmisores urbanos) sanos, desencadenando así una epidemia de Fiebre Amarilla urbana.

Al insertar la vacunación en el modelo original, se decidió introducirla solo en el medio urbano, ya que el paso de los humanos por la región forestal es transitorio, por un corto período de tiempo en la mayoría de los casos. Asimismo, es importante resaltar que, debido a que el bosque es un lugar más remoto y, muchas veces, de difícil acceso, la llegada y almacenamiento de vacunas podría ser inviable.

Por lo tanto, la dinámica de la FA puede modelarse mediante el siguiente sistema de ecuaciones diferenciales. El ciclo forestal viene dado por:

$$\begin{cases} \frac{ds_w}{dt} = \mu_w - \beta_w s_w y_w - \mu_w s_w, \\ \frac{di_w}{dt} = \beta_w s_w y_w - \gamma_w i_w - \mu_w i_w, \\ \frac{dz_w}{dt} = \gamma_w i_w - \mu_w z_w, \\ \frac{dy_w}{dt} = \alpha_w (1 - y_w) i_w + \alpha_m (1 - y_w) i_m - v_w y_w. \end{cases} \quad (1)$$

El ciclo entre humanos en la región del bosque es:

$$\begin{cases} \frac{ds_m}{dt} = \delta s_u - \beta_m s_m y_w - \varepsilon s_m - \mu_u s_m, \\ \frac{di_m}{dt} = \beta_m s_m y_w - \gamma_u i_m - \varepsilon i_m - \mu_u i_m, \\ \frac{dz_m}{dt} = \delta z_u + \gamma_u i_m - \varepsilon z_m - \mu_u z_m + \delta V_u. \end{cases} \quad (2)$$

El ciclo urbano viene dado por:

$$\begin{cases} \frac{ds_u}{dt} = \mu_u - \beta_u s_u y_u - \mu_u s_u - \delta s_u + \varepsilon s_m - f v s_u, \\ \frac{di_u}{dt} = \beta_u s_u y_u - \gamma_u i_u - \mu_u i_u + \varepsilon i_m, \\ \frac{dz_u}{dt} = -\delta z_u + \varepsilon z_m + \gamma_u i_u - \mu_u z_u, \\ \frac{dy_u}{dt} = \alpha_u (1 - y_u) i_u - v_u y_u, \\ \frac{dV_u}{dt} = f v s_u - \delta V_u - \mu_u V_u. \end{cases} \quad (3)$$

Aquí, las variables s , i y z representan las poblaciones de monos y humanos susceptibles, infectados y recuperados, respectivamente. Se utilizaron los subíndices w , m y u para diferenciar cada uno de los ciclos. Los mosquitos infectados están dados por y (no se consideraron los mosquitos recuperados ya que su vida es muy corta, sin tiempo de recuperación) y la población humana urbana vacunada está dada por V_u . Cabe señalar que $f v s_u$ representa la tasa de población de humanos susceptibles que adquieren inmunidad a través de la vacunación.

Las poblaciones totales de cada ciclo comprenden la suma de los individuos presentes en el mismo y están dadas por: N_w (población de monos), N_m (población de humanos viviendo en el bosque), N_u (población de humanos viviendo en la ciudad), M_w (población de *Haemagogus*), M_u (población de *Aedes aegypti*) y N_h (población humana total, $N_m + N_u$).

Los parámetros considerados anteriormente para modelar el problema son:

- μ - tasa de mortalidad natural,
- v_w - tasa de mortalidad de mosquitos *Haemagogus*,
- v_u - tasa de mortalidad de mosquitos *Aedes aegypti*,
- γ - tasa de recuperación de la población,
- δ - porcentaje de humanos que se mudan al bosque,
- ε - porcentaje de humanos que regresan a la ciudad,
- α - transmisión de poblaciones infectadas a mosquitos,
- β - transmisión de mosquitos a susceptibles,
- f - efectividad de la vacuna,
- v - tasa de vacunación.

Dónde:

$$\begin{aligned} \beta_w &= b_w \bar{\beta}_w \frac{M_w}{N_w + N_m}, & \alpha_w &= b_w \bar{\alpha}_w \frac{N_w}{N_w + N_m}, \\ \beta_m &= b_w \bar{\beta}_m \frac{M_w}{N_w + N_m}, & \alpha_m &= b_w \bar{\alpha}_m \frac{N_h}{N_w + N_m}, \\ \beta_u &= b_u \bar{\beta}_u \frac{M_u}{N_u}, & \alpha_u &= b_u \bar{\alpha}_u \frac{N_h}{N_u}, \end{aligned} \quad (4)$$

con:

- $\bar{\beta}_w$: coeficiente de transmisión de *Haemagogus* para animales del bosque;
- $\bar{\beta}_m$: coeficiente de transmisión del *Haemagogus* para migrantes humanos;
- $\bar{\beta}_u$: coeficiente de transmisión de *Aedes aegypti* para humanos;
- $\bar{\alpha}_w$: coeficiente de transmisión de los monos al *Haemagogus*;
- $\bar{\alpha}_m$: coeficiente de transmisión de migrantes humanos al *Haemagogus*;
- $\bar{\alpha}_u$: coeficiente de transmisión humana para *Aedes aegypti*.

3. RESULTADOS Y DISCUSIÓN

A partir de la resolución de las ecuaciones diferenciales mediante el método de Runge-Kutta de 4° orden y 4 etapas, implementado en el *software* Scilab, fue posible obtener una gráfica del comportamiento de cada una de las poblaciones analizadas, asumiendo que la población urbana es, inicialmente, libre de FA, con circulación de la enfermedad en los demás ciclos.

También se consideró que los migrantes humanos permanecerían un mes en la región de selva ($\varepsilon = 1$) y que la tasa de migración δ es de 0,02, es decir, alrededor del 2% de la población urbana se traslada a la zona de selva, por mes.

Aún así, se consideró que las poblaciones totales cumplen: $N_m = \delta N_u / (\varepsilon + \mu_u)$, $N_w = 0,5N_h$, $M_w = 3N_w$ y $M_u = 2N_h$. Además, se consideró que inicialmente no había vacunas y que la tasa de vacunación era del 50% de la población, con una eficacia del 90%. Es importante señalar que la tasa de vacunación es un parámetro muy variable y puede verse influenciado por múltiples factores. Por tanto, este porcentaje del 50% de la población vacunada sólo se aplica a este caso hipotético y debe analizarse con cautela para simular casos reales. La eficacia de la vacuna es una aproximación a un parámetro ya conocido, ya que la vacuna FA tiene una efectividad de aproximadamente el 95%, según Brasil (2021). El tiempo de simulación fue de 120 meses (10 años). El resto de parámetros utilizados en la simulación se pueden encontrar en Esteva *et al.* (2019) y se pueden ver con más detalle en el apéndice, junto con las condiciones iniciales.

En las Figuras 2 y 3 se puede observar el comportamiento de las poblaciones que participan en los ciclos de FA en ambiente con y sin vacunación, en colores rojo y azul, respectivamente.

Al analizar el comportamiento de las poblaciones, especialmente de las poblaciones humanas que participan de la dinámica de la FA en un ambiente sin vacunación, es posible observar que, aun partiendo de ningún individuo infectado

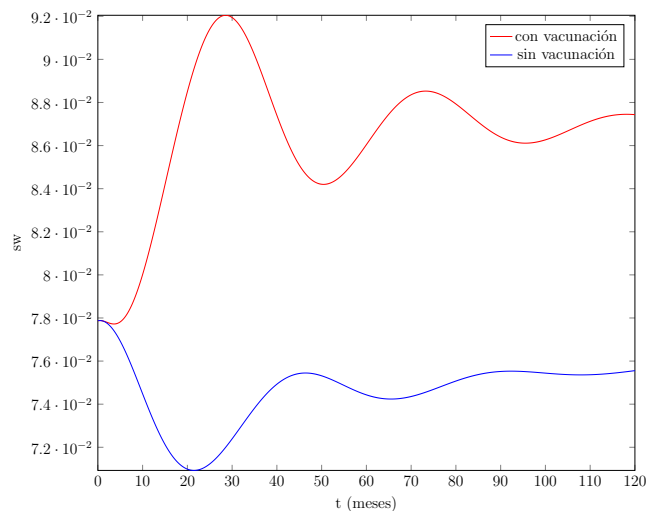


Figura 1: Gráfico del comportamiento de las poblaciones que participan en el ciclo de FA.

en el área urbana (libre de FA), con el tiempo, debido a la migración, la enfermedad se reinserta en el medio urbano, provocando una epidemia. Esta epidemia se puede ver en azul, en la Figura 2f.

Con la inclusión de la vacunación en áreas urbanas, es posible notar que la proporción de humanos susceptibles e infectados disminuye más rápidamente, lo que se puede ver en las Figuras 2 (c), (d), (e) y (f). Una vez que los humanos susceptibles son vacunados, se vuelven inmunes a la FA y no pueden contraer el virus. Así, con el tiempo, más y más personas están siendo vacunadas y, por lo tanto, el número de susceptibles se vuelve cada vez más pequeño. Incluso la disminución de los susceptibles conduce a una rápida disminución del número de personas infectadas, ya que el número de individuos propensos a contraer la enfermedad es menor. El impacto de la vacunación en la población de humanos infectados que residen en áreas urbanas se destaca aquí (Figura 2f).

Las poblaciones de mosquitos infectados también se ven afectadas por la vacunación (Figura 3a y (b)). Se puede observar, en rojo, que hay una disminución en el número de vectores, en ambos casos, y el número de mosquitos infectados en la zona urbana tiende a cero rápidamente. Este último hecho se debe principalmente a la disminución, seguida de la extinción, de humanos infectados en el área urbana (que pueden transmitir el virus a los mosquitos).

Además, al tener en cuenta las poblaciones humanas, se observa que la inserción de la vacunación conduce a una recuperación considerablemente más rápida, en relación al ciclo sin vacunación. Esto se puede ver en la Figura 3d y (e).

4. CONCLUSIONES

Comprender el comportamiento de una enfermedad es extremadamente importante para encontrar formas de prevenirla o incluso erradicarla. Para auxiliar en esta comprensión, se vuelve fundamental el estudio de modelos matemáticos, ya que a través de ellos es posible describir el comportamiento de varias enfermedades infecciosas, teniendo la posibilidad de predecir su propagación así como decidir la mejor estrategia para contenerla, además de poder simular diferentes escenarios, con la inserción de nuevos factores, que pueden llegar a establecerse en esa población.

Con base en un modelo existente, se insertó la variable vacunación y, con ello, fue posible estudiar un modelo epidemiológico para la enfermedad de la FA, teniendo en cuenta el número de vacunados así como la efectividad de la vacuna y, en consecuencia, fue posible verificar cómo estos factores influyen en el control de la infección. De lo anterior, se pudo verificar que el modelo propuesto presenta resultados satisfactorios, indicando que la vacunación es una medida importante en el control de enfermedades, ya que reduce considerablemente las poblaciones de humanos y mosquitos infectados. Es posible notar que, cuando no se aplicaba ninguna medida de control, es decir, cuando aún no se había introducido la vacunación, el proceso de migración terminó por implicar la reinserción de la FA en la zona urbana, provocando una epidemia de la enfermedad. Cuando se tiene en cuenta la vacunación, la epidemia provocada en el área urbana aún se presenta, pero con una duración e intensidad muy bajas. Esta disminución de la intensidad de la epidemia es ciertamente atribuible a la vacunación. En el caso de la Fiebre Amarilla, el papel de la vacunación cobra aún más importancia, ya que no existe un tratamiento específico para la enfermedad, solo medios de prevención, siendo la vacuna el principal.

El contexto abordado en este trabajo, utilizando la migración ciudad-bosque, también puede trasladarse a la movilidad urbana entre barrios o ciudades, lo que permite delinear estrategias de vacunación en áreas metropolitanas.

5. AGRADECIMIENTOS

Agradecemos a GDISPEN, Grupo de Dispersión de Contaminantes e Ingeniería Nuclear de la UFPel, por los valiosos aportes ya CAPES por el apoyo financiero.

A. APÉNDICES

Condiciones iniciales

Las condiciones iniciales utilizadas proceden de cálculos de puntos de equilibrio en diferentes situaciones: para las ecuaciones del ciclo forestal se han utilizado los puntos de equilibrio para el caso en que la FA está circulando únicamente en la zona de bosque (con la excepción de y_w que se calculó sobre la base del estudio de estos puntos); para

el ciclo entre humanos en la región de bosque y para el ciclo urbano, se utilizaron los valores encontrados a través del punto de equilibrio libre de la enfermedad. A continuación se describen las condiciones iniciales utilizadas:

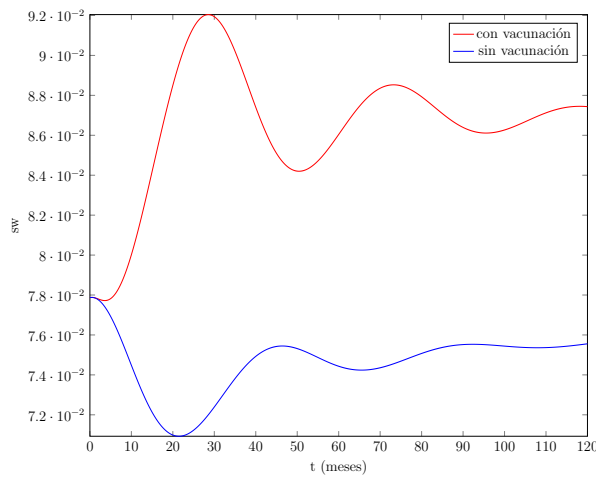
$$\begin{aligned}
 s_w(0) &= \frac{\mu_w}{\beta_w y_w + \mu_w}, \\
 i_w(0) &= \frac{\beta_w \mu_w y_w}{(\beta_w y_w + \mu_w)(\gamma_w + \mu_w)}, \\
 z_w(0) &= 1 - s_w(0) - i_w(0), \\
 y_w(0) &= 0,008203290301, \\
 s_m(0) &= \frac{\delta}{\varepsilon + \mu_u + \delta}, \\
 i_m(0) &= 0, \\
 z_m(0) &= 0, \\
 s_u(0) &= 1 - \frac{\delta}{\varepsilon + \mu_u + \delta}, \\
 i_u(0) &= 0, \\
 z_u(0) &= 0, \\
 V_u(0) &= 0, \\
 y_u(0) &= 0.
 \end{aligned}$$

Parámetros

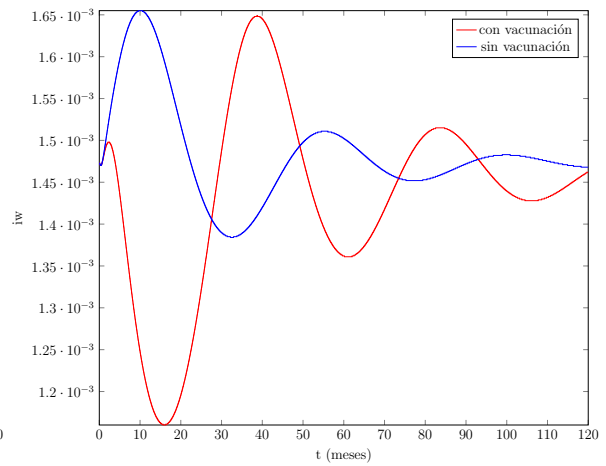
Los parámetros utilizados para la simulación se pueden ver en la siguiente tabla (Tabla 1):

Tabla 1: Parámetros utilizados para la simulación

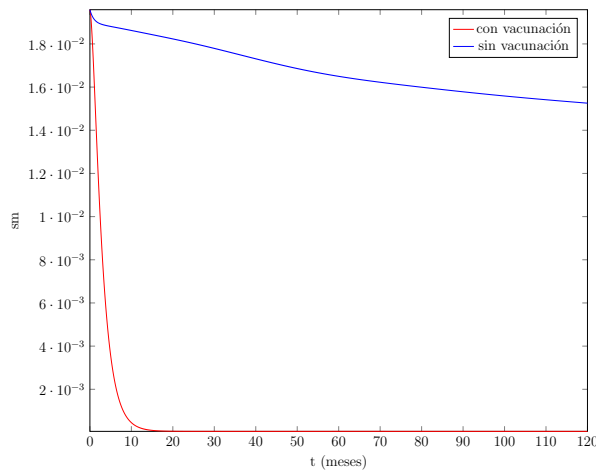
Parámetro	Valor	Referencia
β_w	0,4	Moreno <i>et al.</i> (2015)
β_m	0,25	Esteva <i>et al.</i> (2019)
β_u	0,2	Esteva <i>et al.</i> (2019)
α_w	0,4	Moreno <i>et al.</i> (2015)
α_m	0,4	Esteva <i>et al.</i> (2019)
α_u	0,25	Johnson <i>et al.</i> (2002)
μ_w	0,0048 mês^{-1}	Esteva <i>et al.</i> (2019)
μ_u	0,0012 mês^{-1}	Esteva <i>et al.</i> (2019)
v_w	0,46 mês^{-1}	Raimundo <i>et al.</i> (2016)
v_u	0,913 mês^{-1}	Dengue Vírus Net. (s.d.)
γ_w	3 mês^{-1}	Moreno <i>et al.</i> (2015)
γ_u	4 mês^{-1}	PAHO (2005)
ε	1 mês^{-1}	Esteva <i>et al.</i> (2019)
δ	0,02 mês^{-1}	Esteva <i>et al.</i> (2019)
b_w	6 mês^{-1}	Chadee <i>et al.</i> (1995)
b_u	6 mês^{-1}	Seawright <i>et al.</i> (1997)
f	0,9	Estimado
tv	0,5	Estimado



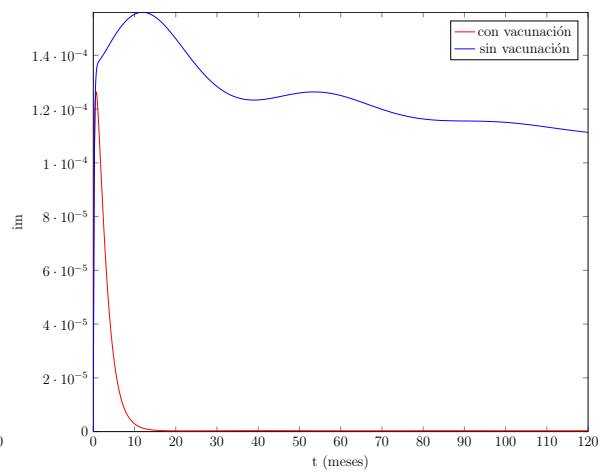
(a) Gráfico de población de monos susceptibles.



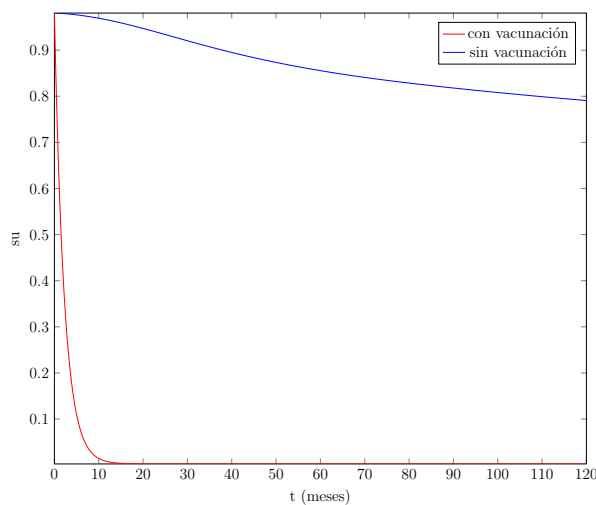
(b) Gráfico de población de monos infectados.



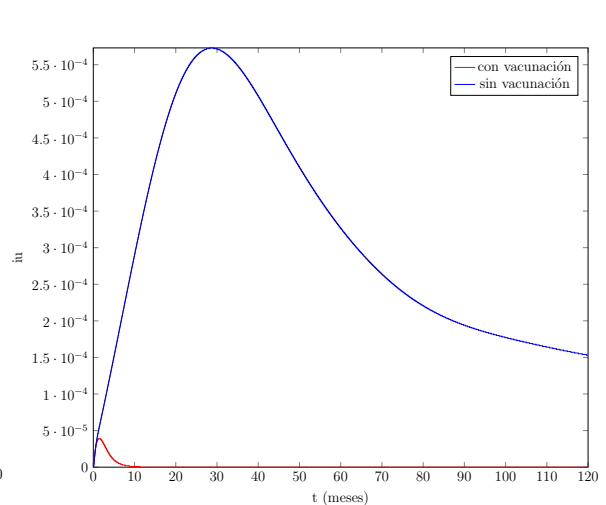
(c) Gráfico de la población de migrantes humanos susceptibles que se encuentran en la región forestal.



(d) Gráfico de la población de migrantes humanos infectados que se encuentran en la región forestal.

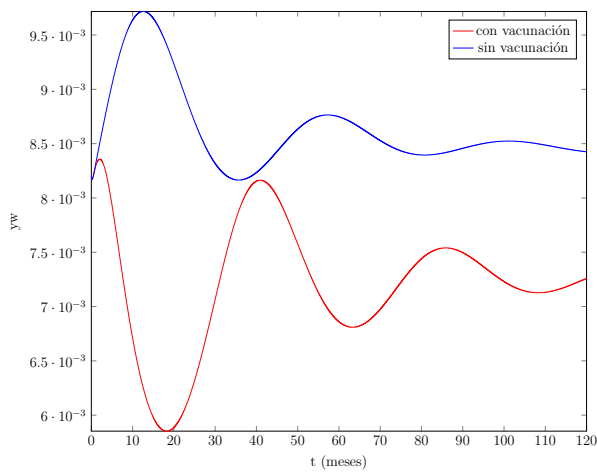


(e) Gráfico de la población de humanos susceptibles que residen en la zona urbana.

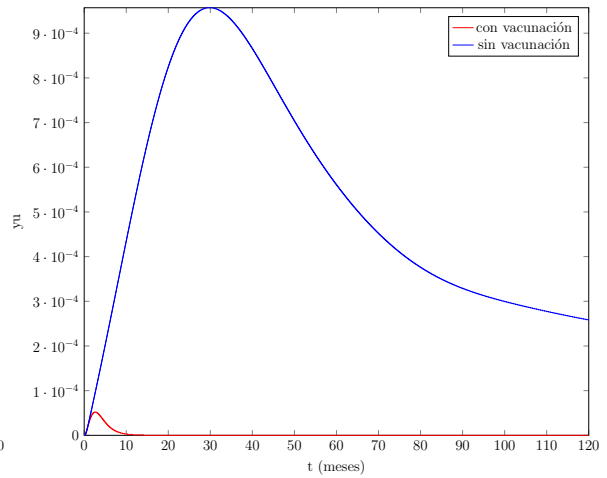


(f) Gráfico de población humana infectada residente en zona urbana.

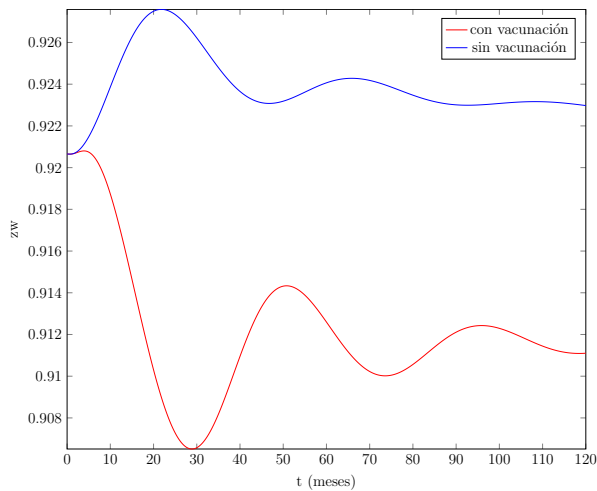
Figura 2: Gráfico del comportamiento de las poblaciones que participan en el ciclo de FA.



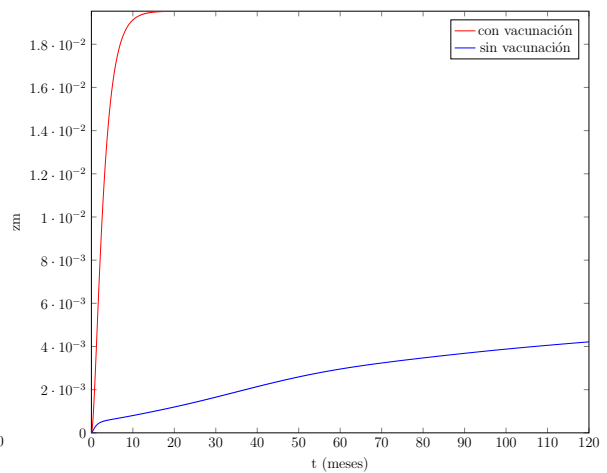
(a) Gráfico de población de mosquitos *Haemagogus* infectados.



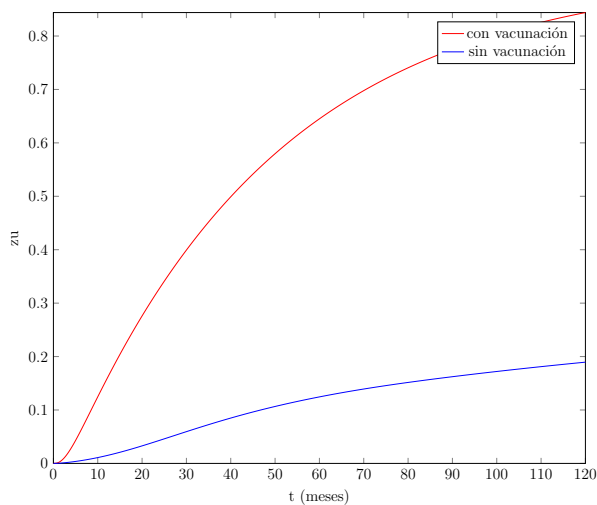
(b) Gráfico de población de mosquitos *Aedes aegypti* infectados.



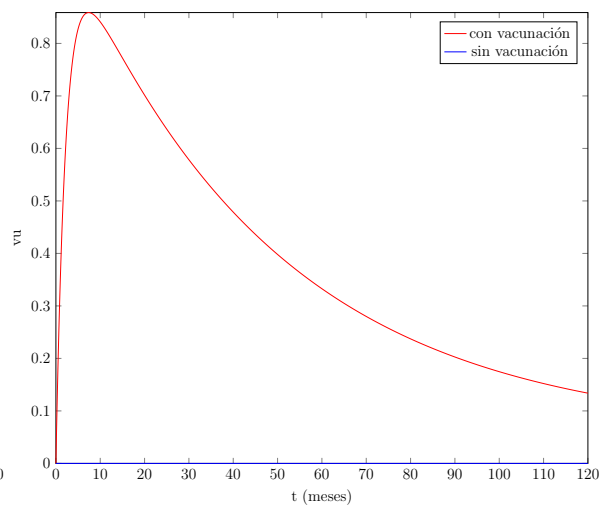
(c) Gráfico de la población de monos recuperados.



(d) Gráfico de la población de migrantes humanos recuperados que se encuentran en la región forestal.



(e) Gráfico de población de humanos recuperados que residen en la zona urbana.



(f) Gráfico de la población vacunada.

Figura 3: Gráfico del comportamiento de las poblaciones que participan en el ciclo de FA.

REFERENCIAS

- Brasil (2021) 'Plano de contingência para resposta às emergências em saúde pública: febre amarela'. Tech. rep., Ministério da Saúde. Secretaria de Vigilância em Saúde. Departamento de Imunização e Doenças Transmissíveis, Brasília.
- CEVS-RS (2021) 'Informativo epidemiológico de arboviroses: Outubro de 2021: Semana epidemiológica 40 (03/10 a 09/10)'. Tech. Rep. 40, Centro Estadual de Vigilância em Saúde do Rio Grande do Sul (CEVS-RS). Governo do Estado do Rio Grande do Sul. Secretaria da Saúde, Rio Grande do Sul.
- Chadee, D., Ganesh, R., Hingwan, J. and Tikasingh, E. (1995) 'Seasonal abundance, biting cycle and parity of the mosquito *Haemagogus leucocelaenus* in trinidad, west indies'. *Medical and Veterinary Entomology*, pp. 372–376.
- Codeço, C.T., Luz, P.M., Coelho, F., Galvani, A.P. and Struchiner, C. (2007) 'Vaccinating in disease-free regions: a vaccine model with application to yellow fever'. *Journal of The Royal Society Interface*, 4(17), pp. 1119–1125. doi:10.1098/rsif.2007.0234.
- Danbaba, U. and Garba, S. (2020) 'Stability analysis and optimal control for yellow fever model with vertical transmission'. *International Journal of Applied and Computational Mathematics*, 6(4), p. 34. doi:10.1007/s40819-020-00860-z.
- Dengue Vírus Net. (s.d.) *Ciclo de vida do Aedes aegypti*. Disponível em: <http://www.denguevirusnet.com/life-cycle-of-aedes-aegypti.html>. Acesso em: 31 jan. 2022.
- Esteva, L., Vargas, C. and Yang, H.M. (2019) 'A model for yellow fever with migration'. *Computational and Mathematical Methods*, 1(6), p. 13. doi:10.1002/cmm4.1059.
- Johnson, B.W., Chambers, T., Crabtree, M.B. *et al.* (2002) 'Vector competence of brazilian *Aedes aegypti* and *Ae. albopictus* for a brazilian yellow fever virus isolate.' *Transactions of the Royal Society of Tropical Medicine and Hygiene*, pp. 611–613.
- Kalra, P. and Ratti, I. (2020) 'Impact of yellow fever with multiple control measures: Mathematical model'. *Journal of Physics: Conference Series*, 1531(1), p. 012066. doi:10.1088/1742-6596/1531/1/012066.
- Martcheva, M. (2015) *An Introduction to Mathematical Epidemiology*. New York: Springer. doi:10.1007/978-1-4899-7612-3.
- Massad, E., Amaku, M., Coutinho, F.A.B., Struchiner, C.J., Lopez, L.F., Wilder-Smith, A. and Burattini, M.N. (2017) 'Estimating the size of aedes aegypti populations from dengue incidence data: Implications for the risk of yellow fever outbreaks'. *Infectious Disease Modelling*, 2(4), pp. 441–454. doi:10.1016/j.idm.2017.12.001.
- Massad, E., Coutinho, F.A.B., Burattini, M.N., Lopez, L.F. and Struchiner, C.J. (2005) 'Yellow fever vaccination: How much is enough?' *Vaccine*, 23(30), pp. 3908–3914. doi:10.1016/j.vaccine.2005.03.002.
- Moreno, E.S., Agostini, I., Holzmann, I., Bitetti, M.S.D. *et al.* (2015) 'Yellow fever impact on brown howler monkeys (*Alouatta guariba clamitans*) in argentina: a metamodeling approach based on population viability analysis and epidemiological dynamics'. *Memórias do Instituto Oswaldo Cruz*, 110(7), pp. 865–876. doi:10.1590/0074-02760150075.
- Organización Panamericana de la Salud – OPS/OMS. (2022) *Febre amarela*. Disponível em: <https://www.paho.org/pt/node/40>. Acesso: 12 feb. 2022.
- PAHO: Pan American Health Organization, (ed.) (2005) *Control of Yellow Fever: Field Guide*, 603. Washington, D.C.: PAHO: Pan American Health Organization. Scientific and Technical Publication.
- Raimundo, S.M., Amaku, M. and Massad, E. (2015) 'Equilibrium analysis of a yellow fever dynamical model with vaccination'. *Computational and Mathematical Methods in Medicine*, 2015, pp. 1–12. doi:10.1155/2015/482091.
- Raimundo, S.M., Yang, H.M. and Massad, E. (2016) 'Modeling vaccine preventable vector-borne infections: yellow fever as a case study'. *Journal of Biological Systems*, 24(02n03), pp. 193–216. doi:10.1142/s0218339016500108.
- Sacchetto, L., Drumond, B.P., Han, B.A., Nogueira, M.L. and Vasilakis, N. (2020) 'Re-emergence of yellow fever in the neotropics — quo vadis?' *Emerging Topics in Life Sciences*, 4(4), pp. 411–422. doi:10.1042/etls20200187.
- Seawright, J., Dame, D. and Weidhaas, D. (1997) 'Field survival and ovipositional characteristics of *Aedes aegypti* and their relation to population dynamics and control'. *Mosquito News*, pp. 62–70.




Citación recomendada: Pitol, L. *et al.* (2023). '*Modelamiento Matemático de la Fiebre Amarilla: un modelo con migración*'. Rev. model. mat. sist. biol. 3(E), e23E02, doi:10.58560/rmmsb.v03.n02.023.05



This open access article is licensed under a Creative Commons Attribution International (CC BY 4.0) <http://creativecommons.org/licenses/by/4.0/>.
Support:

Pattern Formation in a Resource and Two Consumers Discrete Model

Formación de Patrones en un Modelo Discreto de un Recurso y dos Consumidores

 Poliana Kenderli Pacini Selau^{1,2},  Diomar Cristina Mistro² and
 Luiz Alberto Díaz Rodrigues²

✉ Poliana Selau: poli.kenderli@outlook.com

¹ Departamento de Matemática,
Universidade Federal do Rio Grande do Sul,
Porto Alegre, Brasil

² Departamento de Matemática,
Universidade Federal de Santa Maria,
Santa Maria, Brasil

Recepción: 2023-04-05 | Aceptación: 2023-08-21 | Publicación: 2023-10-29

Recommended Citation: Pacini Selau, P. *et al.* (2023). 'Pattern Formation in a Resource and Two Consumers Discrete Model'. Rev. model. mat. sist. biol. 3(E), e23E03, doi:10.58560/rmmsb.v03.n02.023.02



This open access article is licensed under a Creative Commons Attribution International (CC BY 4.0) <http://creativecommons.org/licenses/by/4.0/>. Support: CAPES - Code 001.

ABSTRACT

In this work, we propose a Coupled Map Lattice model to analyse the spatio-temporal dynamics of a system of three interacting species: a resource species and two consumers. The resource is an insect with potential to become an agriculture pest while one of the consumers is a parasitoid and the other, is a predator. All the three species reproduce at the same time scale so that the dynamics is described by a system of three difference equations. The resource grows according to the Beverton-Holt function and the consumption is described by the Holling type III functional response. By means of numerical simulations, we observed that the pattern of species spatial distribution and the temporal density depend on the dynamical as well as on the movement parameters. It can be stable or oscillating heterogeneous spatial distributions but the species can also be homogeneously distributed in space. Finally, we observe that the inclusion of the space does not change the forecast of extinction obtained by the local dynamics only for some parameters.

Keywords:

Coupled Map Lattice, Discrete Models, Resource Consumers models

RESUMEN

En este trabajo proponemos un modelo del tipo Redes de Mapas Acoplados para analizar la dinámica espacio-temporal de un sistema de tres especies interactuantes: una especie recurso y dos consumidores. El recurso es un insecto con potencial para convertirse en plaga agrícola, mientras que uno de los consumidores es un parasitoide y el otro, un depredador. Las tres especies se reproducen en la misma escala temporal, de modo que la dinámica se describe mediante un sistema de tres ecuaciones en diferencias. La especie recurso crece según la función de Beverton-Holt y el consumo se describe mediante la respuesta funcional Holling tipo III. Mediante simulaciones numéricas, observamos que el patrón de distribución espacial de las especies y la densidad temporal dependen tanto de los parámetros de la dinámica como de los de movimiento. Pueden surgir distribuciones espaciales heterogéneas estables u oscilantes, pero las especies también pueden distribuirse homogéneamente en el espacio. Por último, observamos que la inclusión del espacio no modifica la previsión de extinción obtenida únicamente por la dinámica local para algunos parámetros.

Palabras Claves:

Redes de Mapas Acoplados, Modelos Discretos, Modelos Recurso Consumidores

2020 AMS Mathematics Subject Classification: Primary: 92B05; Secondary: 92C42

1 INTRODUCTION

Natural enemies of insects represent an important tool to control insect pest populations in agriculture. They can help keeping the insect pest at acceptable densities and hence, decrease the input of pesticides. Before introducing biological species in the environment, it is important to study the dynamics in order to avoid undesirable effects such the extinction of non target species, for example. Most studies on biological control deal with the interaction of an insect pest and just one enemy. However, in natural habitats, communities of many different species interact and the use of multiple controlling agents in biological control is an important topic for theoretical investigation (Hassel and May, 1986; Jones *et al.*, 1993; Hassell, 2000).

In the present work, we propose a discrete spatio-temporal model to study the dynamics of three interacting species: a resource species and two specialist consumers. The resource species has potential to become an agriculture pest while the consumers are the pest natural enemies. It can be, for example, a rodent and two predators or an insect pest and two parasitoids. For making the description and the interpretation easier, we suppose that the resource species is an insect pest; one of the consumers is a parasitoid and the other is a predator. The resource species participates in the interaction as host and prey at the same time; however, we will refer to it by resource species in order to avoid any confusion. The resource growth process is represented by the Beverton-Holt model and its consumption by both enemies is described by the discrete equivalent to the Holling type III functional response (Kot, 2001). We also assume that all the three species grow at the same time scale.

When the environment is markedly discrete and that the dynamical processes occur at well defined time stages, a model formulated in terms of Coupled Map Lattices (CML) provide a good description (Comins *et al.*, 1992).

The paper is organized as follows: in the *Coupled Map Lattice Model* Section we describe the CML model, the local dynamics and the movement stage. In the section *Results* we present the results of numerical implementations of the proposed model while in the section *Conclusions*, we discuss the results and make conclusions from the ecological point of view.

2 COUPLED MAP LATTICE MODEL

The proposed CML model assumes a two dimensional spatial domain, split in sites arranged as a lattice where each site is identified by the index (i, j) . The state of the site (i, j) is described by three values corresponding to the species density in the site. The dynamics is composed by two different stages: the movement stage and the reaction stage which occurs alternately (?).

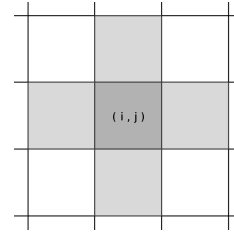


Figure 1: von Neumann neighbourhood (gray sites) of site (i, j) .

During the movement stage, the individuals of each species disperse and are redistributed in the lattice. Several mechanisms can promote the individuals movement such as a random movement in homogeneous habitat; biased movement due to attraction to some source of food as well as repulsion to toxic substances or enemies; it can also be due convection of the fluid where individuals leave such as the wind or a river stream (Edelstein-Keshet, 1998). Here, we consider that the environment is homogeneous and individuals move randomly to its neighbours.

We define the neighbourhood $V_{i,j}$ of site (i, j) as those sites for which the individuals at site (i, j) can migrate. Here we consider that individuals, of all the three species, at a site can migrate to the four nearest sites. That is, we consider the von Neumann neighbourhood defined by:

$$V_{i,j} = \{(i-1, j); (i+1, j); (i, j-1); (i, j+1)\},$$

and illustrated in Figure 1.

We represent by $N'_{i,j,t}$ the density of the resource species and by $P'_{i,j,t}$ and $W'_{i,j,t}$ the density of the parasitoid and predators, respectively, in the site (i, j) , after the movement stage of generation t . At each generation, during the movement stage, a constant fraction of each species: β_N for the resource, β_P for the parasitoid and β_W for the predator, leaves the site (i, j) and evenly migrates to the sites of $V_{i,j}$. Hence, a fraction $1 - \beta_x$, (where $x = N, P$ or W) of each population remains in the site (i, j) .

The equations for the proposed movement stage are:

$$\begin{cases} N'_{i,j,t} = (1 - \beta_N)N_{i,j,t} + \sum_{(x,y) \in V_{i,j}} \frac{\beta_N}{4} N_{x,y,t} \\ P'_{i,j,t} = (1 - \beta_P)P_{i,j,t} + \sum_{(x,y) \in V_{i,j}} \frac{\beta_P}{4} P_{x,y,t} \\ W'_{i,j,t} = (1 - \beta_W)W_{i,j,t} + \sum_{(x,y) \in V_{i,j}} \frac{\beta_W}{4} W_{x,y,t} \end{cases} \quad (1)$$

Moreover equations (1), we consider reflective boundary conditions, so that the fraction β_x ($x = N, P, W$) of individuals located at a boundary site migrate to the three (or two, for the sites in the four corners of the domain) neighbouring sites.

That is, we suppose that the environment is uninhabitable outside the domain and that individuals can sense the habitat quality and decide do not leave it.

After the movement stage, all the interactions occur locally in each site: growth, intra-specific competition of the resource individuals, parasitism and predation. The proposed nondimensional equations for the dynamics are given by:

$$\begin{cases} N_{i,j,t+1} = N'_{i,j,t} f(N'_{i,j,t}) g_1(N'_{i,j,t}, P'_{i,j,t}) g_2(N'_{i,j,t}, W'_{i,j,t}) \\ P_{i,j,t+1} = B_1 N'_{i,j,t} (1 - g_1(N'_{i,j,t}, P'_{i,j,t})) \\ W_{i,j,t+1} = B_2 N'_{i,j,t} (1 - g_2(N'_{i,j,t}, W'_{i,j,t})), \end{cases} \quad (2)$$

where $N_{i,j,t+1}$ is the resource density, $P_{i,j,t+1}$ and $W_{i,j,t+1}$ are the density of the consumers at site (i, j) at the beginning of generation $t + 1$, after the reactions have taken place. B_1 is the number of the parasitoid viable eggs in one resource individual and B_2 represents the predator growth factor. Function $f(N)$ which describes the resource growth, $g_1(N, P)$ and $g_2(N, W)$ which represent the resource density that escape from parasitism and predation, respectively, are given by

$$\begin{aligned} f(N) &= \frac{\lambda}{1 + (\lambda - 1) \frac{N}{k}}, \\ g_1(N, P) &= e^{\left(\frac{-a_1 NP}{1 + (e_1 N)^2} \right)}, \\ g_2(N, W) &= e^{\left(\frac{-a_2 NW}{1 + (e_2 N)^2} \right)}, \end{aligned} \quad (3)$$

where $\lambda, k, a_1, e_1, a_2$ and e_2 are positive parameters.

In the absence of the consumers, the resource grows according to the Beverton-Holt function $f(N)$, which is equivalent to the continuous logistic growth. $\lambda > 1$ is the resource species intrinsic growth rate and k is its carrying capacity. We assume that predators and parasitoids consume the resource with Holling type III functional response. $N(1 - g_x(N, 1))$, $(x = 1, 2)$, is a sigmoidal curve which describes the density of the resource species captured by one consumer during one generation (see Figure 2). It assumes that the consumer is inefficient at low resource densities. On the other hand, consumers have a saturation effect at high resource densities. $\frac{a_x}{(e_x)^2}$, $(x = 1, 2)$, represents the maximum density of the resource species captured by one predator (or killed by one parasitoid) during one generation (Kot, 2001). That is, $\lim_{N \rightarrow +\infty} N(1 - g_x(N, 1)) = \frac{a_x}{e_x^2}$, $(x = 1, 2)$. $\frac{1}{e_x}$ $(x = 1, 2)$ corresponds to the resource density for which the fraction that is captured $(1 - g_x(N, 1))$ by one parasitoid is maximum; that is, $\frac{1}{e_x}$ $(x = 1, 2)$ is the point of maximum of function $1 - g_x(N, 1)$.

In order to identify the relevant groups of parameters, we introduce the nondimensional variables $n_{i,j,t} = e_2 N_{i,j,t}$, $p_{i,j,t} = \frac{e_2}{B_1} P_{i,j,t}$ and $w_{i,j,t} = \frac{a_2}{e_2} W_{i,j,t}$ in system (2) to obtain the

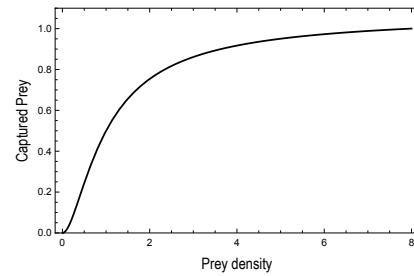


Figure 2: Holling type III functional response: density of resource captured by one predator (or killed by one parasitoid) during a generation. That is, $N(1 - g_x(N, 1))$ where $x = 1, 2$.

following nondimensional equations for the dynamical stage:

$$\begin{cases} n_{i,j,t+1} = n'_{i,j,t} F(n'_{i,j,t}) G_1(n'_{i,j,t}, p'_{i,j,t}) G_2(n'_{i,j,t}, w'_{i,j,t}), \\ p_{i,j,t+1} = n_{i,j,t} (1 - G_1(n'_{i,j,t}, p'_{i,j,t})), \\ w_{i,j,t+1} = \mu_2 n'_{i,j,t} (1 - G_2(n'_{i,j,t}, w'_{i,j,t})), \end{cases} \quad (4)$$

where $n_{i,j,t+1}$ is the resource density, $p_{i,j,t+1}$ and $w_{i,j,t+1}$ are the density of the consumers at site (i, j) at the beginning of generation $t + 1$, after the reactions have taken place. Function $F(n)$ which describes the resource growth, $G_1(n, p)$ and $G_2(n, w)$ which represent the resource density that escape from parasitism and predation, respectively, are given by

$$\begin{aligned} F(n) &= \frac{\lambda}{1 + (\lambda - 1) \frac{n}{\alpha_2}}, \\ G_1(n, p) &= e^{\left(\frac{-\mu_1 np}{1 + \alpha_1 n^2} \right)}, \\ G_2(n, w) &= e^{\left(\frac{-mw}{1 + n^2} \right)}. \end{aligned} \quad (5)$$

The nondimensional parameters are $\mu_1 = \frac{B_1 a_1}{(e_2)^2}$, $\mu_2 = \frac{B_2 a_2}{(e_2)^2}$, $\alpha_1 = \left(\frac{e_1}{e_2}\right)^2$ and $\alpha_2 = e_2 k$.

We observe that the equations for the movement stage (1) in the nondimensional variables do not change.

3 RESULTS

Initially, we study the local dynamics. At each site (i, j) , the system (4) - (5) has five equilibrium solutions:

- $P_1 = (0, 0, 0)$, the trivial equilibrium;
- $P_2 = (\alpha_2, 0, 0)$, the resource only equilibrium;
- $P_3 = (\bar{n}, \bar{p}, 0)$, the predator extinction equilibrium;
- $P_4 = (\bar{n}, 0, \bar{w})$, the parasitoid extinction equilibrium and
- $P_5 = (\bar{n}, \bar{p}, \bar{w})$, the coexistence equilibrium.

The standard Jury criterion for linear stability analysis, indicates that P_1 is never stable, since $\lambda > 1$. P_2 is linearly asymptotically stable given that:

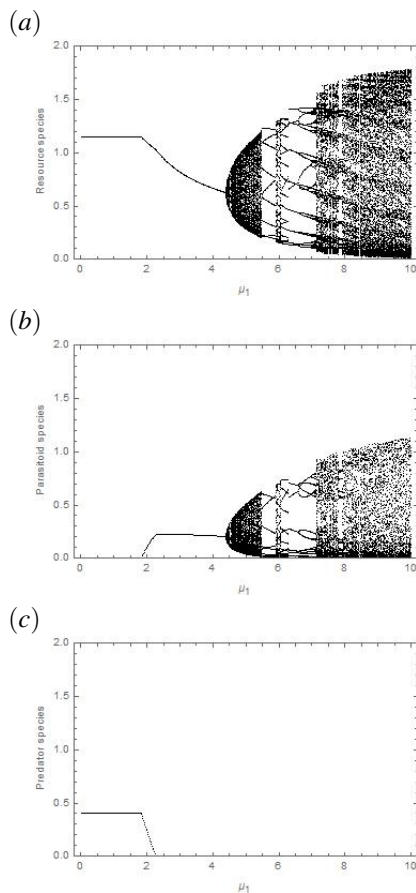


Figure 3: Bifurcation diagrams with respect to μ_1 for (a) resource species, (b) parasitoid and (c) predator, with $\alpha_1 = 1.0764$, $\alpha_2 = 1.8$, $\mu_2 = 1.94$ and $\lambda = 2$.

- 1) $\lambda > 1$;
- 2) $\alpha_2^2(\mu_1 - \alpha_1) < 1$ and
- 3) $\alpha_2^2(\mu_2 - \alpha_1) < 1$.

Due to the complexity of the expressions in system (4) - (5), it is not possible to find neither the analytical expressions for P_3 , P_4 and P_5 nor the conditions for their stability. Numerical simulations indicate the existence and stability of these equilibria as well as p -cycles and periodic limit cycles solutions. Figure 3 illustrates the typical behaviour observed in the dynamics through bifurcation diagrams of the populations with respect to μ_1 . For small values of μ_1 , P_4 is stable; as μ_1 increases, the three species coexist and P_5 is stable. Further increase in μ_1 , which means that the parasitoid effectiveness increases, promotes the extinction of the predator population and then P_3 is stable until a bifurcation leads to the emergence of limit cycles.

In order to study the spatio-temporal dynamics of model (1), (4) and (5), we developed numerical simulations in a 50×50 square lattice for several different dynamical

and movement parameters. Our main interest is identify heterogeneous spatial distribution of the species. All the simulations start from a heterogeneous small perturbation of the asymptotic solution $(\bar{n}, \bar{p}, \bar{w})$, numerically obtained for each set of parameters. That is, $n_{i,j,0} = \bar{n}(1 + 0,1 \xi_{i,j}^1)$; $p_{i,j,0} = \bar{p}(1 + 0,1 \xi_{i,j}^2)$; $w_{i,j,0} = \bar{w}(1 + 0,1 \xi_{i,j}^3)$, where ξ^1 , ξ^2 , $\xi^3 \in [-1, 1]$ are randomly chosen according to the uniform distribution. For dynamical parameters for which the equilibrium is stable, the initial distribution corresponds to a small perturbation of the equilibrium in each site. On the other hand, for parameters promoting oscillating cycles (p -cycles or limit cycles), the initial value in each site corresponds to a perturbation of a solution value.

The classical Turing type patterns appearing in predator-prey systems occur for dynamical parameters for which the local equilibrium is stable. Moreover, movement parameters of prey and predators must be different (Edelstein-Keshet, 1988). In discrete models, heterogeneous patterns in predator prey models have been found from perturbations of the stable equilibrium along with discrepant movement parameters for prey and predators (Rodrigues et al., 2011). Heterogeneous spatial distributions for predator and prey have also been found close to Neimark-Sacker bifurcations (Rodrigues et al., 2011). Since we do not have an analytical criterion for pattern formation with three species in discrete models, we consider the dynamics in different regions of the dynamical parameters space and the movement parameters with different magnitude for the three species.

We present the spatial distribution of the species through density plots in which the dark (light) gray tones indicate high (low) densities. We also show graphs of the total density of each species over time.

In a first numerical experiment, we consider dynamical parameters for which the local coexistence of the three species is stable, that is, $\mu_1 = 2$, $\mu_2 = 1.94$, $\alpha_1 = 1.0764$, $\alpha_2 = 1.8$ and $\lambda = 2$. Furthermore, movement parameters for each species were taken as $\beta_n = 0.91$, $\beta_p = 0.01$ and $\beta_w = 0.01$. The Figure 4 illustrates heterogeneous spatial distribution of the resource (a), parasitoids (b) and predators (c) at time-step $t = 600$. The pattern obtained also depend on the initial perturbation of the species however, the type of pattern is related to the parameters. Figure 5 shows that the total population remains constant over time.

In order to investigate the effects of the movement parameters on the spatio-temporal dynamics, we fixed the dynamical parameters as those in Figure 4 and simulate the equations for different values of β_x . Heterogeneous patterns were obtained when both consumers move at low rates. We obtained homogeneous distributions of the species when at least one of the consumers move at high rate (see Table 1).

Figure 6 shows the spatial distribution of the resource species for $\mu_1 = 4.5$, $\mu_2 = 1.94$, $\alpha_1 = 1.0764$, $\alpha_2 = 1.8$

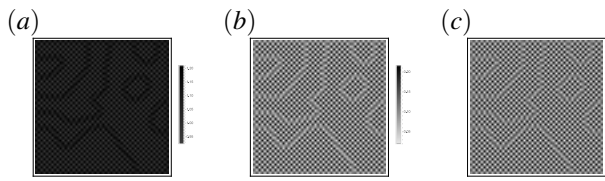


Figure 4: Spatial distribution of: (a) resource species, (b) parasitoids (c) predators, at $t = 600$, for $\mu_1 = 2$, $\mu_2 = 1.94$, $\alpha_1 = 1.0764$, $\alpha_2 = 1.8$, $\lambda = 2$, $\beta_n = 0.91$, $\beta_p = 0.01$ and $\beta_w = 0.01$.

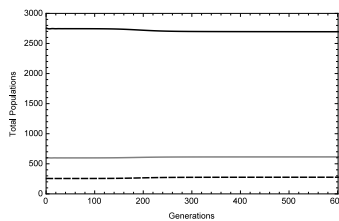


Figure 5: Total populations of the resource species (solid black curve), the parasitoids (dashed curve) and predators (gray curve). The parameters are: $\mu_1 = 2$, $\mu_2 = 1.94$, $\alpha_1 = 1.0764$, $\alpha_2 = 1.8$, $\lambda = 2$, $\beta_n = 0.91$, $\beta_p = 0.01$ and $\beta_w = 0.01$.

Table 1: Spatial distribution for different values of β , with $\mu_1 = 2$, $\mu_2 = 1.94$, $\alpha_1 = 1.0764$, $\alpha_2 = 1.8$ and $\lambda = 2$.

Values of β	Spatial distribution
$\beta_n = 0.01; \beta_p = 0.91; \beta_w = 0.01$	Homogeneous
$\beta_n = 0.01; \beta_p = 0.01; \beta_w = 0.91$	Homogeneous
$\beta_n = 0.91; \beta_p = 0.91; \beta_w = 0.01$	Homogeneous
$\beta_n = 0.01; \beta_p = 0.91; \beta_w = 0.91$	Homogeneous

and $\lambda = 2$, and different values of the movement parameters. For this set of dynamical parameters, the resource and parasitoids species oscillate while the predator species goes extinct in the local dynamics. The spatio-temporal dynamics of the CML, on the other hand, depends on the movement parameters. However, the predator species did not persist for any of the movement rate used in our simulations. The resource and parasitoid spatial distributions exhibited either homogeneous or heterogeneous distributions. Homogeneous distributions were obtained when resource species and parasitoid movement rate were close to each other (for example: $\beta_n = 0.01$; $\beta_p = 0.01$; $\beta_w = 0.9$; and $\beta_n = 0.91$; $\beta_p = 0.98$; $\beta_w = 0.01$, which are not illustrated here for the sake of brevity). On the other hand, when their movement rate were significantly different, heterogeneous distributions were observed (Fig. 6). Since the parasitoid spatial distribution is very similar to the resource one, Figure 6 only presents the spatial distribution of the resource species. Figure 7 illustrates the corresponding total population of the resource species (black continuous curve) and parasitoids (dashed curve). We can observe that the amplitude

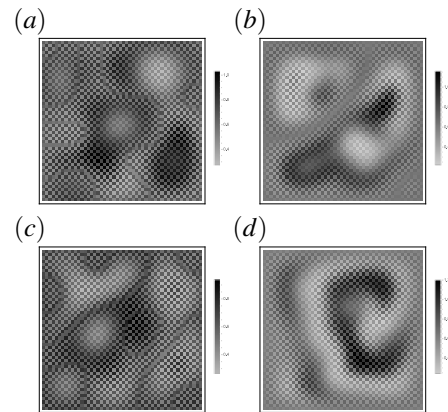


Figure 6: Spatial distribution of the resource species at $t = 600$, for dynamical parameters $\mu_1 = 4.5$, $\mu_2 = 1.94$, $\alpha_1 = 1.0764$, $\alpha_2 = 1.8$ and $\lambda = 2$ and different sets of the movement parameter β :

- (a) $\beta_n = 0.91$; $\beta_p = 0.01$; $\beta_w = 0.01$;
- (b) $\beta_n = 0.01$; $\beta_p = 0.98$; $\beta_w = 0.01$;
- (c) $\beta_n = 0.91$; $\beta_p = 0.01$; $\beta_w = 0.9$;
- (e) $\beta_n = 0.01$; $\beta_p = 0.98$; $\beta_w = 0.9$;

of population oscillations depends on the movement parameters. It is worth noting that Figure 7(e) and (f) correspond to oscillations with homogeneous spatial distributions (spatial distributions are not illustrated in Fig. 6). That is, the populations oscillate in time with the same density in all the sites of the habitat.

We now perform the simulation with parameters for which the local dynamics shows p -cycles of the resource and the predator populations while the parasitoid goes extinct: $\alpha_1 = 1.0764$, $\alpha_2 = 1.8$, $\mu_1 = 1.84$, $\mu_2 = 5.7$ and $\lambda = 2$. The results of spatial model with this set of parameters depend on the species movement rate. Figure 8 shows the resource heterogeneous spatial distributions for different values of β_x ($x = n, p, w$). The predator distribution in space follows the resource one while the parasitoid goes extinct as it occurs in the local dynamics. The total population oscillates with amplitude dependent on the movement parameters (Figure 9). Oscillations with the species homogeneously distributed in space were obtained for movement parameters:

- $\beta_n = 0.91; \beta_p = 0.01; \beta_w = 0.9$;
- $\beta_n = 0.01; \beta_p = 0.01; \beta_w = 0.9$; and
- $\beta_n = 0.01; \beta_p = 0.98; \beta_w = 0.9$.

Figure 9 shows the total population for these parameters; however the corresponding spatial homogeneous distribution are not illustrated in the Figure 8.

We finally simulated the system with parameters for which all the three species persist oscillating when space is not considered: $\mu_1 = 1.84$, $\mu_2 = 1.94$, $\alpha_1 = 1.0764$, $\alpha_2 = 4$ and $\lambda = 2$. The results of the CML model simulations reveal that, depending on the species movement parameters, either

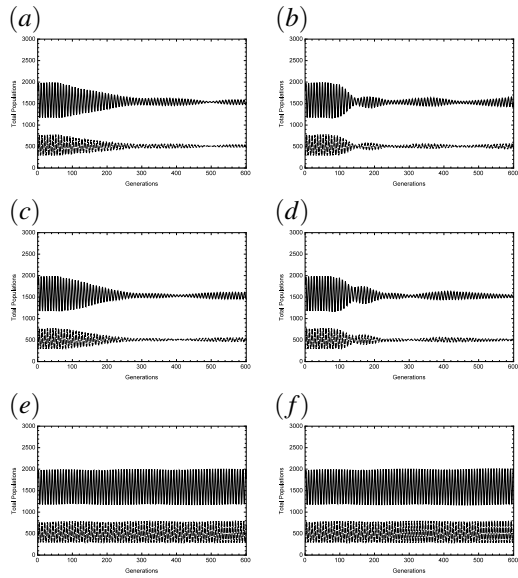


Figure 7: Total populations of the resource species (continuous black curve), parasitoid (dashed curve) and predator species (gray curve) for $\mu_1 = 4.5, \mu_2 = 1.94, \alpha_1 = 1.0764, \alpha_2 = 1.8$ and $\lambda = 2$ and different sets for the movement parameters β :

- (a) $\beta_n = 0.91; \beta_p = 0.01; \beta_w = 0.01;$
- (b) $\beta_n = 0.01; \beta_p = 0.98; \beta_w = 0.01;$
- (c) $\beta_n = 0.91; \beta_p = 0.01; \beta_w = 0.9;$
- (d) $\beta_n = 0.01; \beta_p = 0.98; \beta_w = 0.9;$
- (e) $\beta_n = 0.01; \beta_p = 0.01; \beta_w = 0.9;$
- (f) $\beta_n = 0.91; \beta_p = 0.98; \beta_w = 0.01.$

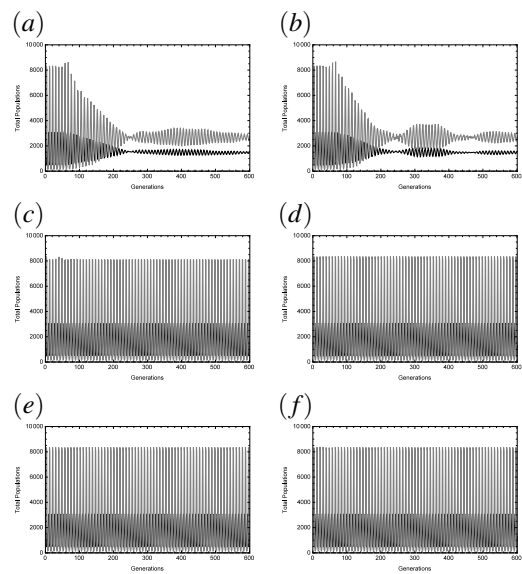


Figure 9: Total populations of the resource species (continuous black curve), the parasitoid species (dashed curve) and the predator species (gray curve) for $\mu_1 = 1.8, \mu_2 = 5.7, \alpha_1 = 1.0764, \alpha_2 = 1.8$ and $\lambda = 2$, and different sets of values for β :

- (a) $\beta_n = 0.91; \beta_p = 0.01; \beta_w = 0.01;$
- (b) $\beta_n = 0.91; \beta_p = 0.98; \beta_w = 0.01;$
- (c) $\beta_n = 0.01; \beta_p = 0.98; \beta_w = 0.01;$
- (d) $\beta_n = 0.91; \beta_p = 0.01; \beta_w = 0.9;$
- (e) $\beta_n = 0.01; \beta_p = 0.01; \beta_w = 0.9;$
- (f) $\beta_n = 0.01; \beta_p = 0.98; \beta_w = 0.9.$

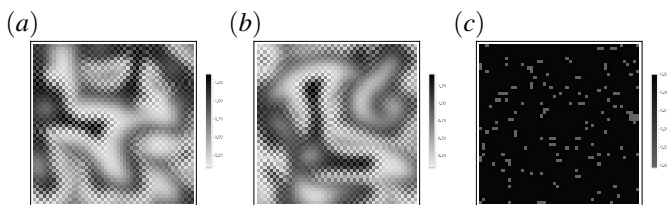


Figure 8: Spatial distribution of resource species at $t = 600$ for $\mu_1 = 1.84, \mu_2 = 5.7, \alpha_1 = 1.0764, \alpha_2 = 1.8$ and $\lambda = 2$ and different sets of values for β :

- (a) $\beta_n = 0.91; \beta_p = 0.01; \beta_w = 0.01;$
- (b) $\beta_n = 0.91; \beta_p = 0.98; \beta_w = 0.01;$
- (c) $\beta_n = 0.01; \beta_p = 0.98; \beta_w = 0.01;$

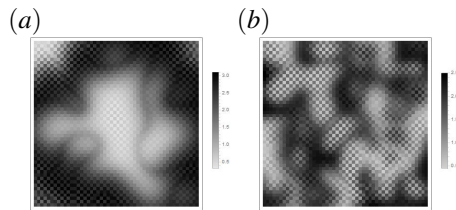


Figure 10: Spatial distribution of resource species at $t = 600$ for $\mu_1 = 1.84$, $\mu_2 = 1.94$, $\alpha_1 = 1.0764$, $\alpha_2 = 4$ and $\lambda = 2$ for the different sets of values of β :

- (a) $\beta_n = 0.91$; $\beta_p = 0.01$; $\beta_w = 0.01$;
- (b) $\beta_n = 0.01$; $\beta_p = 0.01$; $\beta_w = 0.9$.

heterogeneous (see Figure 10) or homogeneous distributions can be obtained. The total populations also oscillate with great amplitude when the distribution is homogeneous (Fig. 11(e) and (f)).

4 CONCLUSIONS

We proposed a CML model for three interacting species in order to analyse the spatio-temporal dynamics of a resource species consumed by two natural enemies: a parasitoid and a predator. The resource species grows according to the Beverton-Holt dynamics while it is consumed through the Holling type III functional response by the two enemies that, implicitly compete exploiting the same resource.

Unfortunately the complexity of the equations for the local dynamics does not allow analytical results. However, through numerical simulations we observed that the local dynamics exhibit coexistence of the three species, which can be either stable or oscillating; coexistence of the resource species and one of the consumers, that is, depending on the parameters, either the parasitoid or the predator can go extinct; extinction of both the consumers and persistence of the resource only.

In the results obtained in our simulations, the movement of the species did not change the local forecast of extinction. That is, when the local dynamics results in the extinction of one the species, the CML model also lead to the extinction of this species regardless its movement rate. It is important to emphasize that this conclusion is limited to the simulations carried out, the extinction forecast of the local model can be changed for other combinations of the parameters. Oscillating local dynamics also oscillates with space with amplitude dependent on the movement parameters.

If from one hand side, the movement parameters do not change the dynamics, on the other hand side, they determine the spatial distribution of the species, whether heterogeneous or homogeneous. Heterogeneous distributions require discrepancy between the species movement rate. However,

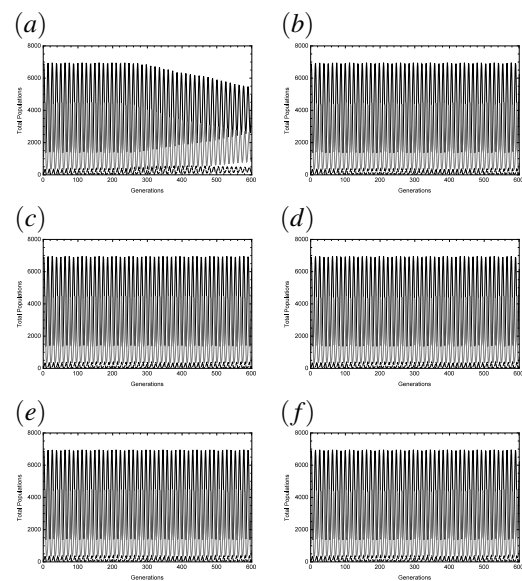


Figure 11: Total populations of the resource species (continuous black curve), the parasitoid species (dashed curve) and the predator species (gray curve) for $\mu_1 = 1.8$, $\mu_2 = 1.94$, $\alpha_1 = 1.0764$, $\alpha_2 = 4$ and $\lambda = 2$, and different sets of values for β :

- (a) $\beta_n = 0.91$; $\beta_p = 0.01$; $\beta_w = 0.01$;
- (b) $\beta_n = 0.01$; $\beta_p = 0.01$; $\beta_w = 0.9$;
- (c) $\beta_n = 0.91$; $\beta_p = 0.01$; $\beta_w = 0.9$;
- (d) $\beta_n = 0.01$; $\beta_p = 0.98$; $\beta_w = 0.01$;
- (e) $\beta_n = 0.01$; $\beta_p = 0.98$; $\beta_w = 0.9$;
- (f) $\beta_n = 0.91$; $\beta_p = 0.98$; $\beta_w = 0.01$.

this is not enough and there is no straightforward relation between the parameters to guarantee the existence of heterogeneous patterns. A criterion for pattern formation induced by diffusion in discrete models can be found for two interacting species (see Rodrigues *et al.* (2011)); however, we do not know, to the best of our knowledge, a similar criterion for three interacting species.

From the ecological point of view, our results suggest that it is necessary to take care with the introduction of two species for the biological control of a pest species since one of the consumers can lead the other to extinction, unless they have similar performance in terms of effectiveness of the resource consumption. The advantages of two natural enemies in biological pest control then demand more investigation and the study of more specific situation are recommended.

SUPPORT

This study was financed in part by the Coordenação de Aperfeiçoamento de Pessoal de Nível Superior – Brasil (CAPES) – Finance Code 001.

REFERENCES

- Comins, H.N., Hassel, M.P. and May, R.M. (1992) ‘The spatial dynamics of host-parasitoid systems’. *Journal of Animal Ecology*, 61, pp. 735–748.
- Edelstein-Keshet, L. (1998) *Mathematical models in biology*. Rondon House.
- Hassel, M.P. and May, R.M. (1986) ‘Generalist and specialist natural enemies in insect predator-prey interactions’. *Journal of Animal Ecology*, 55, pp. 923–994.
- Hassell, M.P. (2000) *The Spatial and Temporal Dynamics of Host-Parasitoid Interactions*. Oxford University Press.
- Jones, T.H., Hassel, M.P. and Pacala, S.W. (1993) ‘Spatial heterogeneity and the population dynamics of a host-parasitoid system’. *Journal of Animal Ecology*, 62, pp. 251–262.
- Kot, M. (2001) *Elements of Mathematical Ecology*. Cambridge University Press.
- Rodrigues, L.A.D., Mistro, D.C. and Petrovskii, S. (2011) ‘Pattern formation, long-term transients, and the Turing-hopf bifurcation in a space- and time-discrete predator-prey system’. *Bulletin of Mathematical Biology*, 73, pp. 1812–1840.

Recommended Citation: Pacini Selau, P. *et al.* (2023). ‘Pattern Formation in a Resource and Two Consumers Discrete Model’. *Rev. model. mat. sist. biol.* 3(E), e23E03, doi:10.58560/rmmsb.v03.n02.023.02



This open access article is licensed under a Creative Commons Attribution International (CC BY 4.0) <http://creativecommons.org/licenses/by/4.0/>. Support: CAPES - Code 001.

Spatial spread of an epidemic in the context of cellular automata

Propagación espacial de una epidemia en el contexto de autómatas celulares

 Marcelo Cargnelutti Rossato¹ and  João Frederico da Costa Azevedo Meyer¹

✉ Marcelo Cargnelutti Rossato: marcelocrossato@gmail.com

¹ Instituto de Matemática, Estatística e Computação Científica,
Universidade Estadual de Campinas,
São Paulo, Brasil

Recepción: 2023-04-05 | Aceptación: 2023-08-25 | Publicación: 2023-10-29

Recommended Citation: Cargnelutti Rossato, M *et al.* (2023). 'Spatial spread of an epidemic in the context of cellular automata'. Rev. model. mat. sist. biol. 3(E), e23E04, doi:10.58560/rmmsb.v03.n02.023.03



This open access article is licensed under a Creative Commons Attribution International (CC BY 4.0) <http://creativecommons.org/licenses/by/4.0/>.
Support:

ABSTRACT

COVID-19 is a disease that has surpassed the mark of 760 million confirmed cases and has caused more than 6.8 million deaths, revealing the importance of seeking and studying strategies to control its spread. Therefore, the objective of this work is to analyze two of the main mechanisms proposed to control the spread of this disease: confinement and vaccination. To do so, a cellular automaton based on a SCEIRDV compartmental model was constructed, with susceptible, confined, exposed, infected, recovered, dead, and vaccinated individuals. Simulations were performed in scenarios with and without confinement and/or vaccination, mainly analyzing the number of deaths, the average number of infected individuals per day, and the maximum number of individuals simultaneously infected. It was concluded that both strategies contributed to the reduction of these indicators, especially when adopted together.

Keywords:

Epidemiology, Compartmental models, Cellular automata, COVID-19

RESUMEN

COVID-19 es una enfermedad que superó la marca de 760 millones de casos confirmados, además de causar más de 6.8 millones de muertes, lo que revela la importancia de buscar y estudiar estrategias para controlar su propagación. Por lo tanto, el objetivo de este trabajo es analizar dos de los principales mecanismos propuestos para controlar la propagación de esta enfermedad: el confinamiento y la vacunación. Para hacerlo, se construyó un autómata celular basado en un modelo compartimental SCEIRDV, con susceptibles, confinados, expuestos, infectados, recuperados, muertos y vacunados. Se realizaron simulaciones en escenarios con y sin confinamiento y/o vacunación, analizando principalmente el número de muertes, el promedio de infectados por día y el máximo de individuos simultáneamente infectados. Se concluyó que ambas estrategias contribuyeron a la reducción de estos indicadores, especialmente cuando se adoptaron conjuntamente.

Palabras Claves:

Epidemiología, Modelos compartimentales, Autómatas celulares, COVID-19

2020 AMS Mathematics Subject Classification: Primary: 92B05; Secondary: 92D30, 37B15

1 INTRODUCTION

COVID-19 is a serious respiratory infection that has a high transmissibility rate, recording more than 760 million cases and 6.8 million deaths around the world (World Health Organization, 2023). A major initial concern, in addition to the number of infections and deaths, was that there were too many people infected simultaneously, which could lead to hospital overload.

Consequently, some social isolation measures were suggested as a strategy to try to avoid this overload and, at the same time, a great mobilization was initiated for the development of a vaccine for the disease. Thus, this work aims to analyze the influence of confinement and vaccination measures in controlling the spread of COVID-19 through the construction of a mathematical model that represents the spatial spread of this disease and the performance of simulations considering the different possible scenarios.

2 SUGGESTED MODEL

One of the first compartmental models in the area of epidemiology was developed by Kermack and McKendrick (1927), in which a system of three differential equations was described to represent the variation of susceptible, infected and recovered individuals. The compartments to be used in a model must be chosen considering the characteristics of the disease to be analyzed and the objective of the model (Hethcote, 2000). Therefore, to describe the spread of COVID-19, we developed a compartmental SCEIRDV model, in which:

- S represents susceptible individuals, who are likely to be infected by the disease or to take measures to protect themselves, such as self-confinement or vaccination;
- C represents confined people, who protect themselves from the disease by remaining isolated and not visiting anyone or receiving visitors;
- E represents those who have had recent exposure to the disease and have not yet developed symptoms, who are less likely than infected people to infect susceptible;
- I represents the infected who have been exposed to the disease for a few days and are symptomatic, being more likely to infect the susceptible;
- R represents recovered individuals, who had the disease and developed a temporary immunity to it;
- D represents those who died from the disease, since deaths from natural causes were not considered, and;
- V represents vaccinated individuals, who cannot be contaminated during the vaccine effect interval, even having contact with exposed or infected people.

The compartment for dead individuals could be removed without affecting any results, as they do not participate in

the transmission dynamics, but we have included it as a simple way to count their numbers. While it may be more informative to assume that vaccination does not provide full protection against infection and does not prevent vaccinated individuals from transmitting the disease, we are considering the best possible scenario, in which vaccinated individuals cannot become infected and therefore cannot transmit the disease. Although it is generally considered that exposed individuals cannot transmit the disease, we decided to consider that they can infect at a lower rate than infected individuals, as was done by Chowell and Brauer (2009).

To carry out the simulations, a cellular automaton was developed, which is a model of discrete states, time and space, in which a state is assigned to each region of the domain, which can be called a cell (De Vries *et al.*, 2006). Thus, an automaton of dimension 100×100 was constructed by the authors, which can be understood as a matrix 100×100 in which each element represents the state (susceptible, confined, exposed, infected, recovered, dead or vaccinated) of the individual living in the corresponding cell.

Initially, only 1 was considered infected near the center of the domain, while all other 9999 individuals were susceptible. In Figure 1, the possible state changes are presented, associated with the parameters that influence these changes.

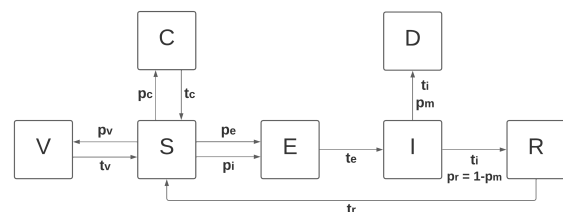


Figure 1: Diagram of the compartmental model SCEIRDV.

Instead of considering that the spatial spread of the disease would occur only through contacts between direct neighbors and following the classic diffusion equation, it was defined that, at each instant of time (which corresponds to one day), each person would randomly interact with others three people within 5 units horizontally and vertically of their position. When there is contact between a susceptible individual and an exposed or infected individual, the susceptible individual may become exposed to the disease with probabilities p_e or p_i , respectively. It should also be noted that the confined and dead do not participate in these interactions, being excluded from the interaction options of other individuals.

It is assumed that individuals exposed to the disease develop symptoms and go to the infected compartment after an incubation time of t_e days and, after t_i days, an infected person can die with probability p_m or recover with probability $p_r = 1 - p_m$. A recovered person becomes susceptible again after t_r days. Finally, at each instant of time, every susceptible individual can confine himself with probability p_c or be vaccinated with probability p_v . The confined remain totally isolated for a period of t_c days, then returning to being susceptible, and the vaccinated remain protected during

an interval of t_v days and then also return to the susceptible compartment.

In this model, we use stochastic components for the probabilities that an individual will be infected, confined, vaccinated, and to determine whether the individual recovers or dies after an infection. However, the times in which he remains vaccinated, confined, exposed, infected or recovered are presented in a deterministic way. An analogous completely stochastic model could be constructed using the relation $p = \frac{1}{t}$, in which, for example, a confined individual would have a probability of $\frac{1}{t_c}$ to leave the confinement each day rather than becoming deterministically susceptible after t_c days.

To estimate the parameters accurately, we reviewed several articles. Li *et al.* (2020) reported an average disease incubation period of 5.2 days in the first 425 COVID-19 patients in Wuhan, while Elias *et al.* (2021) analyzed 99 studies published between January 1, 2020 and January 10, 2021, and found an average incubation time of 6.38 days. Additionally, Wu *et al.* (2022) obtained a mean incubation time of 6.57 days in 142 studies with a total of 8112 patients, which could be even lower considering specific strains. Thus, we set $t_e = 6$ days.

Studies have provided estimates of the infectious period for the disease ranging from 5 to 14 days. The analysis by Acuña-Zegarra *et al.* (2020) estimated infectious periods of 5.97 days for asymptomatic patients and 10.81 days for symptomatic patients. Moreover, viral loads were found to peak around 10 days after symptom onset, according to Zou *et al.* (2020). Byrne *et al.* (2020) reported that the average time from symptom onset to two negative RT-PCR tests was 13.4 days. In this work, we use $t_i = 10$ days.

The duration of protection provided by the COVID-19 vaccine is difficult to pinpoint precisely, but studies suggest a decline in its effectiveness between 3 to 6 months after vaccination. Research has shown that the high initial antibody titers induced by mRNA vaccines diminish by this time frame (Barouch, 2022), with mean antibody levels 4 months after vaccination falling to just 6.3% of peak levels (Khoury *et al.*, 2021). Furthermore, a reduced efficacy against hospitalization within 3 to 4 months post-vaccination has been reported by Collie *et al.* (2022). Based on these observations, we have set $t_v = 120$ days.

While Reynolds *et al.* (2020) reported detecting neutralizing antibodies against SARS-CoV-2 at 16-18 weeks after infection, other studies suggest the potential for reinfection with an average time of 50.5 days (Dos Santos *et al.*, 2021). Additionally, Seow *et al.* (2020) observed that individuals could maintain high levels of neutralizing antibodies for up to 60 days after infection. In order to establish a parameter between these observed values, we define $t_r = 90$ days.

It is assumed that an individual will remain confined for an average of 30 days and may face isolation again in the future. Hence, we set $t_c = 30$ days. The mortality rate is calculated by dividing the number of deaths from the disease by the total number of cases, using data reported by World Health

Organization (2023). This yields $p_m \approx \frac{6,800,000}{760,000,000} \approx 0.009$.

For any interaction between an infected person and a susceptible person, the probability of exposure for the susceptible person is assumed to be 3%. Therefore, we define $p_i = 0.03$. In the case of an interaction with an exposed individual, it is assumed that the probability of exposure for the susceptible person is half of that, or $p_e = 0.015$.

3 SIMULATIONS

In order to analyze the influence of confinement and vaccination on the spread of the disease, the results obtained in simulations with and without confinement and/or vaccination will be presented, mainly evaluating the number of deaths, average infected per day and maximum number of simultaneously infected individuals.

Table 1 presents the parameters used for each simulation, with periodic boundary conditions and a total simulation time of 1,095 days (approximately 3 years). The values of p_c and p_v differ in each simulation, and will be discussed in detail for each of the considered scenarios.

Table 1: Parameters

Parameter	Value	Meaning
t_e	6 days	Incubation time
t_i	10 days	Infectious period
t_c	30 days	Consecutive confinement time
t_r	90 days	Period of immunity from disease
t_v	120 days	Period of vaccine immunity
p_m	0.009	Mortality rate
p_i	0.03	Infection rate by infected individuals
p_e	0.015	Infection rate by exposed individuals
p_c	0.01 – 0.03	Confinement rate
p_v	0.001 – 0.005	Vaccination rate

First, in the simulation without confinement and without vaccination, that is, with $p_c = p_v = 0$, a total of 403 deaths were obtained, which is about 4% of the initial population of 10,000 individuals. The evolution of the number of susceptible, exposed, infected, recovered and dead is shown in Figure 2.

It is possible to observe that, without any containment measures, the virus continues to spread with great intensity even when there is a high number of deaths, with an average of 405.7 people infected per day. The maximum number of people simultaneously infected is 1,255, occurring on day 927. Figures 3a and 3b show the day with the highest number of infected people and the scenario after 1,095 days, respectively.

Similar to the colors in Figure 2, the black squares represent the dead, the green ones are recovered, the red ones are infected and the orange ones are exposed to the disease. The only difference is that the susceptibles, previously displayed in yellow, are now represented by white squares. It is noted that at the end of the simulation there are still several foci of infection, similarly to the day when there is the highest number of infected people.

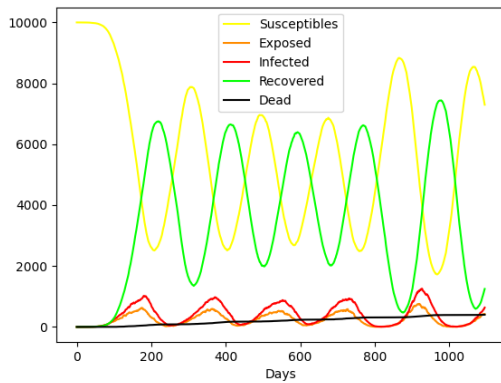


Figure 2: Result of the first simulation, without confinement and vaccination.

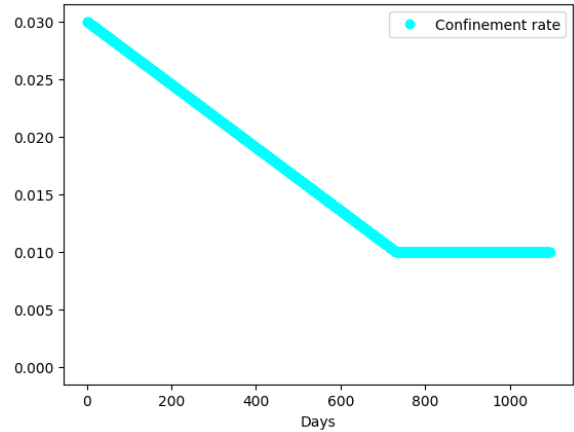


Figure 4: Evolution of the confinement rate over time.

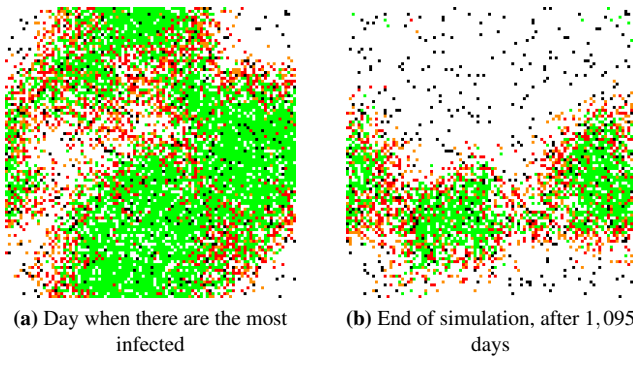


Figure 3: Spatial distributions of the simulation without confinement and vaccination.

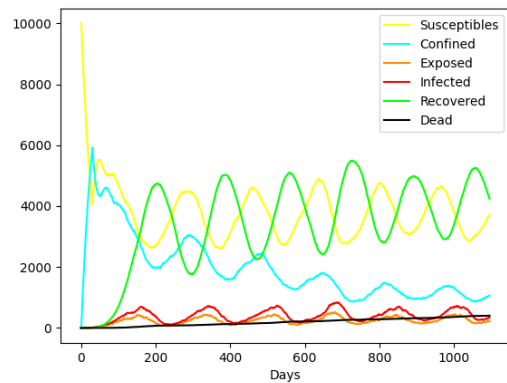


Figure 5: Result of the second simulation, with confinement and without vaccination.

To carry out the second simulation, it was considered that the confinement rate should start high and be reduced over time, since there are several factors that lead people not to isolate themselves at home for a long time, such as the need to go out to work or the desire to meet friends and family, for example.

Thus, an initial confinement probability of $p_c = 0.03$ was defined, which was linearly reduced until reaching $p_c = 0.01$ at the end of 2 years (730 days), remaining constant at this value until the end of the analyzed period, as can be observed in Figure 4.

Again without vaccination ($p_v = 0$), the simulation resulted in 403 deaths, the same as the previous scenario. A summary of this simulation can be seen in Figure 5.

By reducing the number of susceptibles through confinement, it is observed that the oscillations of all compartments are smaller and the peak of infected individuals in one day is also reduced by one third to 837, which can help to avoid overloading hospitals. Even so, the average number of people infected per day is 398.1 people, which indicates that, although confinement manages to reduce the number of people infected simultaneously, there is no significant reduction in the total number of infections, they only occur in a slightly

more homogeneous way over the days. The spatial distribution of the population on day 686, when the number of infected people peaked, and at the end of 1,095 days are shown in Figures 6a and 6b, respectively.

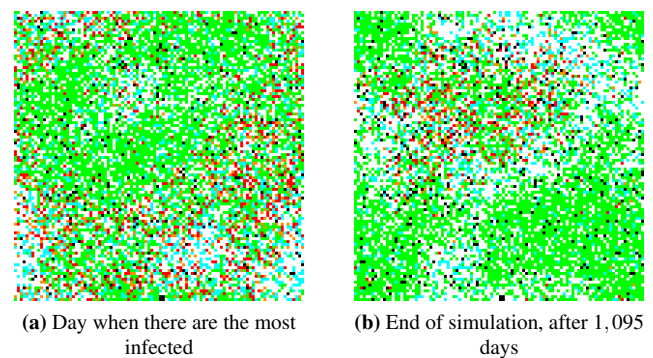


Figure 6: Spatial distributions of the simulation with confinement and without vaccination.

The colors are the same as shown in Figure 3, with the

inclusion of cyan for confined individuals. It is observed that the high number of confined means that the infection cannot reach as many people at the same time as in the previous case, but there is still a considerable oscillation in the number of infected even after approximately 3 years.

The third scenario serves to analyze the impact of vaccination alone, therefore confinement is not carried out ($p_c = 0$). Estimating that people could start vaccinating approximately 1 year after the onset of the disease and that the vaccination rate would increase as more vaccines were purchased and more people could be vaccinated, it was defined that $p_v = 0$ initially, spiking to $p_v = 0.001$ at $t = 365$ days and growing linearly up to $p_v = 0.005$ at $t = 730$ days, remaining constant until the end of the analyzed period. The graph of the vaccination rate over time is shown in Figure 7.

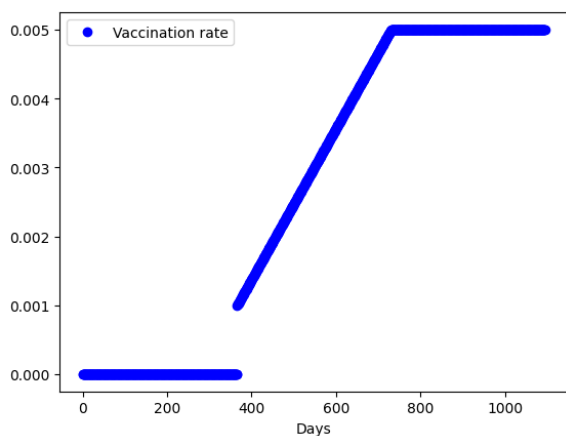


Figure 7: Evolution of the vaccination rate over time.

The evolution of the disease in this case is shown in Figure 8, which shows that there were 306 deaths, a reduction of about 24% compared to previous cases.

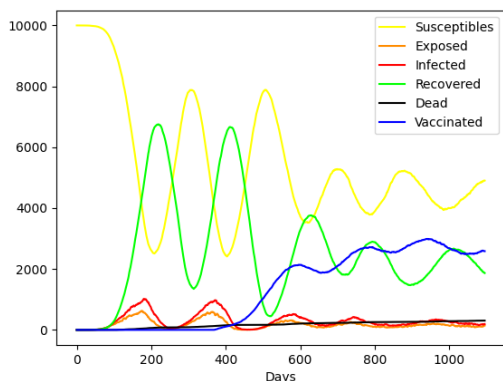


Figure 8: Result of the third simulation, with vaccination and without confinement.

In this simulation, a large difference is observed in the number of infected people before and after the start of vaccination. While there is a peak of 1,022 infected on day 180,

the highest number of individuals simultaneously infected after the start of vaccination (disregarding the first days, as the vaccine began to be applied at a time when the number of infected people was close to maximum value) was 523 people, on the day 582.

In this way, it is possible to observe that the vaccination was able to reduce both the maximum number of infected in one day and the average of infected over the days, which dropped from about 400 to 301.7. The spatial spread on the days when there is the highest number of infected people after the start of vaccination and after 1,095 days can be seen in Figures 9a and 9b, respectively.

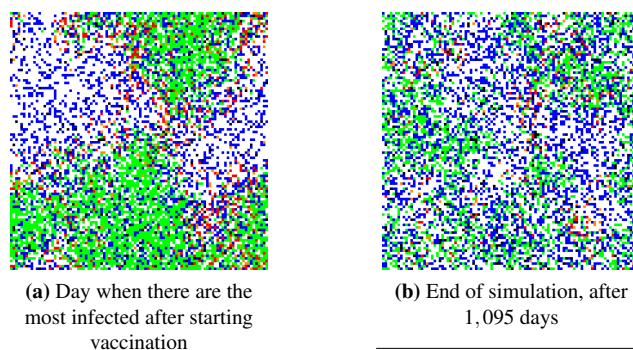


Figure 9: Spatial distributions of the simulation with vaccination and without confinement.

In this case, blue squares are included to represent those vaccinated. Analyzing the two scenarios, it is observed that in Figure 9a, while the vaccination rate was still rising, there are some large groups of susceptibles nearby, which facilitates the spread of the disease. Meanwhile, it is noted that at the end of the 1,095 days, susceptibles are often surrounded by vaccinated and recovered, which makes it difficult for the disease to spread.

Finally, the last simulation analyzes the combined effects of confinement and vaccination. Thus, it starts with $p_c = 0.03$ which decreases linearly to $p_c = 0.01$ in $t = 730$ days, while $p_v = 0$ during the first year, jumping to $p_v = 0.001$ after 365 days and growing linearly up to $p_v = 0.005$ at $t = 730$ days, as used in the two previous simulations. Combining the two mechanisms to control the spread of the disease, there were only 261 deaths, about 35% less than in the first simulation, in which there was no form of control. The evolution of the disease in this simulation is illustrated in Figure 10.

Up to day 365, the results obtained are identical to those shown in Figure 5 and the maximum number of infected individuals is 719 on day 344. After the start of vaccination, there is the lowest peak among all the simulations, with only 515 infected simultaneously on day 528. Figures 11a and 11b illustrate this peak of infected people and the population distribution at the end of the simulation, respectively.

Contrary to the large waves of infection that were observed mainly in Figures 3a and 6a, those infected seem to be more spread out and fewer in this simulation, showing that vacci-

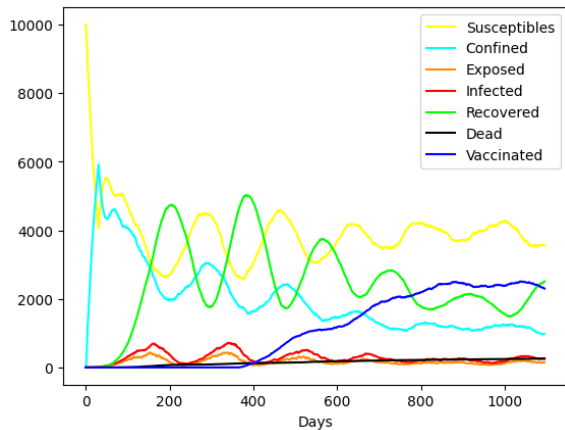


Figure 10: Result of the fourth simulation, with confinement and vaccination.

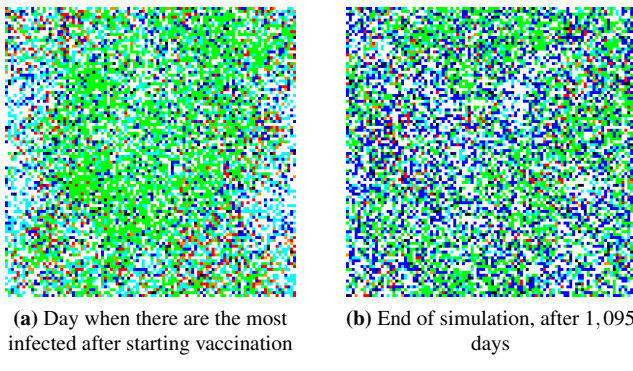


Figure 11: Spatial distributions of the simulation with confinement and vaccination.

nation and confinement managed to curb a little the spread of the disease. Still in this simulation, the lowest average of infected per day was reached, 282.9. A summary of the results obtained in the simulations, considering the peak of infected people after the start of vaccination in the cases in which it was carried out, is presented in Table 2.

Table 2: Summary of simulation results

Simulation	1	2	3	4
Number of deaths	403	403	306	261
Peak of infected	1255	837	523	515
Average number of infected	405.7	398.1	301.7	282.9

Analyzing the table, it is possible to observe that in the second simulation, where there was only confinement, there was no reduction in the number of deaths and the average of infected was less than 2% lower, but the peak of infected was reduced by about 33% when compared to the case without any containment measures.

Meanwhile, considering only vaccination, there was a 24% reduction in the number of deaths, a 58% reduction in the maximum number of simultaneous infections and an av-

erage number of infected people almost 26% lower. Finally, in the simulation with both containment measures, 35% fewer deaths, 59% lower peak of infected people and 30% lower average number of infected people were observed.

4 FINAL CONSIDERATIONS

In this work, the authors developed a cellular automaton based on a SCEIRDV compartmental model to simulate the evolution of COVID-19 using parameters based on real studies on the disease. Analyzing the results summarized in Table 2, it is possible to observe that the implementation of confinement and vaccination measures separately has already caused a reduction in some infection and mortality rates, but the joint application of these two measures has reduced them the number of deaths at about 35%, the peak of infected at almost 59% and the average of infected at more than 30%, being the most favorable strategy among those analyzed.

In future work, there are several implementations that can be considered, such as changing the infection and/or mortality rates over time to consider the different variants of the disease, for example. In addition, a completely stochastic model can be built for comparison and the scenario in which vaccinated people can also be infected can be considered. Finally, another idea is to introduce houses or clusters into the model, to directly consider the possibility of exposure to the disease through other individuals living in the same environment.

REFERENCES

Acuña-Zegarra, M.A., Santana-Cibrian, M. and Velasco-Hernandez, J.X. (2020) ‘Modeling behavioral change and covid-19 containment in mexico: A trade-off between lockdown and compliance’. *Mathematical biosciences*, 325, p. 108370.

Barouch, D.H. (2022) ‘Covid-19 vaccines—immunity, variants, boosters’. *New England Journal of Medicine*, 387(11), pp. 1011–1020.

Byrne, A.W., McEvoy, D., Collins, A.B., Hunt, K., Casey, M., Barber, A., Butler, F., Griffin, J., Lane, E.A., McAloon, C. *et al.* (2020) ‘Inferred duration of infectious period of sars-cov-2: rapid scoping review and analysis of available evidence for asymptomatic and symptomatic covid-19 cases’. *BMJ open*, 10(8), p. e039856.

Chowell, G. and Brauer, F. (2009) ‘The basic reproduction number of infectious diseases: computation and estimation using compartmental epidemic models’. *Mathematical and statistical estimation approaches in epidemiology*, pp. 1–30.

Collie, S., Nayager, J., Bamford, L., Bekker, L.G., Zylstra, M. and Gray, G. (2022) ‘Effectiveness and durability of the bnt162b2 vaccine against omicron sublineages in south africa’. *New Engl and Journal of Medicine*, 387(14), pp. 1332–1333.

De Vries, G., Hillen, T., Lewis, M., Müller, J. and Schöfnisch, B. (2006) *A course in mathematical biology: quantitative modeling with mathematical and computational methods*. SIAM.

Dos Santos, L.A., de Góis Filho, P.G., Silva, A.M.F., Santos, J.V.G., Santos, D.S., Aquino, M.M., de Jesus, R.M., Almeida, M.L.D., da Silva, J.S., Altmann, D.M. *et al.* (2021) ‘Recurrent covid-19 including evidence of reinfection and enhanced severity in thirty brazilian healthcare workers’. *Journal of Infection*, 82(3), pp. 399–406.

Elias, C., Sekri, A., Leblanc, P., Cucherat, M. and Vanhems, P. (2021) ‘The incubation period of covid-19: A meta-analysis’. *International Journal of Infectious Diseases*, 104, pp. 708–710.

Hethcote, H.W. (2000) ‘The mathematics of infectious diseases’. *SIAM review*, 42(4), pp. 599–653.

Kermack, W.O. and McKendrick, A.G. (1927) ‘A contribution to the math-

- ematical theory of epidemics'. *Proceedings of the royal society of london. Series A, Containing papers of a mathematical and physical character*, 115(772), pp. 700–721.
- Khoury, J., Najjar-Debbiny, R., Hanna, A., Jabbour, A., Ahmad, Y.A., Safuri, A., Abu-Sinni, M., Shkeiri, R., Eley, A. and Hakim, F. (2021) 'Covid-19 vaccine–long term immune decline and breakthrough infections'. *Vaccine*, 39(48), pp. 6984–6989.
- Li, Q., Guan, X., Wu, P., Wang, X., Zhou, L., Tong, Y., Ren, R., Leung, K.S., Lau, E.H., Wong, J.Y. *et al.* (2020) 'Early transmission dynamics in wuhan, china, of novel coronavirus–infected pneumonia'. *New England journal of medicine*.
- Reynolds, C.J., Swadling, L., Gibbons, J.M., Pade, C., Jensen, M.P., Diniz, M.O., Schmidt, N.M., Butler, D.K., Amin, O.E., Bailey, S.N. *et al.* (2020) 'Discordant neutralizing antibody and t cell responses in asymptomatic and mild sars-cov-2 infection'. *Science immunology*, 5(54), p. eabf3698.
- Seow, J., Graham, C., Merrick, B., Acors, S., Pickering, S., Steel, K.J., Hemmings, O., O'Byrne, A., Kouphou, N., Galao, R.P. *et al.* (2020) 'Longitudinal observation and decline of neutralizing antibody responses in the three months following sars-cov-2 infection in humans'. *Nature microbiology*, 5(12), pp. 1598–1607.
- World Health Organization (2023) *Covid-19 weekly epidemiological update, edition 135, 22 march 2023*. <https://www.who.int/emergencies/diseases/novel-coronavirus-2019/situation-reports>.
- Wu, Y., Kang, L., Guo, Z., Liu, J., Liu, M. and Liang, W. (2022) 'Incubation period of covid-19 caused by unique sars-cov-2 strains: a systematic review and meta-analysis'. *JAMA network open*, 5(8), pp. e2228008–e2228008.
- Zou, L., Ruan, F., Huang, M., Liang, L., Huang, H., Hong, Z., Yu, J., Kang, M., Song, Y., Xia, J. *et al.* (2020) 'Sars-cov-2 viral load in upper respiratory specimens of infected patients'. *New England journal of medicine*, 382(12), pp. 1177–1179.

Recommended Citation: Cargnelutti Rossato, M *et al.* (2023). 'Spatial spread of an epidemic in the context of cellular automata'. *Rev. model. mat. sist. biol.* 3(E), e23E04, doi:10.58560/rmmsb.v03.n02.023.03



This open access article is licensed under a Creative Commons Attribution International (CC BY 4.0) <http://creativecommons.org/licenses/by/4.0/>. Support:

Using the Chemical Master Equation to model the interaction network of focal adhesion proteins

Utilizando la Ecuación Maestra Química para modelar la red de interacción de las proteínas de adhesión focal.

 Luciana Renata de Oliveira¹,  Júlia Vitória Ribeiro¹  Alícia Groth Becker¹,
 Gabriel Vitorello¹ and  José Carlos Merino Mombach¹

✉ Luciana Renata de Oliveira: lucianarenatadeoliveira@gmail.com

¹ Departamento de Física, Centro de Ciências Naturais e Exatas,
Universidade Federal de Santa Maria,
Santa Maria, RS, Brasil

Recepción: 2023-06-01 | Aceptación: 2023-09-10 | Publicación: 2023-10-29

Recommended Citation: Renata de Oliveira, L. *et al.* (2023). 'Using the Chemical Master Equation to model the interaction network of focal adhesion proteins'. *Rev. model. mat. sist. biol.* 3(E), e23R05, doi:10.58560/rmmsb.v03.n02.023.04



This open access article is licensed under a Creative Commons Attribution International (CC BY 4.0) <http://creativecommons.org/licenses/by/4.0/>.
Support: PIBIC No. 21-2022, PROA 23-25551-0001199-9 (2023)

ABSTRACT

Cells are exposed to mechanical stresses, whether through external forces that are applied to tissues or endogenous forces that are generated within the active cytoskeleton. The differences in the stimuli are sensed by cells and controlled by a network of focal adhesion proteins that regulate signaling pathways and determine cellular responses including cell motility, proliferation, and cell differentiation (cell fate). Together the ability of cells to sense and respond to mechanical stimuli governed by mechanosensors and mechanosignaling proteins can be termed mechanotransduction. Whilst there is intense ongoing research on specific pathways involved in mechanoresponse mechanisms, the experiments alone can only give a global overview of dynamic parameters for the interaction of proteins. The focal adhesion pathway is a complex network and the use of stochastic mathematical algorithms can be an efficient tool to expand and explore this network by building and solving a regulatory interaction map. Exploring the predicted interaction networks can suggest new directions for future experimental research and provide cross-species predictions for efficient interaction mapping. Here we aim to describe the network representing a subset of proteins associated with focal adhesion using the stochastic model Chemical Master Equation and shed further light on how the dynamic of these proteins can direct cell behavior and responses. Our results showed that our model is able to describe the experimental interactions. In addition, it is able to model the temporal cascade of events related to responses to mechanical stimuli and showed different dynamical behaviors based on the kinetic parameters.

Keywords:

Chemical Master equation, Focal Adhesion, Signaling Networks, Stochastic Model

RESUMEN

Las células están expuestas a tensiones mecánicas, ya sea a través de fuerzas externas aplicadas a los tejidos o fuerzas endógenas generadas dentro del citoesqueleto activo. Las diferencias en los estímulos son percibidas por las células y controladas por una red de proteínas de adhesión focal que regulan las vías de señalización y determinan respuestas celulares, incluida la movilidad celular, la proliferación y la diferenciación celular (destino celular). En conjunto, la capacidad de las células para percibir y responder a estímulos mecánicos, gobernada por mecanosensores y proteínas de señalización mecánica, puede denominarse mecanotransducción. Si bien hay una intensa investigación en curso sobre las vías específicas involucradas en los mecanismos de respuesta mecánica, los experimentos por sí solos solo pueden proporcionar una visión general de los parámetros dinámicos para la interacción de las proteínas. La vía de adhesión focal es una red compleja y el uso de algoritmos matemáticos estocásticos puede ser una herramienta eficiente para expandir y explorar esta red mediante la construcción y resolución de un mapa de interacción reguladora. La exploración de las redes de interacción predichas puede sugerir nuevas direcciones para futuras investigaciones experimentales y proporcionar predicciones entre especies para mapeos de interacción eficientes. Aquí nuestro objetivo es describir la red que representa un subconjunto de proteínas asociadas a la adhesión focal utilizando el modelo estocástico de la Ecuación Maestra Química y arrojar más luz sobre cómo la dinámica de estas proteínas puede dirigir el comportamiento y las respuestas celulares. Nuestros resultados mostraron que nuestro modelo es capaz de describir las interacciones experimentales. Además, puede modelar la cascada temporal de eventos relacionados con respuestas a estímulos mecánicos y mostró diferentes comportamientos dinámicos basados en los parámetros cinéticos.

Palabras Claves:

Ecuación Maestra Química, Adhesión Focal, Redes de Señalización, Modelo Estocástico

2020 AMS Mathematics Subject Classification: Primary: 92B05; Secondary: 104A54, 104A62

1 INTRODUCTION

Human anatomy consists of various types of tissues, ranging from the very soft gyri and sulci of the brain to the very hard rigid trabeculae of bones ?. In our tissues, cells experience numerous mechanical stimuli, for example, shear stresses from the blood flow or stretching and compression forces from several tissues associated with muscle activity ?. Adherent cells respond very sensitively not only to biochemical but also to the physical properties of their environment. For example, it has been shown that stem cell differentiation can be guided by substrate rigidity, which is sensed by cells by actively pulling on their environment with actomyosin-generated forces ?. Force, therefore, plays an important role in the shaping, development, and maintenance of tissues and organs. Virtually all organisms have evolved structures from the macroscale (organs, tissues) to the microscale (cells) and nanoscale (molecular assemblies, single proteins) that are sensitive and responsive to myriad forces, including compressive, tensile, shear stress, and hydrostatic pressure ???.

The ability of cells to sense and respond to mechanical stimuli is termed mechanotransduction ?, including not only all components of force, stress, and strain but also substrate rigidity, topology, and adhesiveness. This ability is crucial for the cell to respond to the surrounding mechanical cues and adapt to the changing environment ?. Cells sense their microenvironment using a variety of receptors. Integrins are one of the most prominent receptor families that bind proteins of the extracellular matrix (ECM), which consist of fibrous protein filaments that are organized in aligned fibers (e.g. co-aligned fibers in forming tendons) or highly organized membranous networks (e.g. the basement membranes underneath of epithelial cell layers). The organization, the biochemistry, and the mechanical properties of integrins depend on the type of ECM proteins they are assembled with. With their intracellular domains, integrins associate with a large number of proteins (focal adhesion plaque proteins) that link them to the contractile actomyosin cytoskeleton ????. These multiprotein complexes appear as focused adhesion structures when observed under the fluorescence microscope and hence are called focal adhesions (FAs) (Figure 1) ????

Upon binding to ECM integrins become activated and form initial clusters at the cell membrane. Mechanical forces can support the integrin activation process involving conformational changes of the receptor that promotes not only high-affinity interaction with the ECM but also induces the recruitment of a number of proteins to the intracellular integrin cytoplasmic domain. Two of the critical proteins that connect integrins with the actin cytoskeleton are the adapter proteins talin and vinculin. Because of the key role sensing of their mechanical environment, talin and vinculin are often described as mechanosensors and they have multiple binding sites for other proteins. Talin for example, in addition to vinculin, binds to the focal adhesion kinase (*FAK*), paxillin, RIAM, DLC1, actin, and others ??; vinculin binds to ponsin,

vinexin (a+b), CAP, Arp/2/3, paxillin, and actin ????. Some of these proteins, i.e. *FAK* and paxillin together with the *SRC* kinase trigger signaling pathways that regulate downstream the family of RhoGTPases, a protein family that governs actin polymerization (i.e. through Rac1) and/or myosin-mediated actin bundling and contraction (i.e. *RhoA*). The latter group of proteins can thus be regarded as mechanosignaling proteins that translate the mechanosensory information into chemical signals that coordinate specific cellular responses.

There are many other proteins besides those mentioned above that contribute to mechanotransduction (Figure 1). In fact, mass spectroscopy experiments have identified more than 2,000 proteins and around 60 of them belong to the core adhesion proteins that are directly involved in cell-matrix adhesion regulation ??????. How they work together and coordinate the process of cell-matrix communication is yet unclear.

The trove of quantitative data produced by modern biology has highlighted that the complex behaviors of biological systems, even the simplest ones, are difficult to comprehend with experiments alone ?. These systems are not isolated, but rather subject to intrinsic and extrinsic fluctuations, which leads to a quasi-equilibrium state (homeostasis) ????. An increasing number of experimentalists appreciate the need for mathematical modeling to explain their data and uncover the underlying molecular mechanisms for their biological systems ?.

As illustrated in Figure 1 the focal adhesion pathway is a complex network and the use of stochastic mathematical algorithms can be an efficient tool to expand and explore this network by building and solving a regulatory interaction map. Protein-protein interaction networks are an important ingredient for the system-level understanding of cellular processes. Exploring the predicted interaction networks can suggest new directions for future experimental research and provide cross-species predictions for efficient interaction mapping.

Here we propose using the Chemical Master Equation to understand the dynamic interactions between proteins in the focal adhesion. We specifically show how the biochemical network involving extracellular matrix stimuli can lead to actin polymerization and focal adhesion formation. Next we present the detailed methodology to build the biochemical network and how to build the stochastic model.

2 METHODOLOGY

SIGNALING NETWORK FOR FOCAL ADHESION PROTEINS

We built a signaling network considering the interaction between the focal adhesion proteins *FAK*, *SRC*, Rac, Rho, Myosin light-chain (*MLC*), that leads to actin polymerization and focal adhesion formation (Figures 1 and 2). We choose specifically these proteins because they are involved in many

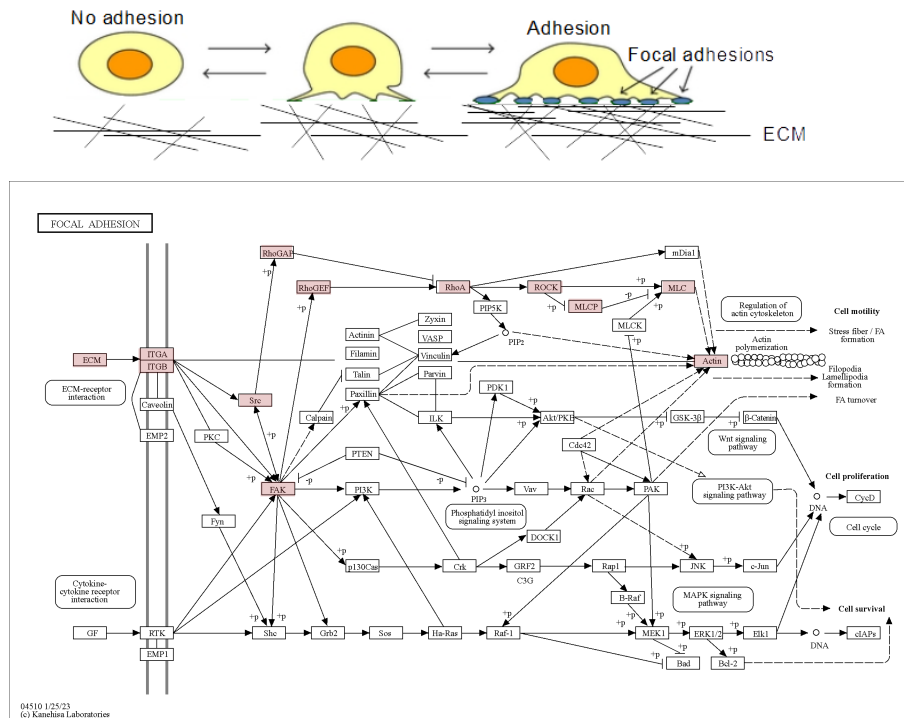


Figure 1: Top: Schematic representation of focal adhesion formation. Bottom: Signaling pathway map for focal adhesion proteins. This figure is a reproduction of the network generated by the Kyoto Encyclopedia of Genes and Genomes (KEGG) (<https://www.genome.jp/pathway/map04510>) for focal adhesion. The proteins modeled in this paper are highlighted.

important cellular processes, including health and disease. *FAK-SRC* interaction is crucial for the initiation and regulation of focal adhesions. Furthermore, *FAK*, plays a role in promoting growth factor- and integrin-stimulated cell motility in both normal and transformed cells and increased *FAK* expression are connected with elevated tumorigenesis. *SRC* activity has a role in normal vascular smooth muscle contractile function and in vascular remodeling in cardiovascular disease. Rho/ROCK pathway is involved in synapses in pathological situations such as spinal cord injury/ischemia, Alzheimer’s disease, Parkinson’s disease, multiple sclerosis, amyotrophic lateral sclerosis (ALS), and spinal muscular atrophy (SMA). And abnormal activation of Rho kinase signaling is closely associated with major cardiovascular diseases such as systemic hypertension, pulmonary hypertension, vasospasm, and adverse cardiac remodeling.

In our study, the signaling network of proteins and their interactions are constructed based on published data, the Kyoto Encyclopedia of Genes and Genomes (KEGG) database and the database for protein-protein interactions Search Tool for the Retrieval of Interacting Genes/Proteins (STRING). In our model, each state of the proteins is considered as one component of the network (for example *FAK* protein (*FAK*) and *FAK* phosphorylated (*p-FAK*), Figure 2). Multiple types of interactions are taken into account, both positive (activation, phosphorylation) and negative (inhibition). Our model is composed of three circuits (Figures 1 and 2): The initial activation by the extracellular matrix and the membrane protein Integrin [8-14] which activates both *FAK*

and *SRC*. *FAK* and *SRC* form a positive feedback loop. *FAK* and *SRC* are connected with the second circuit, the Rho family, *FAK* activates *RhoGEF* and *SRC* activates *RhoGAP*. *RhoGAP* inhibits and *RhoGEF* activates *RhoA*. *RhoA* indirectly activates *MLC*. The cell fate is actin polymerization that will lead to focal adhesion formation. Valencia-Expósito et. al proved that actomyosin contractility is controlled primarily by reversible phosphorylation of the myosin-II regulatory light chain (*MLC*) through the action of myosin kinases and phosphatases. Their results demonstrate that actomyosin oscillations in which the combination of cooperative binding of actin filaments in conjunction with actin filament dissociation from the bundle, due to myosin-induced tension, is sufficient to generate cell-autonomous oscillations in myosin and F-actin content. With these results here we are associating the behavior of *MLC* with the actin, which is the output of the model. This signaling network is used to build the stochastic mathematical model as presented in the next section.

MATHEMATICAL MODEL FOR PROTEIN INTERACTIONS

In biochemistry, Michaelis–Menten kinetics is the simplest case of enzyme kinetics, applied to enzyme-catalysed reactions of one substrate and one product. It takes the form of an equation describing the rate reaction rate v (rate of formation of product P , with concentration $[P]$) to $[S]$, the concentration of the substrate S Its formula is given by the

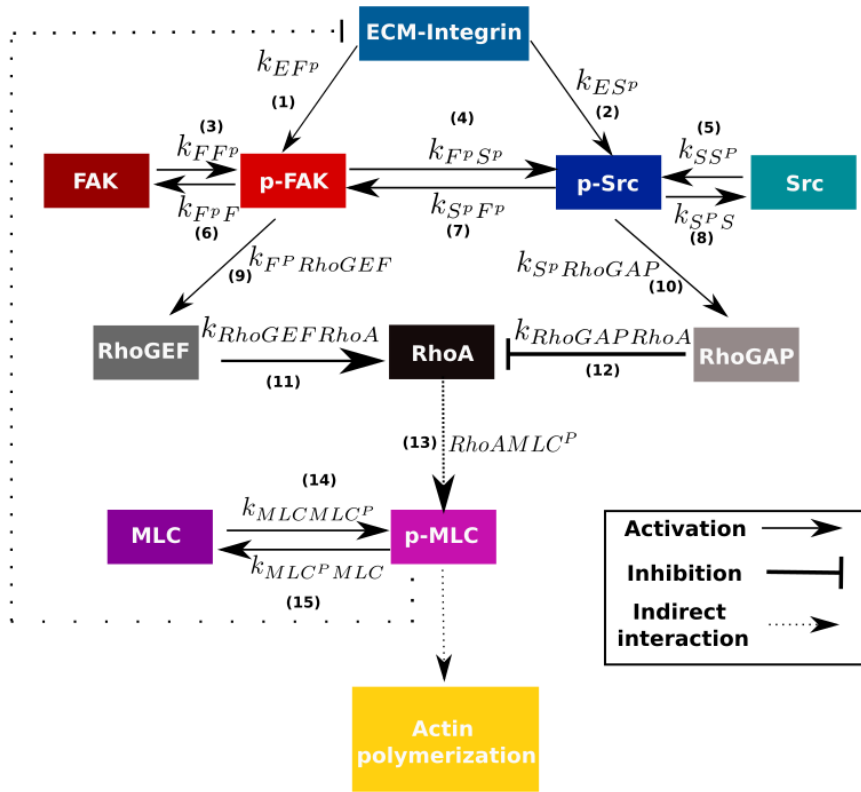


Figure 2: Network considering the pathway of proteins involved in the ECM mediated mechanosensing leading to actin polymerization. The numbers correspond to the equations in Table 1.

Michaelis–Menten equation:

$$v = \frac{dp}{dt} = \frac{k_{SP}[S][P]}{K_m + [P]} \tag{1}$$

where $V = k_{SP}[S]$ represents the limiting rate approached by the system at saturating substrate concentration for a given enzyme concentration. When the value of the Michaelis constant K_m is numerically equal to the substrate concentration, the reaction rate is half of V .

This kind of approach can be used to model protein-protein interactions as we are interested in this paper. To illustrate how to build the system with differential equations to describe the interactions we brought three kinds of examples in Figure 3. Let’s consider that we have two types of proteins A and B , which can interact as represented in Figure 3. For our network, we can represent the interactions as (1) $A \rightarrow B$, where protein A activates protein B , such a process can be represented by a Michaelis-Menten reaction equation. The concentration of protein B , which is represented as $[B]$ increases as the product of protein A and the transition rate of activation of B by A that is represented by k_{AB} in Table 1. (2) $B \rightarrow A$ represents the Degradation of protein B to A with a rate k_{BA} in Table 1. (3) $A \dashv B$ represents the inhibition of B due to A . This dynamic interaction is also represented by a Michaelis-Menten equation such as represented in Table 1.

Taking the interactions for our network in Figure 2, we

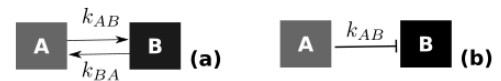


Figure 3: Mathematical representation of a biochemical network. (a) Activation and degradation of proteins. (b) Inhibition of proteins.

have the equations corresponding to each interaction in Table 1 in the Appendix. With these equations representing the interactions, we can build a system of differential equations to study the time evolution of the network in Figure 2, as follows.

Table 1: List of equations for each reaction represented in Figure 3.

Reaction	Equation	Reaction kind
$A \rightarrow B$	$\frac{k_{AB}[A][B]}{k_j + [B]}$	Activation
$B \rightarrow A$	$\frac{k_{BA}[B]}{k_j + [B]}$	Degradation
$A \dashv B$	$\frac{k_{AB}[A][B]}{k_j + [B]}$	Inhibition

$$\begin{aligned}
 \frac{d[FAK^P]}{dt} &= \frac{k_{EFP}([ECMINT] - [p - MLC])[FAK]}{k_1 + [FAK]} + \\
 &\frac{k_{FFP}[FAK][p - FAK]}{k_3 + [p - FAK]} + \frac{k_{SPFP}[p - SRC][FAK]}{k_7 + [FAK]} + \\
 &-k_{FFP}[p - FAK] - \frac{k_{FPP}[p - FAK][SRC]}{k_4 + [SRC]} + \\
 &- \frac{k_{FPRhoGEF}[p - FAK][RhoGEF]}{k_8 + [RhoGEF]} \\
 \\
 \frac{d[SRC^P]}{dt} &= \frac{k_{ESP}([ECMINT] - [p - MLC])[SRC]}{k_2 + [SRC]} + \\
 &+ \frac{k_{FPP}[p - FAK][SRC]}{k_4 + [SRC]} + \frac{k_{SSP}[SRC][p - SRC]}{k_6 + [p - SRC]} - k_{SS}[p - SRC] - \\
 &- \frac{k_{SPFP}[p - SRC][FAK]}{k_7 + [FAK]} + \frac{k_{SPRhoGAP}[p - SRC][RhoGAP]}{k_9 + [RhoGAP]} \\
 \\
 \frac{d[RhoGEF]}{dt} &= \frac{k_{FPRhoGEF}[p - FAK][RhoGEF]}{k_8 + [RhoGEF]} + \\
 &- \frac{k_{RhoGEFRhoA}[RhoGEF][RhoA]}{k_{10} + [RhoA]} \\
 \\
 \frac{d[RhoGAP]}{dt} &= \frac{k_{SPRhoGAP}[p - SRC][RhoGAP]}{k_9 + [RhoGAP]} + \\
 &- \frac{k_{RhoGAPRhoA}[RhoGAP][RhoA]}{k_{11} + [RhoA]} \\
 \\
 \frac{d[RhoA]}{dt} &= \frac{k_{RhoGEFRhoA}[RhoGEF][RhoA]}{k_{10} + [RhoA]} + \\
 &- \frac{k_{RhoGAPRhoA}[RhoGAP][RhoA]}{k_{11} + [RhoA]} \\
 \\
 \frac{d[p - MLC]}{dt} &= \frac{k_{RHOAMLC^P}[RhoA][MLC]}{k_{12} + [MLC]} + \\
 &+ \frac{k_{MLCPMLC^P}[MLC][p - MLC]}{k_{13} + [MLC]} - k_{MLC^P}[p - MLC]
 \end{aligned}$$

The term $[ECMINT] - [p - MLC]$ in the equations represents the negative feedback that the actin polymerization will send to the extracellular matrix. In nature, the signal is not continuous and stops once the actin polymerization starts and it is represented by the balance between the extracellular matrix concentration $[ECM]$ and the actin signal $[p - MLC]$?. We are assuming the conservation of proteins and the concentrations of inactive FAK , SRC , and MLC can be derived from the total number of molecules and the number of phosphorylated proteins. Next, we discuss how to build the stochastic model from the differential equations.

CHEMICAL MASTER EQUATION FOR THE DESCRIPTION OF PROTEIN MECHANOSIGNALING

The Chemical Master Equation is a class of discrete-state, continuous-time Markov processes that describe the time evolution of a system that can be modeled as a probabilistic combination of states ?. For the mechanosignaling network (Figure 2) the states are represented by the concentration of proteins in inactive, or active states usually determined by phosphorylation and/or conformational changes. The concentration of proteins is modeled as temporal variables assuming positive values represented by $[protein]$, that is the number of individuals in each protein state, for example, the number of molecules in inactive FAK ($[FAK]$) or phosphorylated FAK ($[p - FAK]$). The time evolution of the variable's concentrations is modeled by rates representing their interactions, where activation rates represent the interactions for which there is an increase in the protein concentration, for example, the increment in the concentration of phosphorylated SRC ($[p - SRC]$) due to k_{SSP} and the inhibition rates represent the interactions for which there is a decrease in the concentration of the protein, for example in the dephosphorylation of phosphorylated MLC ($[p - MLC]$) due to k_{MLC^P} (Figure 2). It is important to note that the system of equations describes one protein concentration in correspondence with the concentration of the others ??. The chemical master equation for the system is written as

$$\begin{aligned}
 \frac{dp([protein])}{dt} &= r([protein] + 1, t)p([protein] + 1, t) + \\
 &+ g([protein] - 1, t)p([protein] - 1, t) + \\
 &- (r(n_{protein}, t) + g(n_{protein}, t))p(n_{protein}, t)
 \end{aligned} \quad (2)$$

Where each protein is represented by a combination of the gain term ($g([protein], t)$) responsible for the increment of the concentration of the protein ($[protein]$ to $[protein] + 1$) and the recombination term ($r([protein], t)$) responsible for the decrease of the concentration of the protein ($[protein]$ to $[protein] - 1$), the generation and recombination of each protein are described in Table 2. $p([protein], t)$ is the occupation probability per unit of time of a determined state in the system. In our case, it is represented by the concentration of a protein. The generation and recombination terms used to build the stochastic model using the chemical master equation for each reaction in our network (Figure 2) are represented in Table 2.

3 RESULTS: SOLUTION OF THE PATHWAY LEADING TO ACTIN POLYMERIZATION

Here we are interested in exploring the signaling network of focal adhesion proteins leading to actin polymerization and focal adhesion formation (Figures 1 and 2) to illustrate the use of stochastic models such as the Chemical Master Equation for the understanding of protein interactions leading to different cell fates. The network was built considering the interaction between the focal adhesion proteins (see Section

Table 2: List of generation and recombination terms used to build the stochastic model using the chemical master equation.

Protein	Chemical Master equation term
$p - FAK$	$g([p - FAK], t) = \frac{k_{EFP}([ECMINT] - [p - MLC])[FAK]}{k_1 + [FAK]} + \frac{k_{FFP}[FAK][p - FAK]}{k_3 + [p - FAK]} + \frac{k_{SPFP}[p - SRC][FAK]}{k_7 + [FAK]}$
$p - FAK$	$r([p - FAK], t) = k_{FFP}[p - FAK] + \frac{k_{FPSP}[p - FAK][SRC]}{k_4 + [SRC]} + \frac{k_{FFPRhoGEF}[p - FAK][RhoGEF]}{k_8 + [RhoGEF]}$
$p - SRC$	$g([p - SRC], t) = \frac{k_{ESP}([ECMINT] - [p - MLC])[SRC]}{k_2 + [SRC]} + \frac{k_{FPSP}[p - FAK][SRC]}{k_4 + [SRC]} + \frac{k_{SSP}[SRC][p - SRC]}{k_6 + [p - SRC]}$
$p - SRC$	$r([p - SRC], t) = k_{SPS}[p - SRC] + \frac{k_{SPFP}[p - SRC][FAK]}{k_7 + [FAK]} + \frac{k_{SPRhoGAP}[p - SRC][RhoGAP]}{K_9 + [RhoGAP]}$
$RhoGEF$	$g([RhoGEF], t) = \frac{k_{FFPRhoGEF}[p - FAK][RhoGEF]}{k_8 + [RhoGEF]}$
$RhoGEF$	$r([RhoGEF], t) = \frac{k_{RhoGEFRhoA}[RhoGEF][RhoA]}{k_{11} + [RhoA]}$
$RhoGAP$	$g([RhoGAP], t) = \frac{k_{SPRhoGAP}[p - SRC][RhoGAP]}{K_9 + [RhoGAP]}$
$RhoGAP$	$r([RhoGAP], t) = \frac{k_{RhoGAPRhoA}[RhoGAP][RhoA]}{k_{11} + [RhoA]}$
$RhoA$	$g([RhoA], t) = \frac{k_{RhoGEFRhoA}[RhoGEF][RhoA]}{k_{10} + [RhoA]}$
$RhoA$	$r([RhoA], t) = \frac{k_{RhoGAPRhoA}[RhoGAP][RhoA]}{k_{11} + [RhoA]}$
$p - MLC$	$g([p - MLC], t) = \frac{k_{RHOAMLC}[RhoA][MLC]}{k_{12} + [MLC]} + \frac{k_{MLCPMLC}[MLC][p - MLC]}{k_{13} + [MLC]}$
MLC^p	$r([p - MLC], t) = k_{MLC^pMLC}[p - MLC]$

2) and the solution for the dynamic interactions of the proteins is given by the solution of the Chemical Master Equation (Eq. 2) with the corresponding generation and recombination terms (as shown in Section 2). The output of this model is the dynamic interactions of proteins, which can be seen as the distribution of molecules in each protein state per time (Figure 4). The system of equations is solved numerically using the Gillespie algorithm [17]. The input parameters are the initial distribution of proteins, the total time of simulation, and the values of the transition rates (see Tables 3 and 4 for details). Experiments alone cannot give exactly the values of protein concentration or transition rates, because the methodologies used to describe protein dynamics such as Fluorescence recovery after photobleaching (FRAP) or single molecule tracking follows one protein at a time and only tag a sub-population of proteins due to diffraction effects [18]. But we used experimental data to estimate the range of transition rate values and initial protein concentration used in the simulations [19].

In Figure 4 we show the results for Case 1 in Tables 3 and 4. We can see that $p - FAK$ and $p - SRC$ are the first to be activated, followed by the Rho family and later by MLC and $p - MLC$ (Figure 4a). This cascade effect behaves as expected by the construction of the model and the experimental information we had about the system. The higher values of the transition rates k_{EFP} , k_{ESP} and k_{FFP} were chosen to guarantee that these reactions would happen often and coordinate all the other events. In Figure 4b we have the detailed behavior for all 4 circuits in our model. The results showed that the activity of FAK and $p - FAK$ occurs only at the beginning of the process (Figure 4b(i)) and $p - FAK$ reached its peak activity at around 30 MCS. SRC and $p - SRC$ continue to be activated longer in simulation (Figure 4b(ii)), and $p - SRC$ achieved its peak at around 1300MCS. Another interesting behavior we can observe for $p - SRC$ is that it has other peaks later in time, meaning that it is activated in waves. The activation of $RhoGAP$ and $RhoGEF$ (peaks at around 2600 MCS

and around 120 MCS respectively) leads to the activation of $RhoA$, with maximum activity at around 1500 MCS. The circuit MLC-pMLC increased its activity later on reaching its peak at around 3500 MCS for $p - MLC$. The concentration of MLC goes to zero when the $p - MLC$ reaches its stability. This behavior is occurring because MLC is not regulated by any other protein and its role is to activate $p - SRC$. Once $p - SRC$ is activated the protein degrades. It is interesting to notice that the sequence of events is: activation of $p - FAK$ followed by activation of $RhoGEF$, then $p - SRC$ followed by $RhoGAP$ and $RhoA$ then the output $p - SRC$ to reach stability (Figures 2 and Figure 4). For Case 1 MLC reaches a plateau.

For the purpose of validation, we also tested a negative proof for the model, where we considered $ECM-INT=0$, which is equivalent to a null focal adhesion signal. In this scenario, all the other parameters were maintained constant and it resulted in a flat distribution and no interaction was observed in the system (data not shown).

In Figure 5 results for perturbations are shown. We take into account one perturbation at a time. In Figure 5a(i) we simulate the Case 2 in Tables 3 and 4. This case shows the effects to take $k_{EFP} = 1$ ten times greater than the reference in Case 1. It is equivalent to saying that the FAK would be more activated than SRC from the extracellular signal. Comparing Figure 5a(i) with Figure 4b(i), we can see that the concentration of $p - FAK$ is great for case 2 and also that the concentration of $p - SRC$ is reduced. The results for the output protein MLC and $p - SRC$ are shown in Figure 5(b)(i). For case 2 it also reached a plateau.

In Figure 5a(ii) we simulate the Case 3 in Tables 3 and 4. In this case, we increased the initial concentration of $FAK_0 = 20$. The behavior of the proteins $p - FAK$ and $p - SRC$ are not distinguishable from case 1 (Figures 5a(ii) and 4). But the behavior of MLC changes, we can see that $p - SRC$ starts to oscillate around a mean value and it is not a smooth plateau anymore.

In Figure 5a(iii) we simulate the Case 4 in Tables 3 and 4. In this case, we increased the rate of interaction of SRC, $k_{ESP} = 1$. The concentration of the protein $p - FAK$ decreases with respect to case 1 (Figures 5a(iii) and 4). We can see that the amplitude of the oscillations of $p - SRC$ decrease in relation to those in case 3 (Figure 5b(ii)). Finally, in Figure 5a(iv) we simulate the Case 5 in Tables 3 and 4. In this case, we increased the initial concentration of $SRC_0 = 20$. The concentrations of $p - FAK$ and $p - SRC$ are not distinguishable from case 1 (Figures 5a(iv) and 4). We can see that the amplitude of the oscillations of $p - SRC$ have the same range as in case 3 (Figure 5b(ii)).

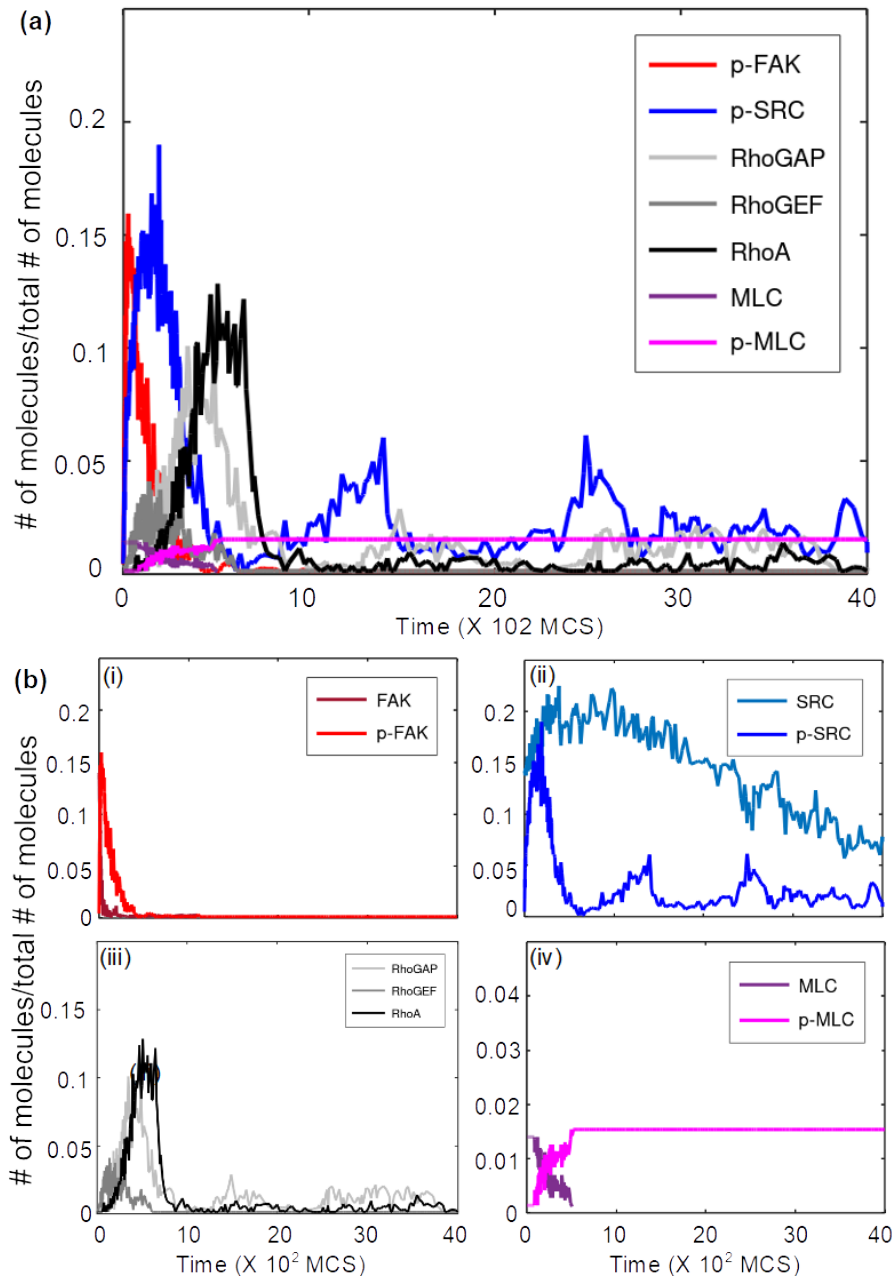


Figure 4: Normalized distribution of proteins per Monte Carlo step (MCS). (a) Dynamic activation of key signaling proteins of the base network. (b) The detailed dynamic of each circuit in the network: (i) FAK (ii) SCR (iii) Rho family and (iv) MLC was zoomed-in protein concentration, for a max concentration of 0.05. All the plots show the mean of 10 simulations. For visualization purposes, each point represents the mean of the concentration for 10-time steps. The parameters used for these simulations are detailed in Tables 3 and 4.

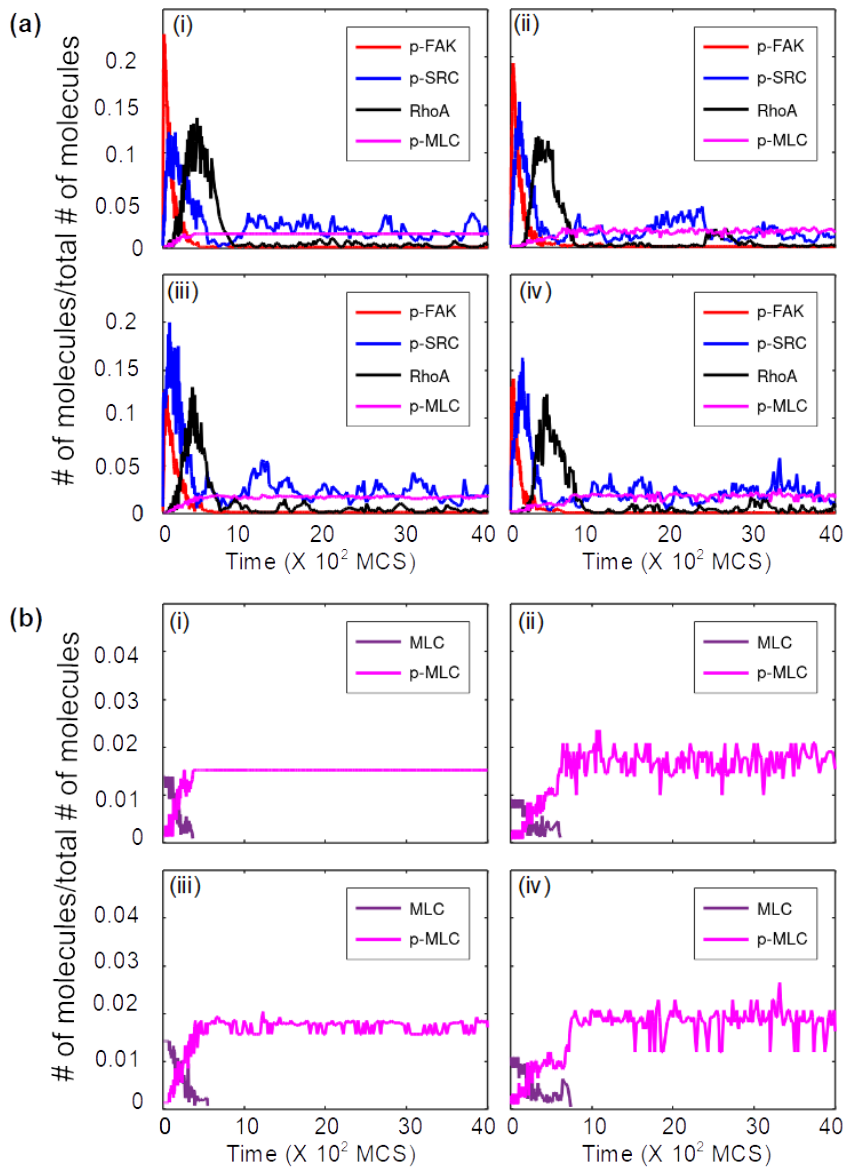


Figure 5: Comparison of the perturbations made in the parameters of the model. (a) The concentration of the key proteins in the system ($p-FAK$, $p-SRC$, $RhoA$ and $p-MLC$) the figures show only the initial 400 MCS for the purpose to see how the early proteins are behaving. (b) The concentration of proteins for the output MLC and $p-MLC$. The subdivision of the figures are (i) Case 2; (ii) Case 3; (iii) Case 4 (iv) Case 5. The parameters used for these simulations are detailed in Tables 3 and 4.

4 DISCUSSION

We proposed a stochastic mathematical model using the solution of the Chemical Master equation to understand the network of proteins involving extracellular matrix stimuli that can lead to actin polymerization and focal adhesion formation. Our signaling network was built considering the interaction between the focal adhesion proteins *FAK*, *Src*, *Rac*, *Rho*, *Myosin light-chain (MLC)* (Figures 1 and 2). Our data showed the capacity of the model to predict expected behaviors by reproducing a cascade of events and dependence on the activation of proteins of a known signaling pathway, as follows.

Our results have shown that *FAK* activity is lower than *Src* activity (see figures 4 and 5), which confirms what was experimentally observed by Caron-Lormier and Berry [?]. Furthermore, we observed that the increase of activation rate of *p-FAK* (Case 2, Figure 5a(i)) did not influence the dynamic of other proteins, only the initial concentration of *p-FAK*. A behavior that was observed experimentally by Stutchbury *et. al* [?].

For cases 3, 4, and 5 oscillations in the dynamics of *p-MLC* were observed (Figures 5b (ii), (iii) and (iv)). These oscillations are more evident in the cases we are varying the initial concentration of *FAK* and *SRC* (Figures 5b (ii), and (iv), respectively). Which can be associated with a stiff substrate and higher protein recruitment to the focal adhesion. Stutchbury *et. al* [?] showed that a modular composition of FAs with the mobile behavior of protein subsets responded differently when encountering environments of different rigidities.

In summary, we proposed a stochastic model considering the dynamic of focal adhesion proteins leading to actin polymerization. Our model was built in a combination of experimental and theoretical observations and was able to demonstrate a variety of behaviors for the different proteins and circuits within the network. Furthermore, we showed the effect of variation in the parameters that can lead to different cell fates.

SUPPORT

Research partially supported by:

- National Council for Scientific and Technological Development (CNPQ), Ministry of Science and Technology, Brazil. PIBIC No. 21-2022 Process 107099-2023-3 (2023). *Programa Institucional de Bolsas de Iniciação Científica*
- Fundação de Amparo à Pesquisa do Estado do Rio Grande do Sul, Brazil. PROA 23-25551-0001199-9 (2023). *Network of interaction of proteins. Decision between apoptosis and senescence.*

CONTRIBUTION OF THE AUTHORS (CREDIT)

Conceptualization: Luciana Renata de Oliveira

Data curation: Luciana Renata de Oliveira, Júlia Vitória Ribeiro, Alícia Groth Becker, Gabriel Vitorello, José Carlos Merino Mombach.

Investigation: Luciana Renata de Oliveira, Júlia Vitória Ribeiro, Alícia Groth Becker, Gabriel Vitorello

Writing – original draft: Luciana Renata de Oliveira and José Carlos Merino Mombach.

APPENDIX

A LIST OF EQUATIONS FOR EACH INTERACTION

The list of equations for each reaction represented in Figure 2. The indexes correspond to those in Figure 2, the equation and the kind of reaction are also represented in the table.

B PARAMETERS FOR THE SIMULATIONS

The list of equations for each reaction represented in Figure 2. The indexes correspond to those in Figure 2, the equation and the kind of reaction are also represented in the table.

Table 3: List of equations for each reaction represented in Figure 2. The indexes correspond to those in Figure 2, the equation and the kind of reaction are also represented in the table.

Index	Reaction	Equation	Reaction kind
1	$ECMINT \rightarrow p - FAK$	$\frac{k_{EFP}([ECMINT] - [p - MLC])[FAK]}{k_1 + [FAK]}$	Michaelis-Menten
2	$ECMINT \rightarrow p - SRC$	$\frac{k_{ESP}([ECMINT] - [p - MLC])[SRC]}{k_2 + [SRC]}$	Michaelis-Menten
3	$FAK \rightarrow p - FAK$	$\frac{k_{FFP}[FAK][p - FAK]}{k_3 + [p - FAK]}$	Michaelis-Menten
4	$p - FAK \rightarrow p - SRC$	$\frac{k_{FPP}[p - FAK][SRC]}{k_4 + [SRC]}$	Michaelis-Menten
5	$SRC \rightarrow p - SRC$	$\frac{k_{SSP}[SRC][p - SRC]}{k_6 + [p - SRC]}$	Michaelis-Menten
6	$p - FAK \rightarrow FAK$	$k_{FPF}[p - FAK]$	Degradation
7	$p - SRC \rightarrow p - FAK$	$\frac{k_{SPP}[p - SRC][FAK]}{k_7 + [FAK]}$	Michaelis-Menten
8	$p - SRC \rightarrow SRC$	$k_{SPS}[p - SRC]$	Degradation
9	$p - FAK \rightarrow RHOGEF$	$\frac{k_{FPRhoGEF}[p - FAK][RhoGEF]}{k_8 + [RhoGEF]}$	Michaelis-Menten
10	$p - SRC \rightarrow RHOGAP$	$\frac{k_{SPRhoGAP}[p - SRC][RhoGAP]}{k_9 + [RhoGAP]}$	Michaelis-Menten
11	$RHOGEF \rightarrow RHOA$	$\frac{k_{RhoGEFRhoA}[RhoGEF][RhoA]}{k_{10} + [RhoA]}$	Michaelis-Menten
12	$RHOGAP \rightarrow RHOA$	$\frac{k_{RhoGAPRhoA}[RhoGAP][RhoA]}{k_{11} + [RhoA]}$	Inhibition
13	$RHOA \rightarrow p - MLC$	$\frac{k_{RHOAMLCp}[RhoA][MLC]}{k_{12} + [MLC]}$	Michaelis-Menten
14	$MLC \rightarrow p - MLC$	$\frac{k_{MLCPMLCp}[MLC][p - MLC]}{k_{13} + [MLC]}$	Michaelis-Menten
15	$p - MLC \rightarrow MLC$	$k_{MLCpMLC}[p - MLC]$	Degradation

Table 4: List of equations for each reaction represented in Figure 2. The indexes correspond to those in Figure 2, the equation and the kind of reaction are also represented in the table.

Rate(/s)	Case 1	Case 2	Case 3	Case 4	Case 5
1	$ECMINT \rightarrow p - FAK$	$\frac{k_{EFP}([ECMINT] - [p - MLC])[FAK]}{k_1 + [FAK]}$	Michaelis-Menten		
2	$ECMINT \rightarrow p - SRC$	$\frac{k_{ESP}([ECMINT] - [p - MLC])[SRC]}{k_2 + [SRC]}$	Michaelis-Menten		
3	$FAK \rightarrow p - FAK$	$\frac{k_{FFP}[FAK][p - FAK]}{k_3 + [p - FAK]}$	Michaelis-Menten		
4	$p - FAK \rightarrow p - SRC$	$\frac{k_{FPP}[p - FAK][SRC]}{k_4 + [SRC]}$	Michaelis-Menten		
5	$SRC \rightarrow p - SRC$	$\frac{k_{SSP}[SRC][p - SRC]}{k_6 + [p - SRC]}$	Michaelis-Menten		
6	$p - FAK \rightarrow FAK$	$k_{FPF}[p - FAK]$	Degradation		
7	$p - SRC \rightarrow p - FAK$	$\frac{k_{SPP}[p - SRC][FAK]}{k_7 + [FAK]}$	Michaelis-Menten		
8	$p - SRC \rightarrow SRC$	$k_{SPS}[p - SRC]$	Degradation		
9	$p - FAK \rightarrow RHOGEF$	$\frac{k_{FPRhoGEF}[p - FAK][RhoGEF]}{k_8 + [RhoGEF]}$	Michaelis-Menten		
10	$p - SRC \rightarrow RHOGAP$	$\frac{k_{SPRhoGAP}[p - SRC][RhoGAP]}{k_9 + [RhoGAP]}$	Michaelis-Menten		
11	$RHOGEF \rightarrow RHOA$	$\frac{k_{RhoGEFRhoA}[RhoGEF][RhoA]}{k_{10} + [RhoA]}$	Michaelis-Menten		
12	$RHOGAP \rightarrow RHOA$	$\frac{k_{RhoGAPRhoA}[RhoGAP][RhoA]}{k_{11} + [RhoA]}$	Inhibition		
13	$RHOA \rightarrow p - MLC$	$\frac{k_{RHOAMLCp}[RhoA][MLC]}{k_{12} + [MLC]}$	Michaelis-Menten		
14	$MLC \rightarrow p - MLC$	$\frac{k_{MLCPMLCp}[MLC][p - MLC]}{k_{13} + [MLC]}$	Michaelis-Menten		
15	$p - MLC \rightarrow MLC$	$k_{MLCpMLC}[p - MLC]$	Degradation		

REFERENCES

- Aguda, B. and Friedman, A. (2008) *Models of cellular regulation*. Oxford University Press.
- Atherton, P., Stutchbury, B., Jethwa, D. and Ballestrem, C. (2016) 'Mechanosensitive components of integrin adhesions: Role of vinculin'. *Experimental cell research*, 343(1), pp. 21–27.
- Berro, J. (2018) "'essentially, all models are wrong, but some are useful"—a cross-disciplinary agenda for building useful models in cell biology and biophysics'. *Biophysical Reviews*, 10(6), pp. 1637–1647.
- Calderwood, D.A., Campbell, I.D. and Critchley, D.R. (2013) 'Talins and kindlins: partners in integrin-mediated adhesion'. *Nature reviews Molecular cell biology*, 14(8), pp. 503–517.
- Carisey, A., Tsang, R., Greiner, A.M., Nijenhuis, N., Heath, N., Nazgiewicz, A., Kemkemer, R., Derby, B., Spatz, J. and Ballestrem, C. (2013) 'Vinculin regulates the recruitment and release of core focal adhesion proteins in a force-dependent manner'. *Current biology*, 23(4), pp. 271–281.
- Caron-Lormier, G. and Berry, H. (2005) 'Amplification and oscillations in the fak/src kinase system during integrin signaling'. *Journal of theoretical biology*, 232(2), pp. 235–248.
- Chen, H., Choudhury, D.M. and Craig, S.W. (2006) 'Coincidence of actin filaments and talin is required to activate vinculin'. *Journal of Biological Chemistry*, 281(52), pp. 40389–40398.
- Dai, Y., Luo, W. and Chang, J. (2018) 'Rho kinase signaling and cardiac physiology'. *Current opinion in physiology*, 1, pp. 14–20.
- De Oliveira, L.R. (2014) 'Master equation: Biological applications and thermodynamic description'.
- Del Rio, A., Perez-Jimenez, R., Liu, R., Roca-Cusachs, P., Fernandez, J.M. and Sheetz, M.P. (2009) 'Stretching single talin rod molecules activates vinculin binding'. *Science*, 323(5914), pp. 638–641.
- Giampieri, E., Remondini, D., De Oliveira, L., Castellani, G. and Lió, P. (2011) 'Stochastic analysis of a mirna-protein toggle switch'. *Molecular BioSystems*, 7(10), pp. 2796–2803.
- Gillespie, D.T. (1977) 'Exact stochastic simulation of coupled chemical reactions'. *The journal of physical chemistry*, 81(25), pp. 2340–2361.
- Hirata, H., Chiam, K.H., Lim, C.T. and Sokabe, M. (2014) 'Actin flow and talin dynamics govern rigidity sensing in actin-integrin linkage through talin extension'. *Journal of The Royal Society Interface*, 11(99), p. 20140734.
- Hsia, D.A., Mitra, S.K., Hauck, C.R., Streblov, D.N., Nelson, J.A., Ilic, D., Huang, S., Li, E., Nemerow, G.R., Leng, J. *et al.* (2003) 'Differential regulation of cell motility and invasion by fak'. *The Journal of cell biology*, 160(5), pp. 753–767.
- Jansen, K., Atherton, P. and Ballestrem, C. (2017) 'Mechanotransduction at the cell-matrix interface'. In *Seminars in cell & developmental biology*, vol. 71. Elsevier, pp. 75–83.
- Jaqaman, K., Loerke, D., Mettlen, M., Kuwata, H., Grinstein, S., Schmid, S.L. and Danuser, G. (2008) 'Robust single-particle tracking in live-cell time-lapse sequences'. *Nature methods*, 5(8), pp. 695–702.
- Kanchanawong, P., Shtengel, G., Pasapera, A.M., Ramko, E.B., Davidson, M.W., Hess, H.F. and Waterman, C.M. (2010) 'Nanoscale architecture of integrin-based cell adhesions'. *Nature*, 468(7323), pp. 580–584.
- Kumar, A., Ouyang, M., Van den Dries, K., McGhee, E.J., Tanaka, K., Anderson, M.D., Groisman, A., Goult, B.T., Anderson, K.I. and Schwartz, M.A. (2016) 'Talin tension sensor reveals novel features of focal adhesion force transmission and mechanosensitivity'. *Journal of Cell Biology*, 213(3), pp. 371–383.
- Lessey, E.C., Guilluy, C. and Burridge, K. (2012) 'From mechanical force to rhoa activation'. *Biochemistry*, 51(38), pp. 7420–7432.
- Lippincott-Schwartz, J., Snapp, E.L. and Phair, R.D. (2018) 'The development and enhancement of frap as a key tool for investigating protein dynamics'. *Biophysical journal*, 115(7), pp. 1146–1155.
- MacKay, C.E. and Knock, G.A. (2015) 'Control of vascular smooth muscle function by src-family kinases and reactive oxygen species in health and disease'. *The Journal of physiology*, 593(17), pp. 3815–3828.
- Martin-Camara, O., Cores, A., Lopez-Alvarado, P. and Menéndez, J.C. (2021) 'Emerging targets in drug discovery against neurodegenerative diseases: Control of synapsis dysfunction by the rhoa/rock pathway'. *European Journal of Medicinal Chemistry*, 225, p. 113742.
- Nagano, M., Hoshino, D., Koshikawa, N., Akizawa, T., Seiki, M. *et al.* (2012) 'Turnover of focal adhesions and cancer cell migration'. *International journal of cell biology*, 2012.
- de Oliveira, L.R. and Jaqaman, K. (2019) 'Fisik: Framework for the inference of in situ interaction kinetics from single-molecule imaging data'. *Biophysical journal*, 117(6), pp. 1012–1028.
- Pertz, O. (2010) 'Spatio-temporal rho gtpase signaling—where are we now?' *Journal of cell science*, 123(11), pp. 1841–1850.
- Raaijmakers, J.G. (1987) 'Statistical analysis of the michaelis-menten equation'. *Biometrics*, pp. 793–803.
- Roca-Cusachs, P., Del Rio, A., Puklin-Faucher, E., Gauthier, N.C., Biais, N. and Sheetz, M.P. (2013) 'Integrin-dependent force transmission to the extracellular matrix by α -actinin triggers adhesion maturation'. *Proceedings of the National Academy of Sciences*, 110(15), pp. E1361–E1370.
- Soriano, O., Alcón-Pérez, M., Vicente-Manzanares, M. and Castellano, E. (2021) 'The crossroads between ras and rho signaling pathways in cellular transformation, motility and contraction'. *Genes*, 12(6), p. 819.
- Srinivasan, B. (2022) 'A guide to the michaelis-menten equation: steady state and beyond'. *The FEBS journal*, 289(20), pp. 6086–6098.
- Stutchbury, B., Atherton, P., Tsang, R., Wang, D.Y. and Ballestrem, C. (2017) 'Distinct focal adhesion protein modules control different aspects of mechanotransduction'. *Journal of cell science*, 130(9), pp. 1612–1624.
- Szklarczyk, D., Gable, A.L., Lyon, D., Junge, A., Wyder, S., Huerta-Cepas, J., Simonovic, M., Doncheva, N.T., Morris, J.H., Bork, P. *et al.* (2019) 'String v11: protein-protein association networks with increased coverage, supporting functional discovery in genome-wide experimental datasets'. *Nucleic acids research*, 47(D1), pp. D607–D613.
- Valencia-Expósito, A., Grosheva, I., Míguez, D.G., González-Reyes, A. and Martín-Bermudo, M.D. (2016) 'Myosin light-chain phosphatase regulates basal actomyosin oscillations during morphogenesis'. *Nature communications*, 7(1), p. 10746.
- Van Kampen, N.G. (1992) *Stochastic processes in physics and chemistry*, vol. 1. Elsevier.

Recommended Citation: Renata de Oliveira, L. *et al.* (2023). 'Using the Chemical Master Equation to model the interaction network of focal adhesion proteins'. Rev. model. mat. sist. biol. 3(E), e23R05, doi:10.58560/rmmsb.v03.n02.023.04



This open access article is licensed under a Creative Commons Attribution International (CC BY 4.0) <http://creativecommons.org/licenses/by/4.0/>.
Support: PIBIC No. 21-2022, PROA 23-25551-0001199-9 (2023)



UTEM

UNIVERSIDAD
TECNOLÓGICA
METROPOLITANA

del Estado de Chile



EDICIONES UNIVERSIDAD
TECNOLÓGICA METROPOLITANA

VERSIÓN EN LÍNEA: ISSN 2735-6817

revistammsb.utm.cl